

AD-A118 696

HONEYWELL POWER SOURCES CENTER-HORSHAM PA
HIGH EFFICIENCY LITHIUM-THIONYL CHLORIDE CELL.(U)

F/G 10/3

AUG 82 N DODDAPANENI

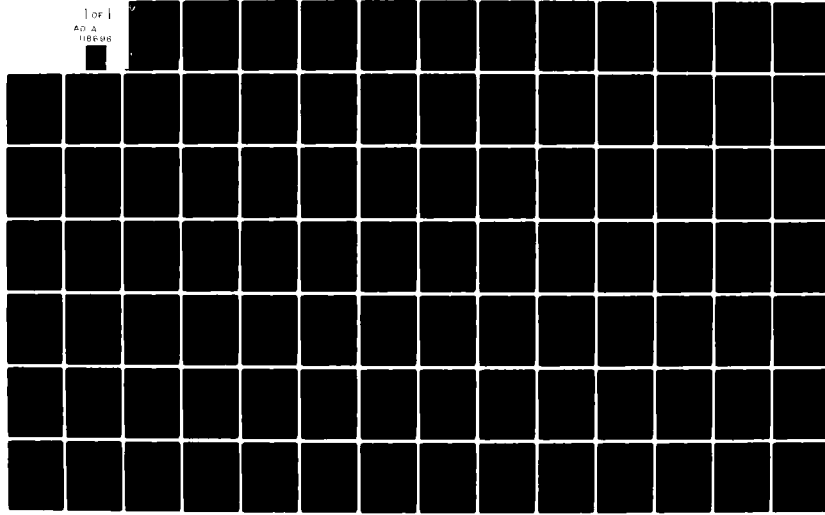
DAAK20-81-C-0381

DELET-TR-81-0381-F

NL

UNCLASSIFIED

1 of 1
AD A
118696





(12)

AD A118696

Research and Development Technical Report

DELET-TR-81-0381-F

HIGH EFFICIENCY LITHIUM-THIONYL CHLORIDE CELL

Dr. Narayan Doddapaneni
Honeywell Power Sources Center
104 Rock Road
Horsham, PA 19044

August 1982

FINAL REPORT for PERIOD 10 APRIL 1981 to 9 MAY 1982

APPROVED FOR PUBLIC RELEASE: DISTRIBUTION UNLIMITED

Prepared for:

ELECTRONICS TECHNOLOGY AND
DEVICES LABORATORY

DCASMA, PHILADELPHIA
P.O. BOX 7699
PHILADELPHIA, PA 19101

AUG 27 1982

E

ERADCOM

US ARMY ELECTRONICS RESEARCH AND DEVELOPMENT COMMAND
FORT MONMOUTH, NEW JERSEY 07703

82

HISA-FM 195-78

SECURITY CLASSIFICATION OF THIS PAGE (When Data Entered)

Unclassified

REPORT DOCUMENTATION PAGE		READ INSTRUCTIONS BEFORE COMPLETING FORM
1. REPORT NUMBER DELET-TR-81-0381-F	2. GOVT ACCESSION NO. <u>AD-A118 696</u>	3. RECIPIENT'S CATALOG NUMBER
4. TITLE (and Subtitle) High Efficiency Lithium-Thionyl Chloride Cell	5. TYPE OF REPORT & PERIOD COVERED 4-10-81 to 5-9-82 Final Report	
7. AUTHOR(s) Narayan Doddapaneni	6. PERFORMING ORG. REPORT NUMBER DAAK20-81-C-0381	
9. PERFORMING ORGANIZATION NAME AND ADDRESS Honeywell Power Sources Center 104 Rock Road Horsham, Pa. 19044	10. PROGRAM ELEMENT PROJECT TASK AREA & WORK UNIT NUMBERS 11162705AH94-11-211	
11. CONTROLLING OFFICE NAME AND ADDRESS U.S. Army Elect Tech & Dvcs Laboratory ATTN: DELET-PR <u>Fort Monmouth, NJ 07703</u>	12. REPORT DATE August 1982	
14. MONITORING AGENCY NAME & ADDRESS (if different from Controlling Office) DCASMA, Philadelphia P.O. Box 7699 Philadelphia, Pa. 19101	13. NUMBER OF PAGES 91 pages	
15. SECURITY CLASS. (of this report) Unclassified		
15a. DECLASSIFICATION/DOWNGRADING SCHEDULE		
16. DISTRIBUTION STATEMENT (of this Report) Approved for Public Release: Distribution Unlimited		
17. DISTRIBUTION STATEMENT (of the abstract entered in Block 20, if different from Report)		
18. SUPPLEMENTARY NOTES		
19. KEY WORDS (Continue on reverse side if necessary and identify by block number) Thionyl chloride, lithium, high discharge rates, low temperatures, catalysis, metal phthalocyanine complexes, cyclic voltammetry, AC impedance.		
20. ABSTRACT (Continue on reverse side if necessary and identify by block number) The polarization characteristics and the specific cathode capacity of Teflon bonded carbon electrodes in the Li/SOCl ₂ system have been evaluated. Doping of electrocatalysts such as cobalt and iron phthalocyanine complexes improved both cell voltage and cell rate capability. High efficiency Li/SOCl ₂ cells were thus achieved with catalyzed cathodes. The electrochemical reduction of SOCl ₂ seems to undergo modification at		

Unclassified

SECURITY CLASSIFICATION OF THIS PAGE(When Data Entered)

catalyzed cathode. For example, the reduction of SOCl_2 at FePc catalyzed cathode involves $2\frac{1}{2} \text{ e}^-/\text{mole}$ of SOCl_2 . Furthermore, the reduction mechanism is simplified and unwanted chemical species are eliminated by the catalyst. Thus a potentially safer high efficiency Li/ SOCl_2 can be anticipated.

The operating temperature strongly influences the cell voltage and its efficiency. The changes in electrolyte conductivity and viscosity, particularly at low temperatures, inhibit the rate capability and useful life of Li/ SOCl_2 cells. With catalyzed cathodes significant improvements were made, however, the intrinsic properties of LiAlCl₄/ SOCl_2 electrolytes play a major role in the efficiency of high rate Li/ SOCl_2 cells at low operating temperatures.

Unclassified

SECURITY CLASSIFICATION OF THIS PAGE(When Data Entered)

TABLE OF CONTENTS

	<u>Page</u>
I. INTRODUCTION	1
II. EVALUATION OF CATHODE OVERPOTENTIAL	3
A. Introduction	3
B. Laboratory Cell Measurements	4
C. Kinetic and Mechanistic Studies	25
D. Impedance Measurements	
III. CATHODE PERFORMANCE IMPROVEMENTS	55
A. Introduction	55
B. Evaluation of Cathode Performance	56
IV. SUMMARY AND CONCLUSIONS	81
V. RECOMMENDATIONS	83
VI. REFERENCES	85
VII. ACKNOWLEDGEMENTS	86

Accession For		
NTIS GRA&I	<input checked="" type="checkbox"/>	<input type="checkbox"/>
DTIC TAB	<input type="checkbox"/>	<input type="checkbox"/>
Unpublished	<input type="checkbox"/>	<input type="checkbox"/>
Justification	<hr/>	
By _____	<hr/>	
Distribution	<hr/>	
Available in Codes	<hr/>	
_____ Dist. _____ _____ Dist. _____	<input type="checkbox"/>	<input type="checkbox"/>
A	<input type="checkbox"/>	<input type="checkbox"/>



LIST OF FIGURES

	<u>Page</u>
1 Flow Diagram of Cathode Fabrication Process	5
2 Laboratory Cell	7
3 Details of Two-Plate Laboratory Cell	8
4 Polarization Characteristics of Li/SOCl ₂ Laboratory Cells at 75° F	9
5 Polarization Characteristics of Li/SOCl ₂ Laboratory Cells at 32° F	10
6 Polarization Characteristics of Li/SOCl ₂ Cells at 0° F	11
7 Polarization Characteristics of Li/SOCl ₂ Cells at -20° F	12
8 Polarization Characteristics of Li/SOCl ₂ Cells at -40° F	13
9 Effect of Operating Temperature on Laboratory Li/SOCl ₂ Cell Limiting Current	15
10 Effect of Operating Temperature on Cell Limiting Current Density	16
11 Discharge Characteristics of Li/SOCl ₂ Laboratory Cells at 20 mA/cm ² and 75° F	17
12 Discharge Characteristics of Li/SOCl ₂ Cells at 20 mA/cm ² and 32° F.	18
13 Discharge Characteristics of Li/SOCl ₂ Laboratory Cells at 20 mA/cm ² and 0° F.	19
14 Discharge Characteristics of Li/SOCl ₂ Cells at 20 mA/cm ² and -20° F	20
15 Discharge Characteristics of Laboratory Li/SOCl ₂ Cells at 15 mA/cm ² and -40° F	21
16 Discharge Characteristics of Li/SOCl ₂ Cells at 5 mA/cm ² and -40° F	22
17 Discharge Characteristics of Li/SOCl ₂ Laboratory Cells at 5 mA/cm ² and -20° F	23
18 Average Discharge Voltage of Li/SOCl ₂ Cells versus Discharge Rate at 72° F	26

18	Average Discharge Voltage of Li/SOCl ₂ Cells versus Discharge Rate at 72° F	26
19	Discharge Performance of Li/SOCl ₂ Cells with 1.5M LiAlCl ₄ /SOCl ₂ at 23°C	27
20	Cyclic Voltammograms at Pressure Annealed Pyrolytic Graphite	29
21	Effect of Sweep Rate on Cyclic Voltammograms at Pressure Annealed Pyrolytic Graphite Electrode	30
22	Current Peak Height (i_p) versus Square Root of Sweep Rate	31
23	Current Peak Height (i_p) versus Square Root of Sweep Rate	32
24	Current Peak Height (i_p) versus Square Root of Sweep Rate, Glassy Carbon Electrode	33
25	Effect of Temperature on Cyclic Voltammograms at Polycrystalline Carbon Electrode	34
26	Effect of Temperature on Cyclic Voltammograms at Polycrystalline Carbon Electrode	35
27	Arrhenius-type Temperature Dependence of Current Peak Heights	36
28	Plot of $1/i_p$ VS $1/\sqrt{\omega}$ From the Rotating Disk Data for Glassy Carbon Electrode	39
29	Plot of $1/i_p$ VS $\omega^{-1/2}$ From the Rotating Disk Data for Glassy Carbon Electrode	40
30	Plot of i^{-1} VS $\omega^{-1/2}$ at Different Potentials From the Rotating Disk Data for Glassy Carbon Electrode	41
31	Plot of $1/i_p$ VS $\omega^{-1/2}$ from the Relative Disc Data for Glassy Carbon Electrode	43
32	Effect of Temperature on the Conductivity of LiAlCl ₄ /SOCl ₂ Electrolyte	45
33	Effect of Temperature on LiAlCl ₄ /SOCl ₂ Electrolyte Viscosity	46
34	Impedance of Stress Annealed Pyrolytic Graphite Electrode in 1.5M LiAlCl ₄ /SOCl ₂ Containing FePc Catalyst	49
35	Impedance of Stress Annealed Pyrolytic Graphite Electrode in 1.5M LiAlCl ₄ /SOCl ₂ Electrolyte at 75°F	50
36	Impedance of Stress Annealed Pyrolytic Graphite Electrode at a Discharge Rate of 34 μ A/cm ² in 1.5M LiAlCl ₄ /SOCl ₂ + FePc	51
37	Impedance of Stress Annealed Pyrolytic Graphite Electrode	52
38	Impedance of Stress Annealed Pyrolytic Graphite Electrode	53

39	Impedance of Stress Annealed Pyrolytic Graphite Electrode	54
40	Effect of Teflon Content on the Cathode Density	57
41	Effect of Cathode Variables on Discharge Performance	59
42	Effect of Cathode Variables on Discharge Performance	60
43	Effect of Cathode Variables on the Discharge Performance	61
44	Effect of Cathode Variables on the Discharge Performance	62
45	Effect of Cathode Variables on Voltage	63
46	Effect of Cathode Variables on the Discharge Performance	64
47	Effect of Cathode Variables on Voltage	65
48	Effect of Cathode Variables	66
49	Effect of Cathode Variables	67
50	Effect of Cathode Variables	68
51	Effect of Carbon Substrates on Cell Discharge Time	69
52	Effect of Cathode Thickness on Discharge Characteristics	70
53	Effect of Cathode Thickness on Discharge Performance Characteristics	71
54	Effect of Cathode Thickness on Discharge Performance with Catalyzed Cathode	72
55	Effect of Cathode Thickness on Discharge Characteristics with Catalyzed Cathode	73
56	Polarization Characteristics of Li/SOCl ₂ Cells at 75° F	76
57	Polarization Characteristics of Li/SOCl ₂ Cells with Optimized Cathodes at 32° F	77
58	Discharge Characteristics at 20 mA/cm ² and 75° F	78

LIST OF TABLES

	<u>Page</u>
1 Discharge Characteristics of Li/SOCl ₂ Cells at 10 mA/cm ² in 1.5M LiAlCl ₄ /SOCl ₂	24
2 Effect of Temperature on Discharge Characteristics of Li/SOCl ₂ Cells with Optimized Cathodes and 1.5M LiAlCl ₄ /SOCl ₂ at 10 mA/cm ²	79
3 Effect of Temperature on Discharge Characteristics of Li/SOCl ₂ Cells with Optimized Cathodes and 1.5M LiAlCl ₄ /SOCl ₂ at 20 mA/cm ²	80

I. INTRODUCTION

The lithium-thionyl chloride electrochemistry (1-4) has the potential of being one of the best primary systems having the combined characteristics of high rate and high energy density capability, long shelf life, and wide operating temperature range. However, many of these advantages have not yet been achieved in the development of a practical cell. The operating capabilities of the Li/SOCl₂ system are limited, to a large extent, by the Teflon-bonded porous carbon electrode. High cathodic overpotentials due to the non-uniformity of current distribution and electrode kinetics impede this system from attaining its full usage. The extent of cathode polarization depends on several variables such as applied current density, operating temperature, cathode structure, and electrolyte composition.

The porous carbon cathode, where the reduction of SOCl₂ occurs, has a limited capacity for retaining solid lithium chloride as it precipitates in the pore structure. As the lithium chloride accumulates, the porosity of the electrode is reduced to where mass transport, particularly of the cathode depolarizer, can no longer be maintained at a rate commensurates with the required current density. When this happens, polarization becomes excessive and denotes the end of useful battery life.

At high rate discharges and low operating temperatures, the cathode polarization becomes very severe. Analysis of the porous electrode after high rate discharge showed only a small part of the available cathode thickness was utilized in the electrochemical process. Furthermore, the reaction zone thickness was found to depend strongly on the cathode thickness and composition. The purpose of this program was to identify and minimize the effects of these variables on cathode overpotential and reaction zone thickness so that a high efficiency lithium-thionyl chloride cell can be realized in practical hardwares. Specifically, the main objectives of the program were to:

- (a) evaluate the polarization characteristics of Teflon-bonded porous carbon cathodes.
- (b) improve cathode performance at high discharge rates and/or low operating temperatures.

Several experimental methods such as half-cell measurements, discharge performance characteristics, cyclic voltammetric studies and AC impedance measurements were carried out to evaluate the cathode polarization. These studies were made with our cathodes with and without electrocatalyst. The catalysts* studies were:

CATALYST A = Cobalt Phthalocyanine monomer, CoPc

CATALYST B = Iron Phthalocyanine monomer, FePc

CATALYST C = Cobalt Phthalocyanine polymer $(CoPc)_n$

Significant improvements in both Li/SOCl₂ cell voltage and specific cathode capacity were achieved with electrocatalysts. Cathode variables such as density and thickness also influenced the efficiency of the cell. At low operating temperature, the electrolyte conductivity and viscosity influenced the rate as well as performance capabilities.

*Patents pending.

II. EVALUATION OF CATHODE OVERPOTENTIAL

A. INTRODUCTION

The overpotential of an electrode system is defined as the difference between the measured potential under working conditions and the thermodynamic potential. Both physical and chemical processes taking place at the electrode interphase influence the extent of overpotential, commonly referred to as polarization.

The voltage of an electrochemical cell during discharge is given by the open circuit voltage (OCV) minus all the resistance and polarization losses throughout the cell. Thus, for cell discharge

$$E_D = OCV - i\sum R - \Sigma\eta_c - \Sigma\eta_a \quad (1)$$

where,

i = applied current

$\sum R$ = sum of electrolyte, electrode and lead resistance

$\Sigma\eta_c$ = sum of concentration polarization at the anode and cathode

$\Sigma\eta_a$ = sum of activation polarizations at the anode and cathode

Concentration polarization is anticipated to be severe in the Li/SOCl₂ system at low operating temperatures. Poor electrolyte conductivity and high viscosity contribute severely to the diffusion rate of the depolarizer. Furthermore, LiCl precipitation in the pore structure adversely effects both IR drop and concentration polarization.

Activation polarization arises from the irreversibility of both chemical and electrochemical processes taking place. Therefore, the electron transfer processes and hence the discharge rate influence the activation overpotential. It is known that SOCl₂ reduction proceeds smoothly at porous carbon cathodes

at low discharge rates. High discharge rates are achieved (5) only at cathodes doped with electrocatalysts.

Ohmic overpotential arises from the non-uniformity of current distribution over the porous electrode. In addition, electrolyte conductivity and viscosity and LiCl precipitation in pore structure contribute to this overpotential. Therefore, IR drop can have a severe effect on the Li/SOCl₂ cell potential, especially under high discharge rate and low temperature conditions.

All three types of overpotential contribute to cathode polarization in a Li/SOCl₂ system. The magnitude of each type depends on the operating temperature, electrolyte conductivity and viscosity. During the program, we attempted to improve cell voltage by lowering the activation overpotential of Teflon-bonded carbon cathode. This was achieved by the use of electrocatalysts.

B. LABORATORY CELL MEASUREMENTS

1. Experimental

Cathodes. Our baseline cathode contained 95% Shawinigan Acetylene Black (100% compressed-grade) and 5% Teflon-6. The standard cathode fabrication process is summarized in Figure 1.

Our best improved cathodes contained either iron phthalocyanine monomer, FePc or in-house synthesized polymeric cobalt phthalocyanine (CoPc)_n.* FePc was found to be soluble in the electrolyte, therefore, it was dissolved in the electrolyte before cells were activated. (CoPc)_n was impregnated onto carbon from a concentrated H₂SO₄ solution by diluting with ice water. The material was washed thoroughly with distilled water and dried at 120° C. This catalyst-carbon mix was then heat treated between 500-600° C in an inert atmosphere to activate the catalyst. The heat treatment renders the catalyst insoluble in SOCl₂ electrolytes. Cathodes were fabricated according to standard procedure. The final cathode composition was 5% (CoPc)_n, 90% SAB and 5% Teflon-6.

* The (CoPc)_n catalyst was synthesized by the heat treatment of a mixture of 3,3', 4,4' benzophenone tetracarboxylicdianhydride, cobalt sulfate, urea and ammonium molybdate at 180° ± 10° C for 2 hours.

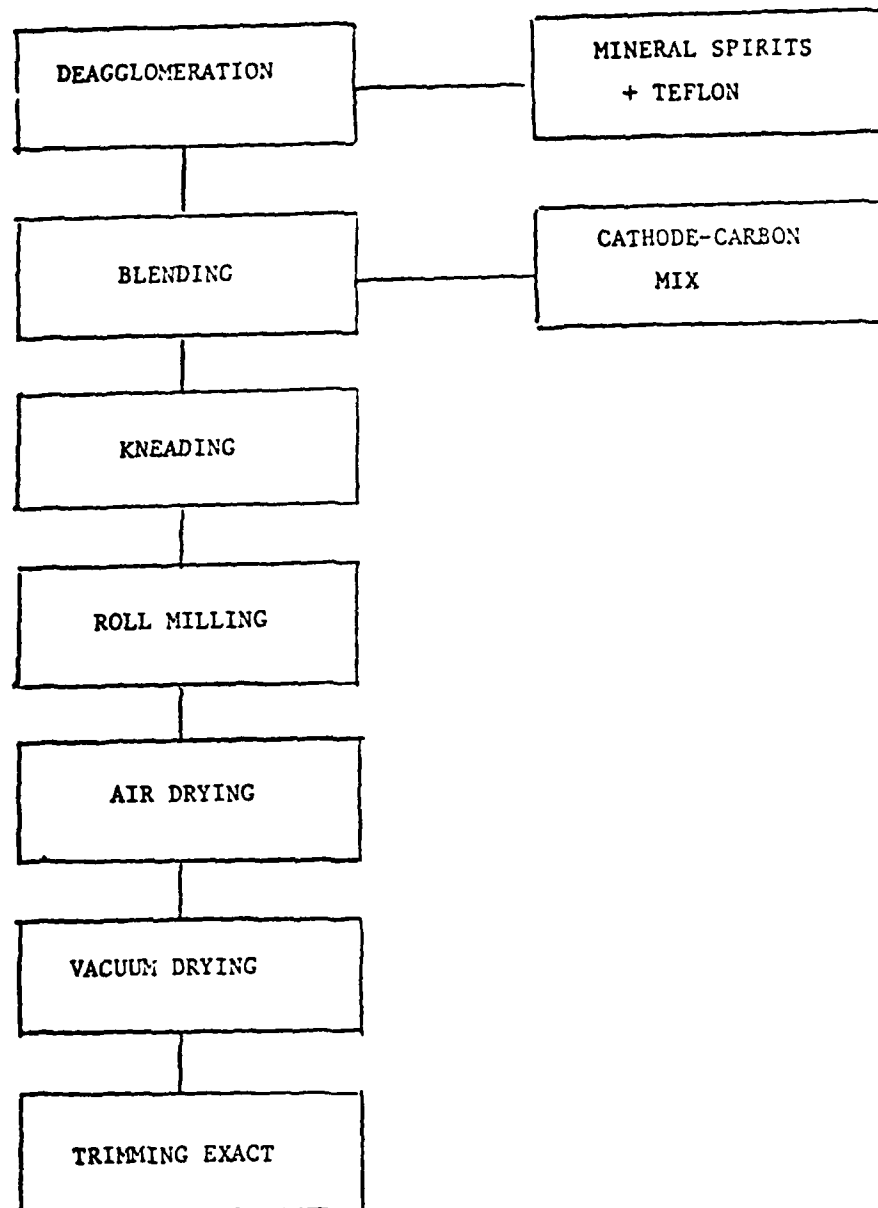


Figure 1. Flow Diagram of Cathode Fabrication Process.
Workability of the process not restricted to
specific carbon type. Rolling incurs excellent
mechanical integrity on the cathode.

Electrolytes. 1.5M LiAlCl₄/SOCl₂ electrolyte was manufactured by dissolving required AlCl₃ and LiCl salts in thionyl chloride. Analytical grade AlCl₃ (Fluka-grade), LiCl (MCB) and SOCl₂ (MCB-TX535) were used without further purification.

Laboratory Cell. The laboratory cell used for both polarization and discharge characterization experiments was a sealed electrochemical fixture (Figure 2) which contained a basic cell structure of two plate prismatic electrodes (Figure 3), one Teflonated carbon electrode and one lithium anode, both pressed onto nickel grid current collectors.

The cathodes studied were 0.5" (wide) x 1.0" (high) x 0.020" (thick)^{*}, and the anodes had the same apparent surface area but used a thickness of 0.01". Two layers of 0.005" thick each Manning Glass separators were used. All cells were activated at ambient temperature using 2 cc of electrolyte. Low temperature experiments were carried out after placing them at the operating temperature for 2 hours. Experiments were carried out in duplication at ambient temperature, +32°F, 0°F, -20°F and -40°F.

2. Half-Cell Measurements

Three types of cathodes were examined for their polarization behavior between -40 and 75°F. They were (a) baseline cathode, (b) FePc catalyzed cathode, and (c) (CoPc)_n doped cathode. The potential dependence of current was determined by measuring steady-state electrode potential relative to a lithium reference electrode at various controlled currents. At low applied currents (<5 mA/cm²), 2-5 minutes was needed to reach steady state, whereas less than a minute was needed at higher applied currents.

Figures 4-8 show the polarization characteristics of the above described three cathodes at operating temperatures of 75, 32, 0, -20 and -40°F. With catalyzed cathodes, the cathode polarization is reduced significantly. FePc catalyzed cathodes has the lowest polarization. The decrease in voltage loss with catalyzed cathodes is due mainly to the lowering of activation polarization associated with SOCl₂ adsorption and electron transfer processes.

* Cathodes of 0.20" thick were used throughout the program - unless specified otherwise.

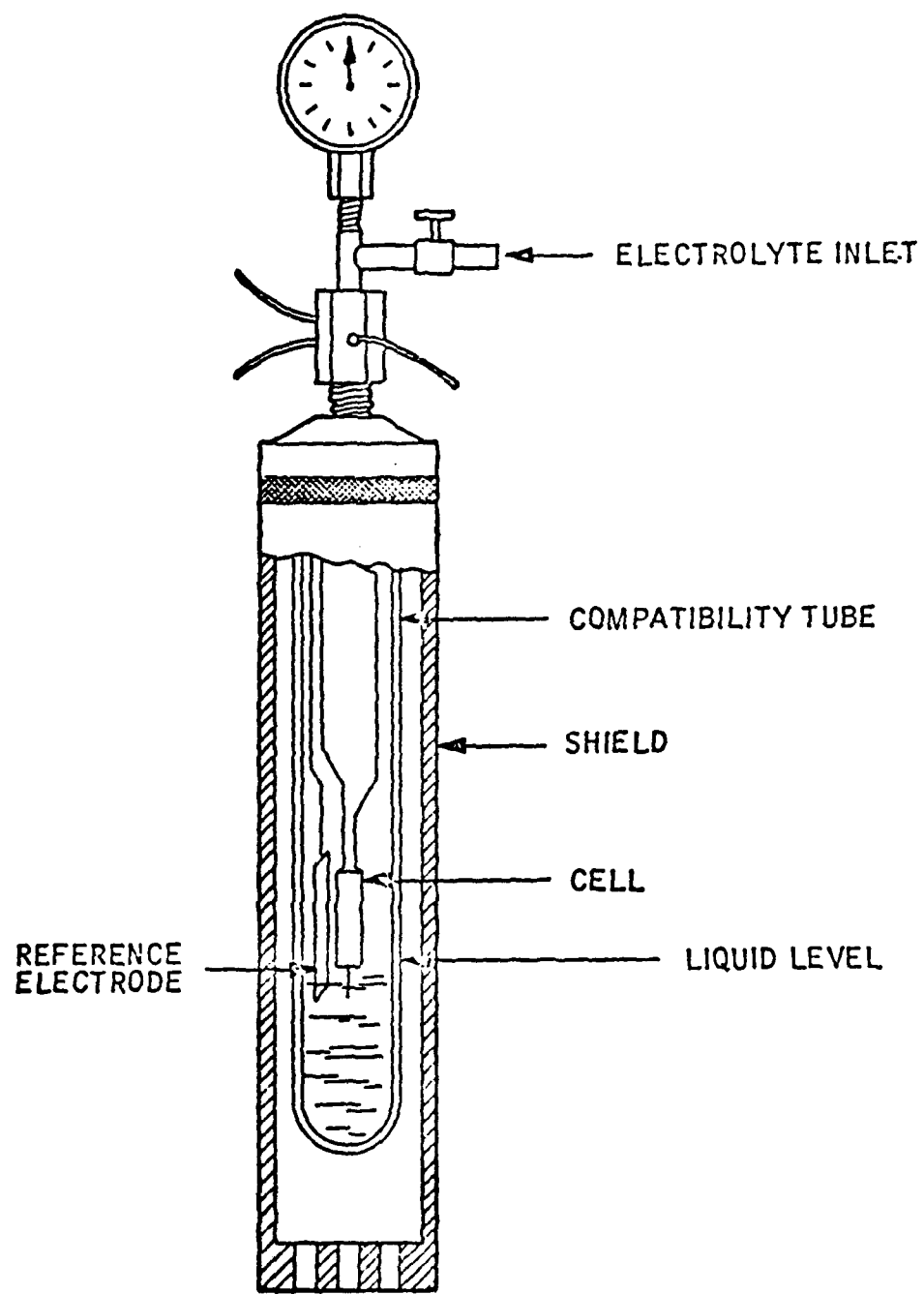


Figure 2. Laboratory Cell. Employed to study the polarizations and discharge performance of cathodes.

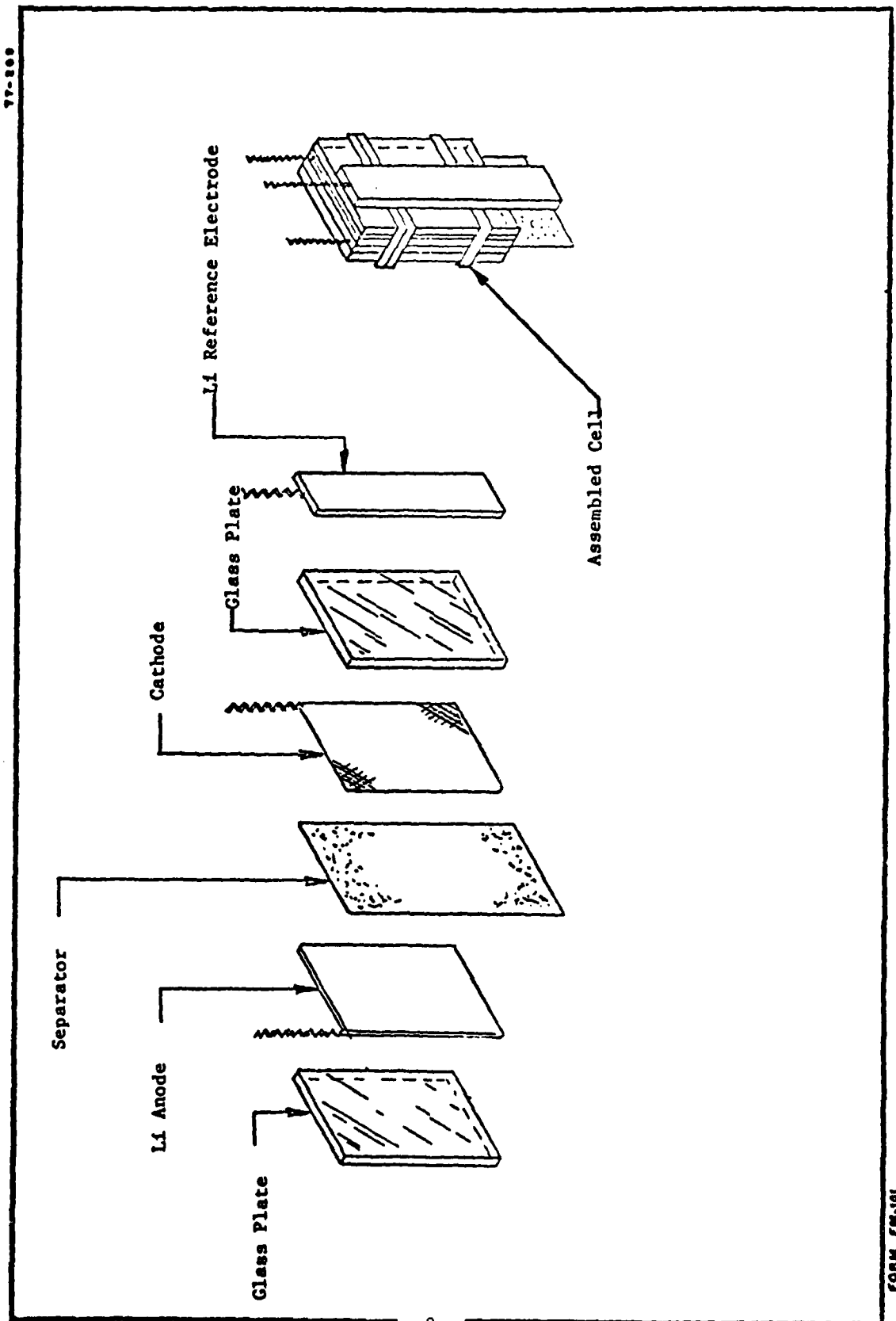


Figure 3. Details of Two-Plate Laboratory Cell.

81-063

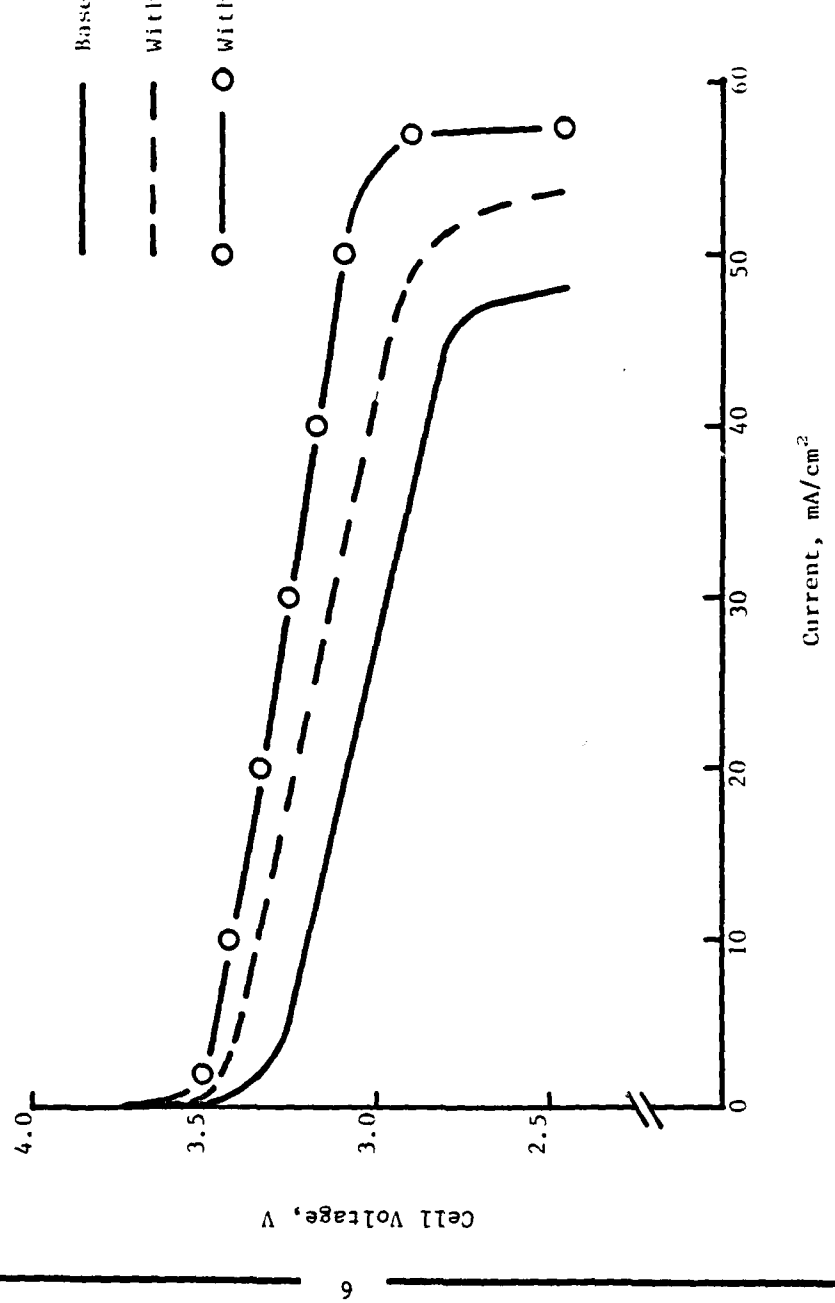


Figure 4 . Polarization characteristics of Li/SOCl_2 Laboratory cells at 75°F

81-068

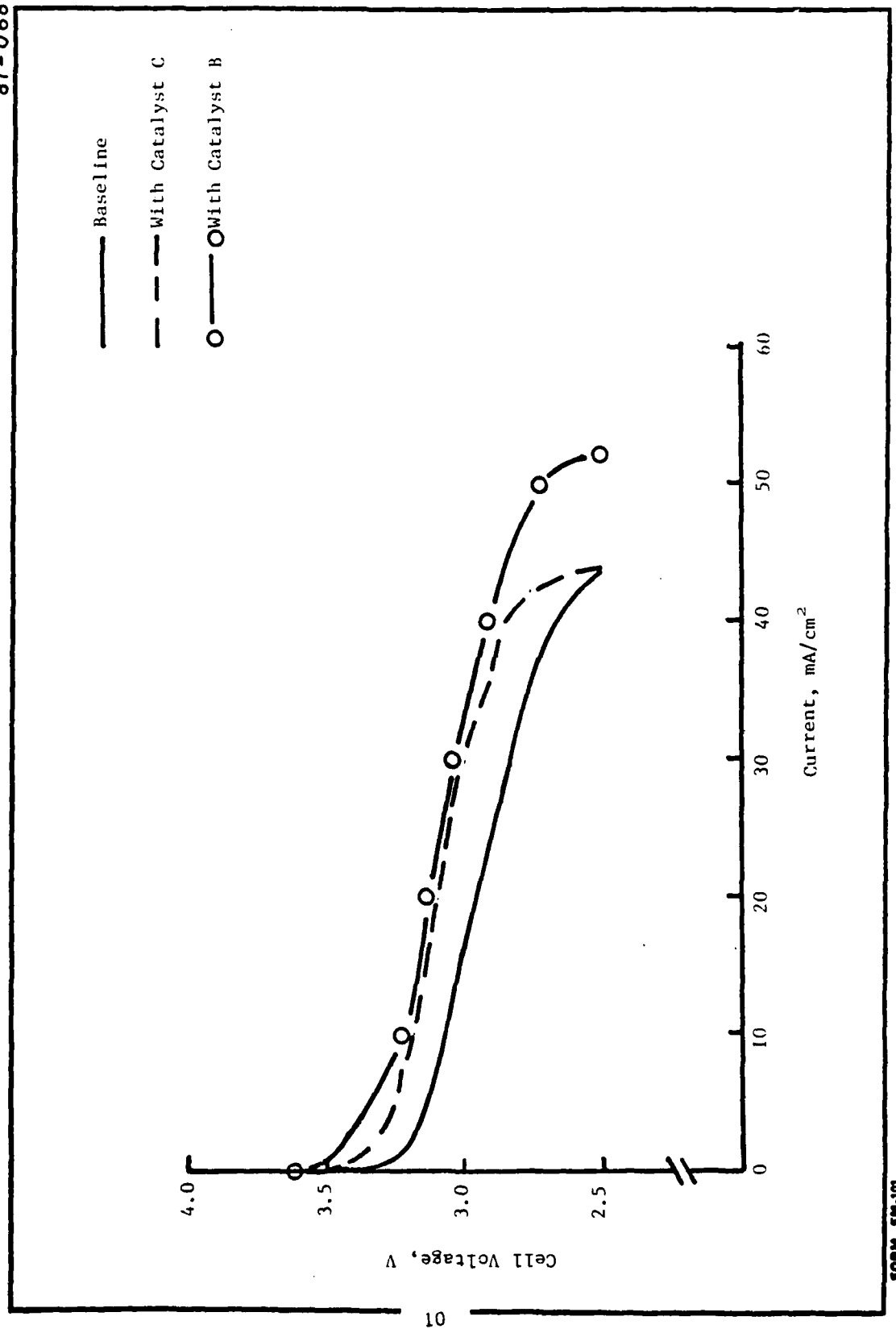


Figure 5. Polarization Characteristics of Li/SOCl_2 Laboratory Cells at 32°F .

FORM FM-101

81 - 071

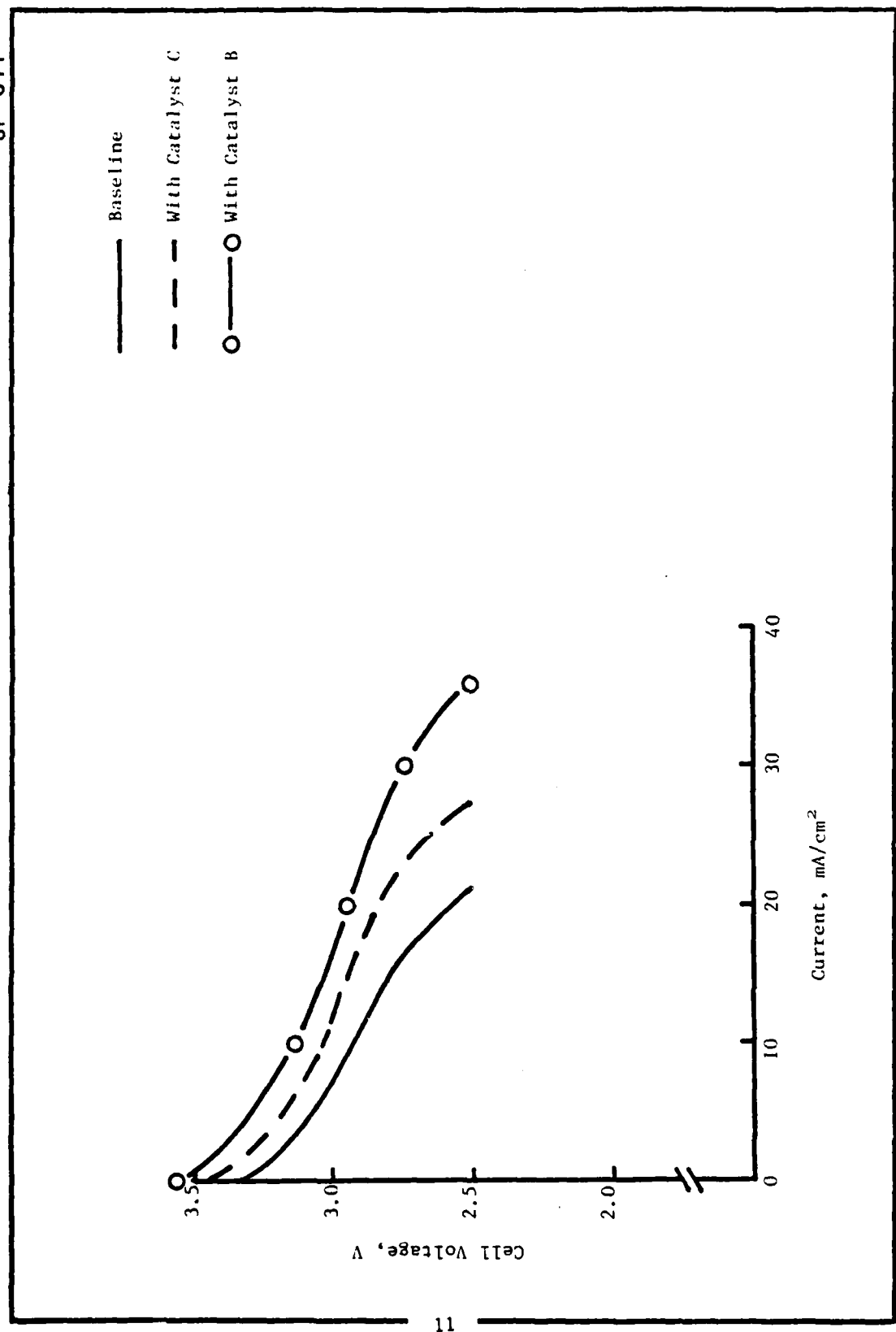


Figure 6. Polarization Characteristics of Li/SOCl_2 Cells at 0°F .

FORM FM-101

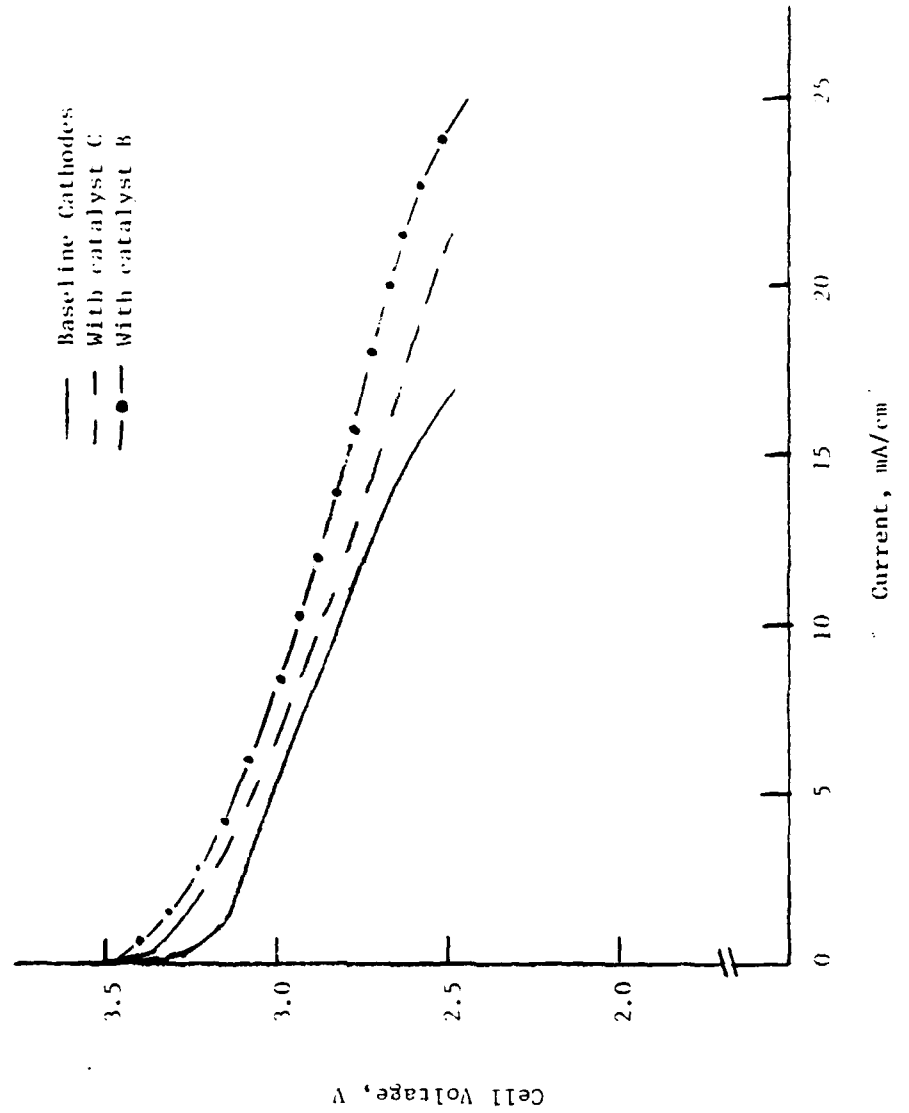


Figure 7. Polarization Characteristics of Li/SOCl₂ Cells at -20° F

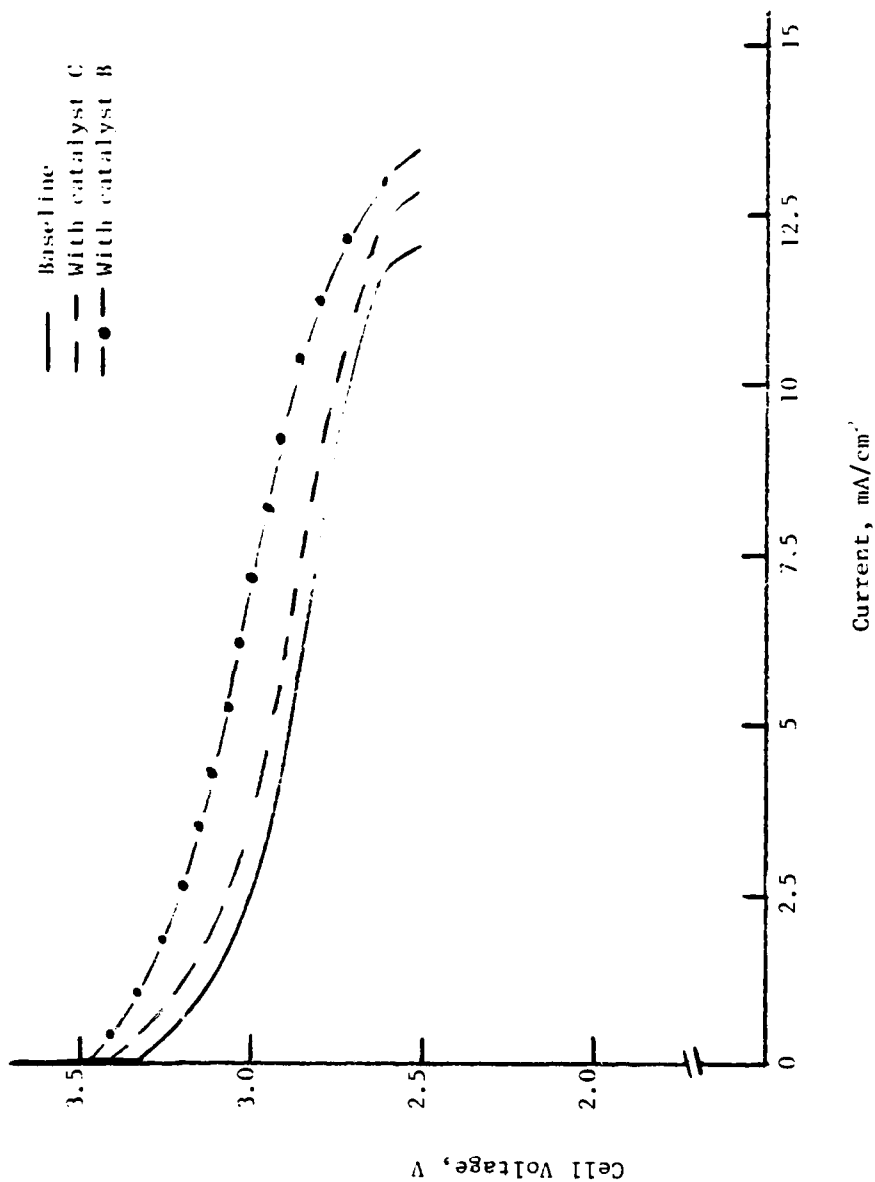


Figure 8. Polarization Characteristics of $\text{Li}/\text{SOCl}_2/\text{Cu11S}$ at -40°F

Electrode polarization, in general, becomes severe with the lowering of operating temperature. Furthermore, limiting current, hence rate capability, decreases with decreasing temperatures. A linear relationship between the limiting current and reciprocal temperature (Figure 9) exists for all three types of cathodes. An Arrhenius-type temperature dependence of limiting current are shown in Figure 10 for the three cathodes. At low temperature, the deviation from linearity is apparent and could be attributed to changes in electrolyte conductivity and viscosity, reaction mechanisms and mass transport rates. It should be noted that similar deviations are observed for Arrhenius-type temperature dependence of conductivity and viscosity.

At all operating temperatures, catalyzed cathodes exhibit higher limiting currents than baseline cathodes. The improvement is approximately 10% for $(CoPc)_n$ and 25% for FePc catalyzed cathodes. The higher limiting current can be used as an indication of modified cathode reaction mechanisms at catalyzed cathodes.

3. Discharge Performance

The objective of laboratory cell measurements was to evaluate the discharge performance characteristics of cathodes with and without catalysts between -40 and 75°F. These cathodes were discharged at rates of 10 and 20 mA/cm². All cells were discharged under constant current using a Hewlett-Packard DC current source #6181B. The data were collected with a Fluka 2240B datalogger. All experiments were duplicated and, in most cases, the results were reproducible.

Figures 11-14 show the discharge characteristics of laboratory cells at 20 mA/cm² on the three described cathodes at 75, 32, 0 and -20°F. Dramatic improvement, in both cell voltage and discharge time are observed with catalyzed cathodes, irrespective of the operating temperatures. The overall performance of Li/SOCl₂ cells with FePc catalyzed cathodes is superior to the cells with $(CoPc)_n$ doped cathodes.

At -40°F, however, none of the three electrodes sustained reasonable discharge times at 20 mA/cm². Therefore, these cells were discharged at 15 and 5 mA/cm² and their discharge characteristics are shown in Figures 15 and 16, respectively. To demonstrate the effect of temperature, additional discharge characteristics at 5 mA/cm² for -20°F is shown in Figure 17 and in Table 1 for 10 mA/cm².

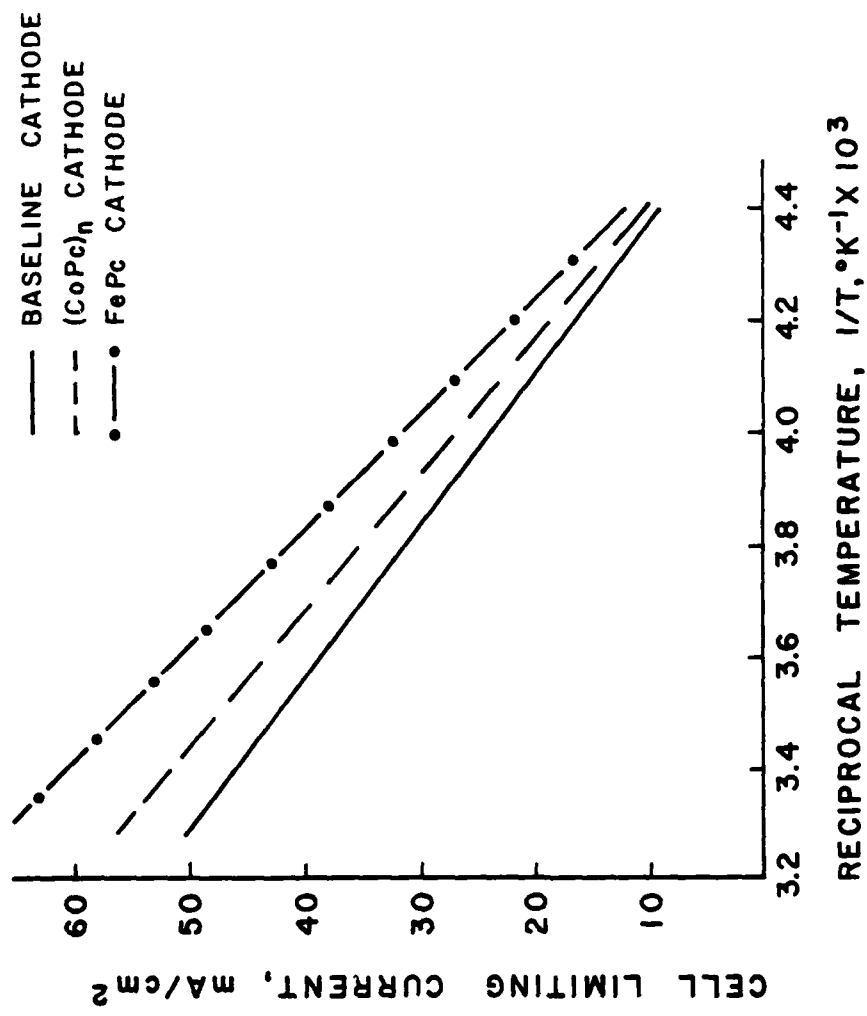


Figure 9. Effect of Operating Temperature on Laboratory Li/SOCl₂ Cell Limiting Current

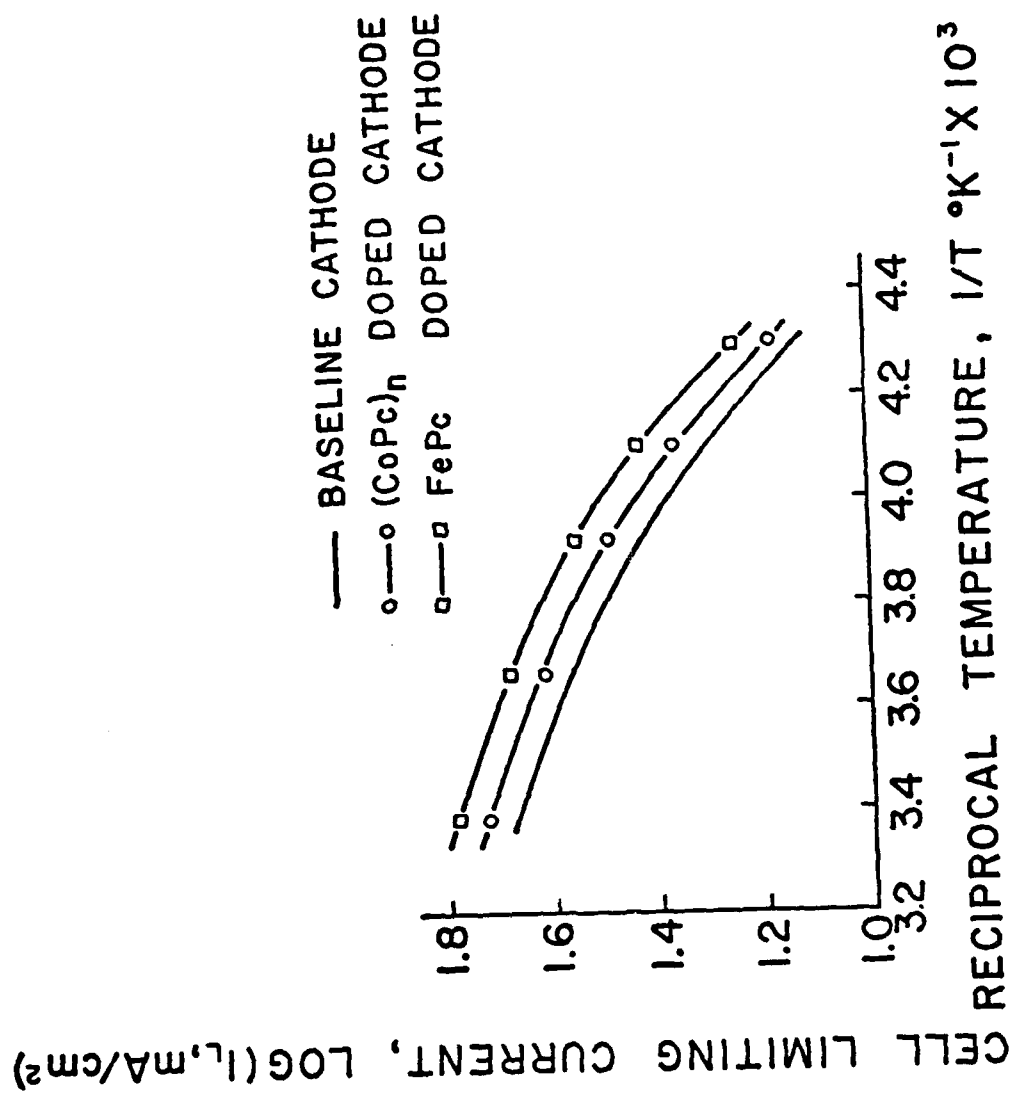


Figure 10. Effect of Operating Temperature on Cell Limiting Current Density

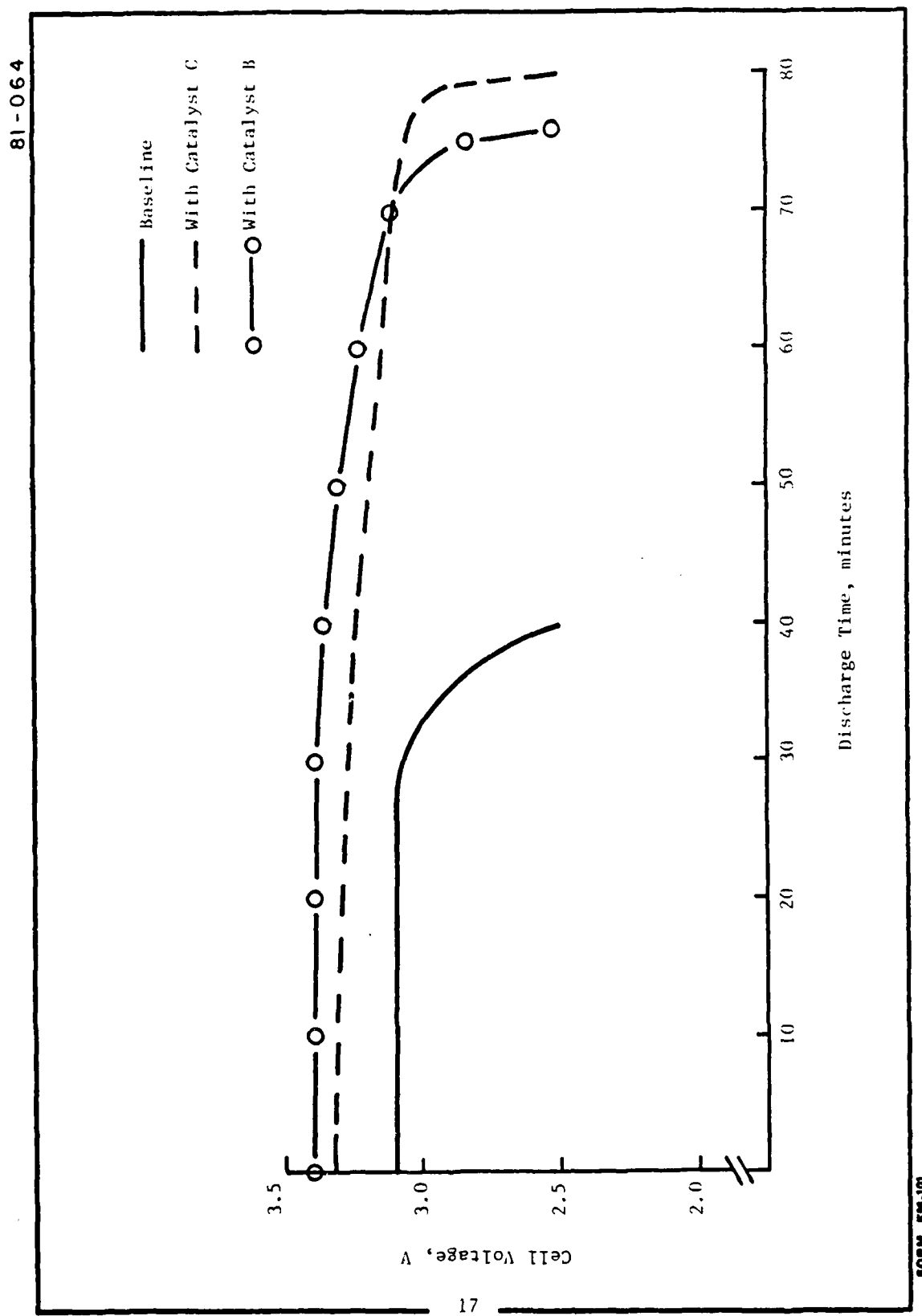
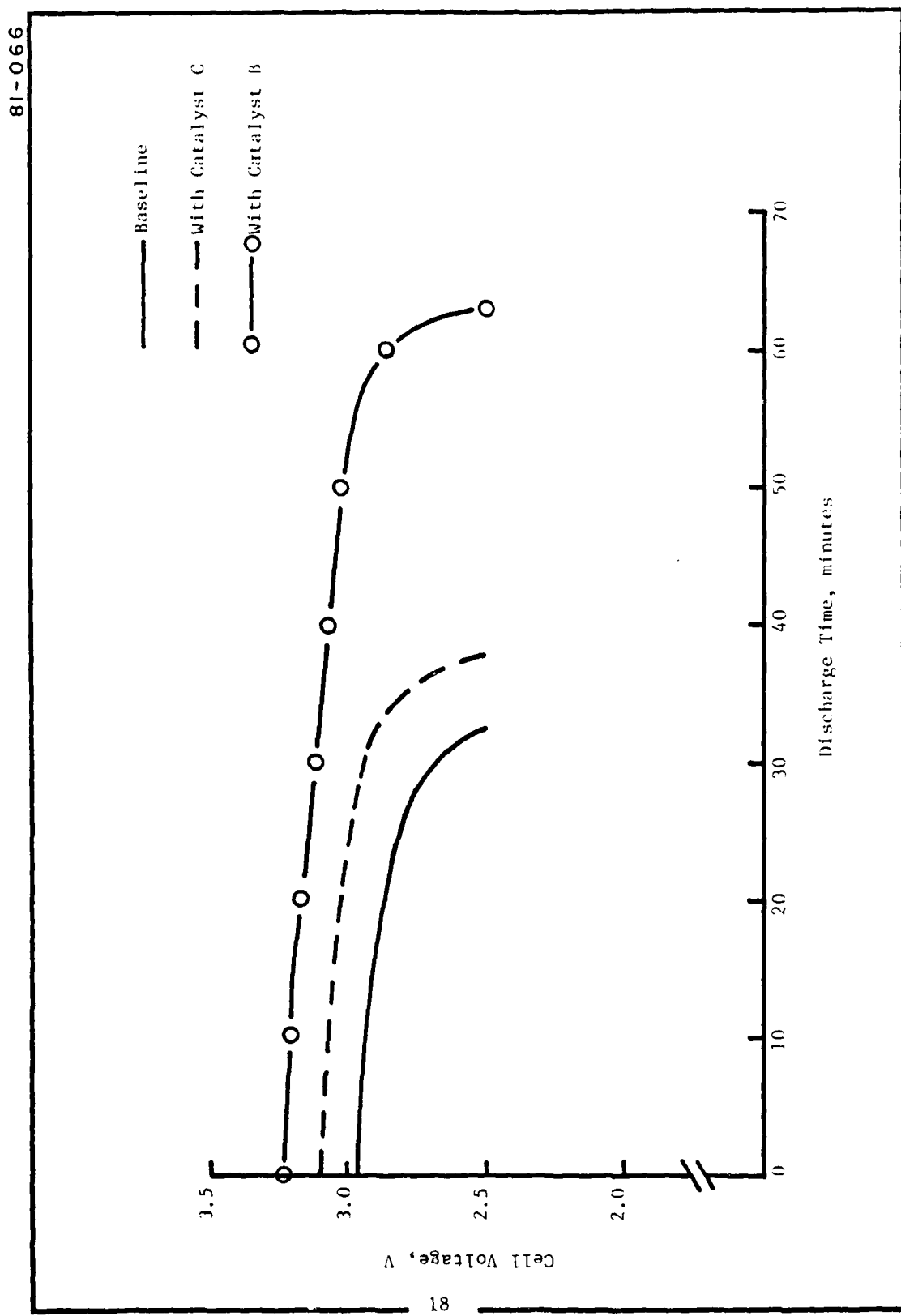


Figure 11. Discharge characteristics of Li/SOCl₂ laboratory cells at 20 mA/cm² and 75° F

Figure 12. Discharge characteristics of Li/SOCl₂ cells at 20 mA/cm² and 30° F.



81-070

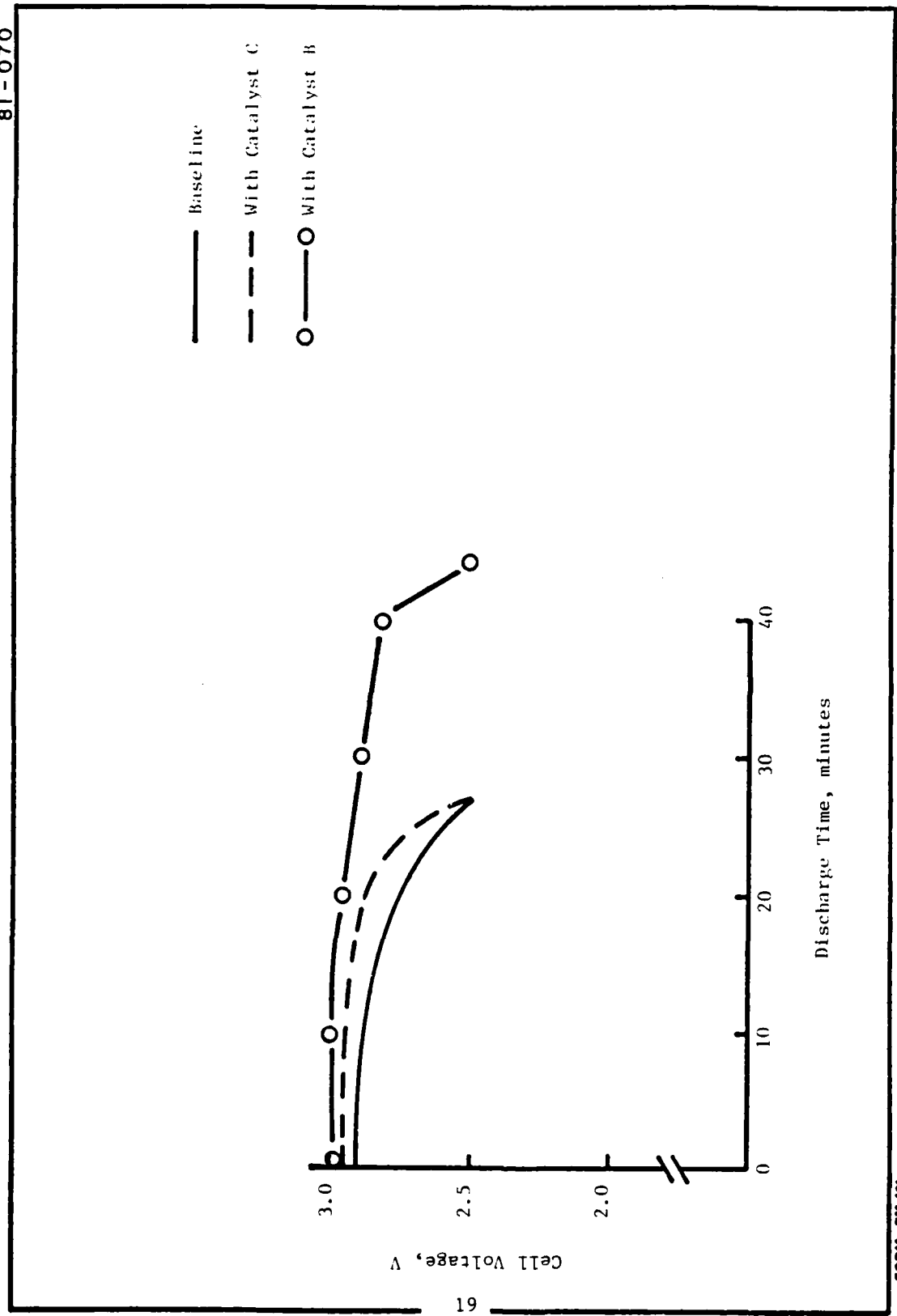


Figure 13. Discharge characteristics of Li/SOCl₂ laboratory cell, at 20 mA/cm² and 0°F.

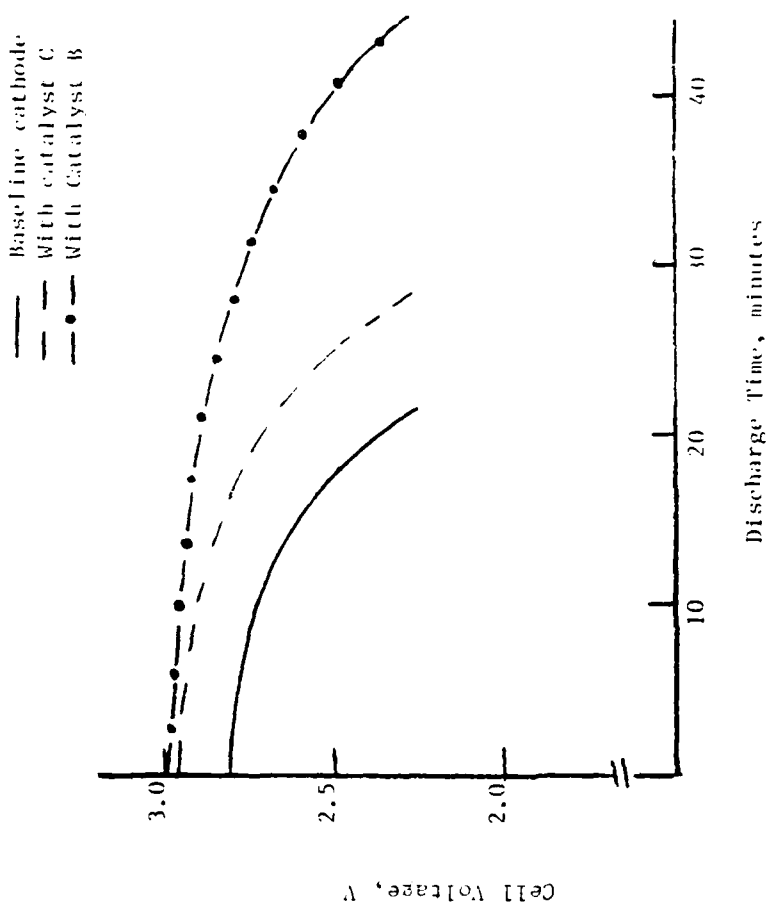


Figure 14. Discharge Characteristics of Li/SOCl₂ Cells at 20 mA/cm² and ~20°F.

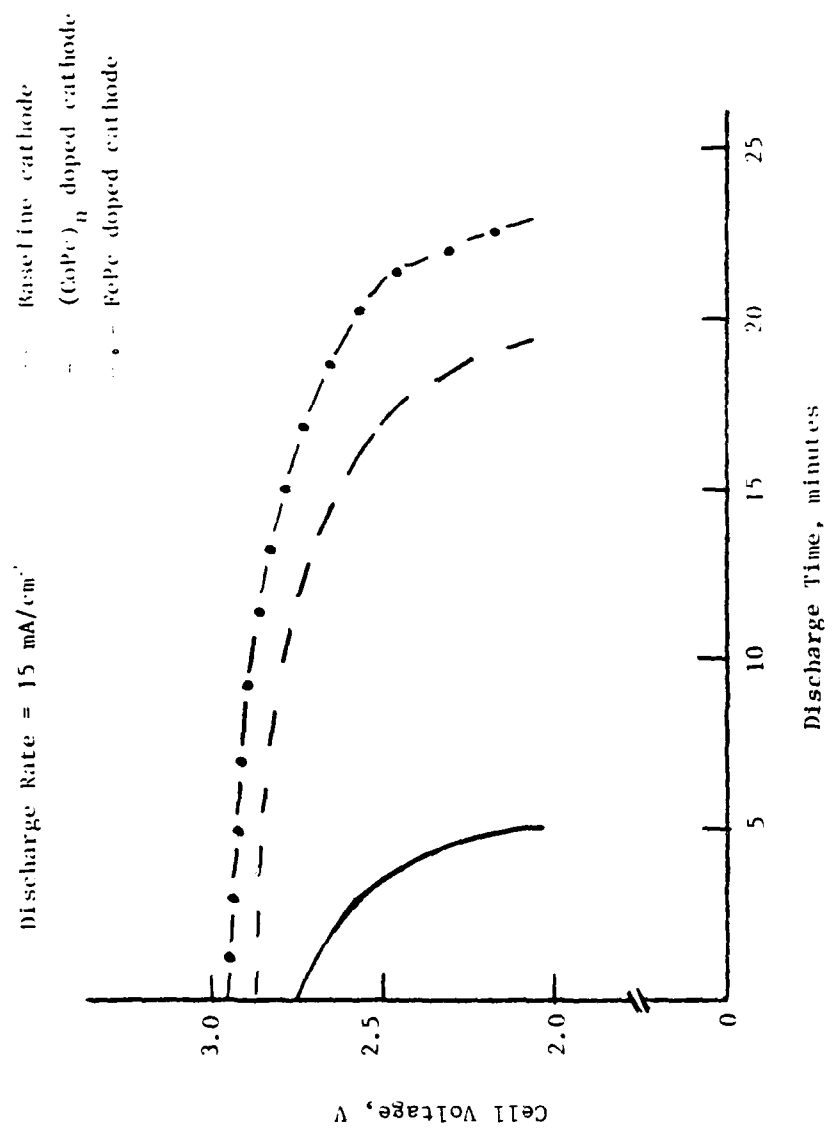


Figure 15. Discharge Characteristics of Laboratory Li/SOCl₂ Cells at 15 mA/cm² and -40°F.

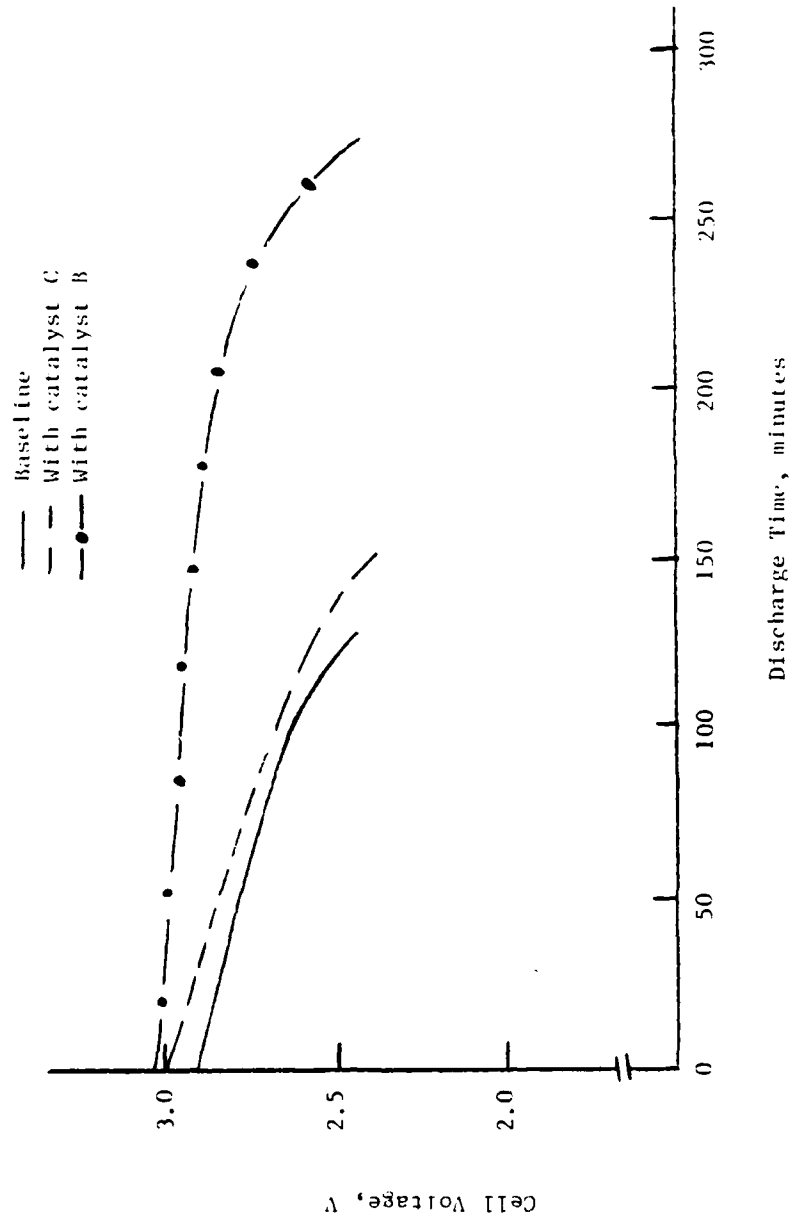


Figure 16. Discharge Characteristics of Li/SOCl_2 Cells at 5 mA/cm^2 and -40°F .

81-072

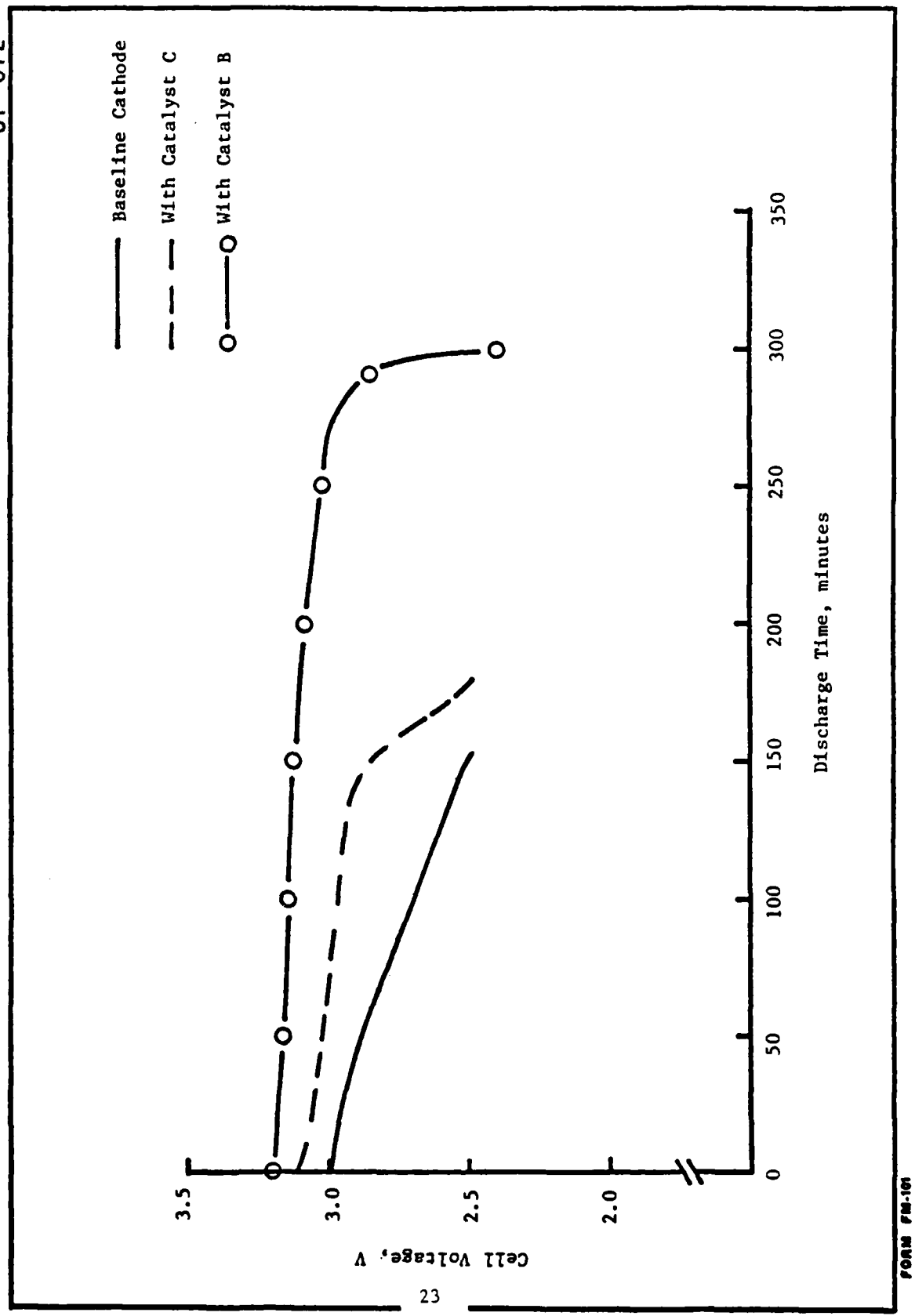


Figure 17. Discharge Characteristics of Li/SOCl_2 Laboratory Cells at 5 mA/cm^2 and -20°F

Table 1. Discharge Characteristics of Li/SOCl₂ Cells at 10 mA/cm²
in 1.5M LiAlCl₄/SOCl₂.

Temp., °F	Baseline Cathode			With Catalyst B			With Catalyst C		
	Avg. Cell Voltage, V.	Discharge Time, min.	Avg. Cell Voltage, V.	Discharge Time, min.	Avg. Cell Voltage, V.	Discharge Time, min.	Avg. Cell Voltage, V.	Discharge Time, min.	Avg. Cell Voltage, V.
75	3.11	125	3.41	162*	3.30	180			
32	3.01	85	3.20	135	3.12	105			
0	2.99	60	3.21	89	3.06	86			
-20	2.80	55	2.89	76	2.90	64			

* Low value is attributed to variation in cathode thickness and/or cell assembly technique.

With respect to cell voltage and specific cathode capacity, the attained improvements by catalyzed cathodes, over a wide range of discharge rates are demonstrated in Figures 18 and 19, respectively.

In summary, we believe that the longer discharge times achieved with catalyzed cathodes are attributed to changes in both reaction mechanisms and reaction zone thickness. Furthermore, the cell performance in general deteriorates with decreasing temperatures regardless of cathode types; i.e., catalyzed or not. Key factors causing this temperature effect are electrolyte conductivity and viscosity.

C. KINETIC AND MECHANISTIC STUDIES

1. Introduction

There is a considerable disagreement on the overall reaction mechanisms of SOCl_2 reduction at porous carbon cathode. Since both the reaction mechanism and reaction products contribute to the performance of a battery, it is desirable to understand these two important factors. For this program, some understanding of reaction mechanism(s) were obtained via cyclic voltammetry and rotating-disc electrode techniques.

2. Cyclic Voltammetric Studies

a. Experimental. Thionyl chloride from MCB was refluxed over lithium metal and distilled twice and the solvent was stored at 0°F . A conventional electrochemical cell with three electrodes was employed. Pressure annealed pyrolytic graphite ($A=0.178 \text{ cm}^2$), polycrystalline carbon ($A=0.178 \text{ cm}^2$), glassy carbon ($A=0.44 \text{ cm}^2$) and platinum ($A=0.178 \text{ cm}^2$) were used as working electrodes. The working electrodes were sealed in Teflon rods. At the end of each cyclic voltammogram, the electrodes were cleaned employing established techniques, to produce reproducible surfaces. The reference and counter electrodes were made freshly by pressing lithium foil onto nickel grids. Catalysts were added to electrolyte (1M $\text{LiAlCl}_4/\text{SOCl}_2$) before studies. The cyclic voltammetric studies were carried out in a dry room using Princeton Applied Research Model 170 Electrochemistry System.

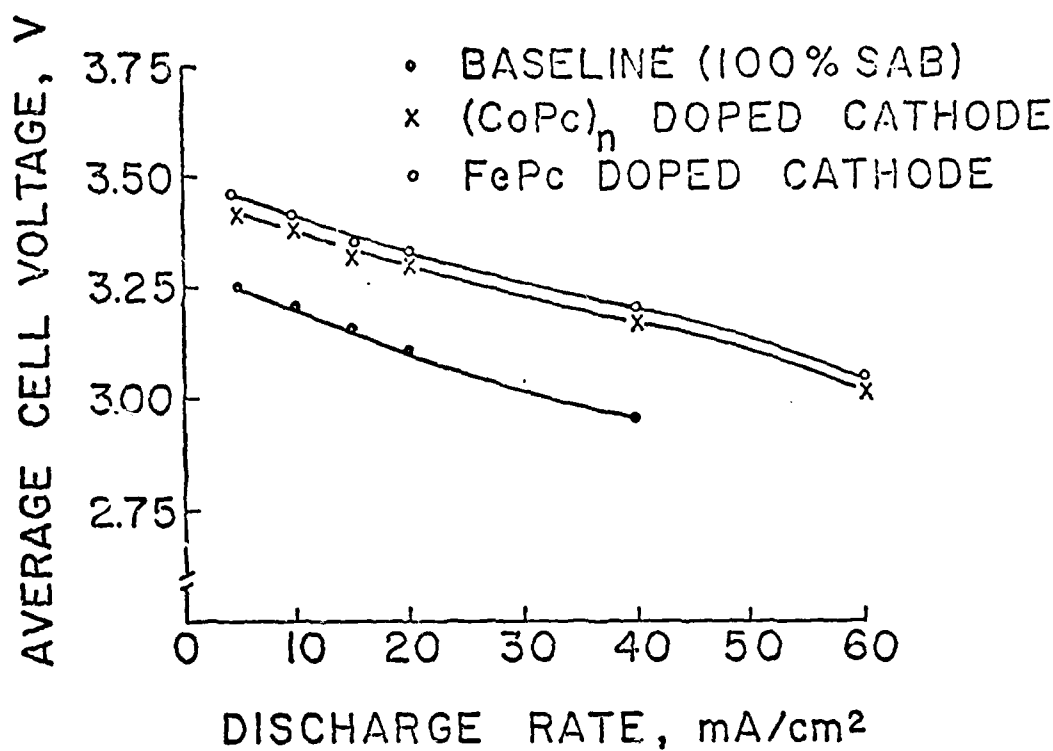


Figure 18. Average Discharge Voltage of Li/SOCl₂ Cells versus Discharge Rate at 72° F

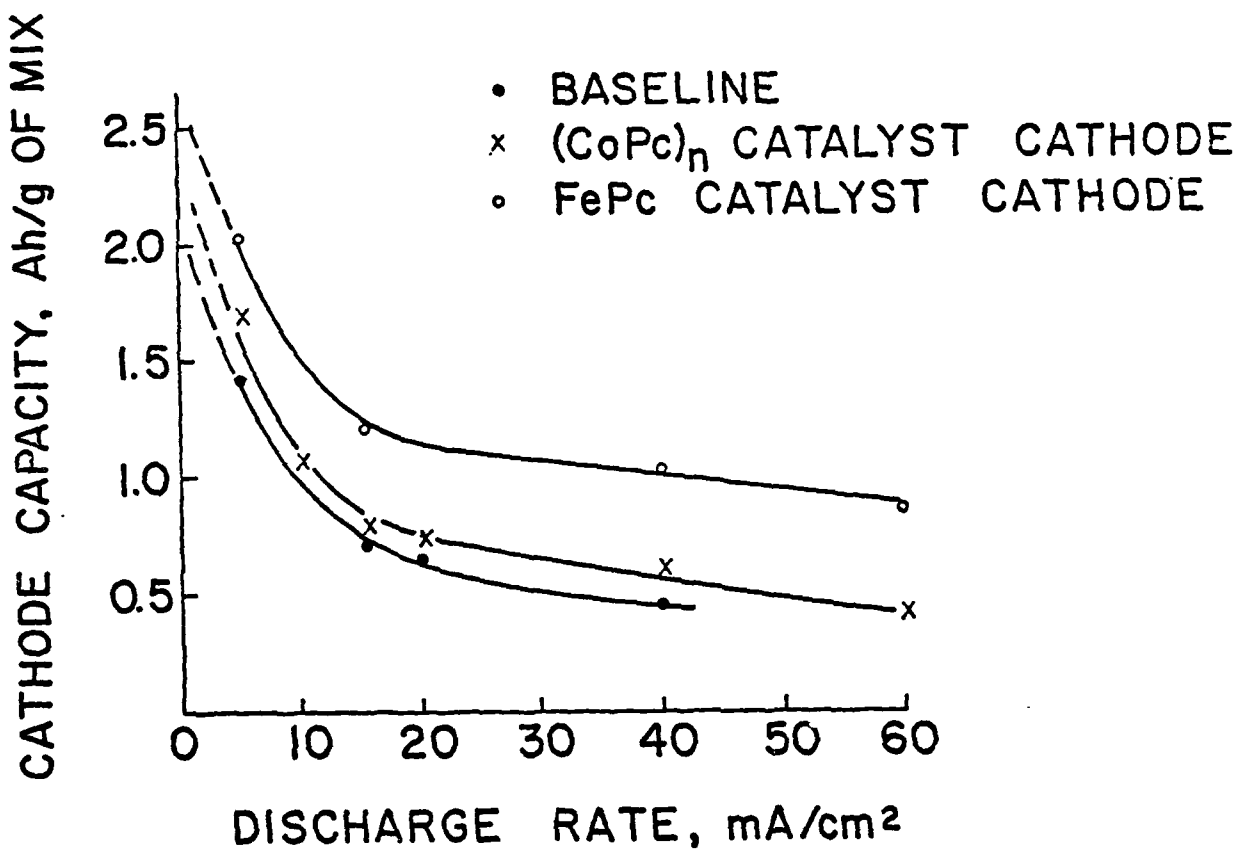


Figure 19. Discharge Performance of Li/SOCl₂ Cells with 1.5M LiAlCl₄/SOCl₂ at 23°C (2.5V Cutoff)

b. Effect of Catalyst. Cyclic voltammograms at a pressure annealed pyrolytic graphite electrode with and without electrocatalyst in 1.0M LiAlCl₄/SOCl₂ electrolyte are shown in Figure 20. At a fresh and dry electrode surface, SOCl₂ is reduced in two steps as evidenced by two reduction peaks in the cyclic voltammogram. At CoPc catalyzed cathode, the two peaks merge and shift toward more positive potential. Moreover, the peak height increases threefold. With metal-free phthalocyanine, the reduction peak does not shift even though the peak height increases. Furthermore, no other reduction or oxidation peaks are observed with catalyzed cathodes between 3.6 and 1 volt versus Li reference electrode. The simplified cyclic voltammograms could be due to electrode blocking by strongly adsorbed reduction products. Similar catalytic effect is achieved with FePc catalyst.

c. Effect of Sweep Rate. In Figure 21, the effect of sweep rate on cyclic voltammograms at pressure annealed pyrolytic graphite electrode in 1.0M LiAlCl₄/SOCl₂ electrolyte at 75°F is shown. Both peak height and position change with sweep rate as anticipated. Similar behavior is also observed with FePc catalyst. In both cases, a linear relation between peak height and square root of sweep rate is observed (Figure 22), thus indicative of a diffusion controlled system. Similar behavior is also observed at platinum electrode (Figure 23) and glassy carbon electrode (Figure 24).

d. Effect of Temperature. At low operating temperature, the electrolyte viscosity and conductivity strongly influence the peak positions. The change in peak height should indicate the extent of electrolyte influence on the rate capability of an electrode. In Figures 25 and 26, the effect of temperature on SOCl₂ reduction peak position and peak height in cyclic voltammograms at polycrystalline carbon electrodes in 1.0M LiAlCl₄/SOCl₂ containing with and without FePc catalyst are shown. In both cases, the reduction peak decreases with lowering of operating temperature. This decrease can be attributed directly to the electrolyte properties which influence the diffusion coefficients.

The reduction peak height with and without catalyst showed a linear relationship with reciprocal temperature. The energies of activation derived from Log i_p vs 1/T relationship (Figure 27), based on data shown in Figures 25 and 26, are 1.83 and 1.65 Kcals, respectively. Such small change in activation energies indicates

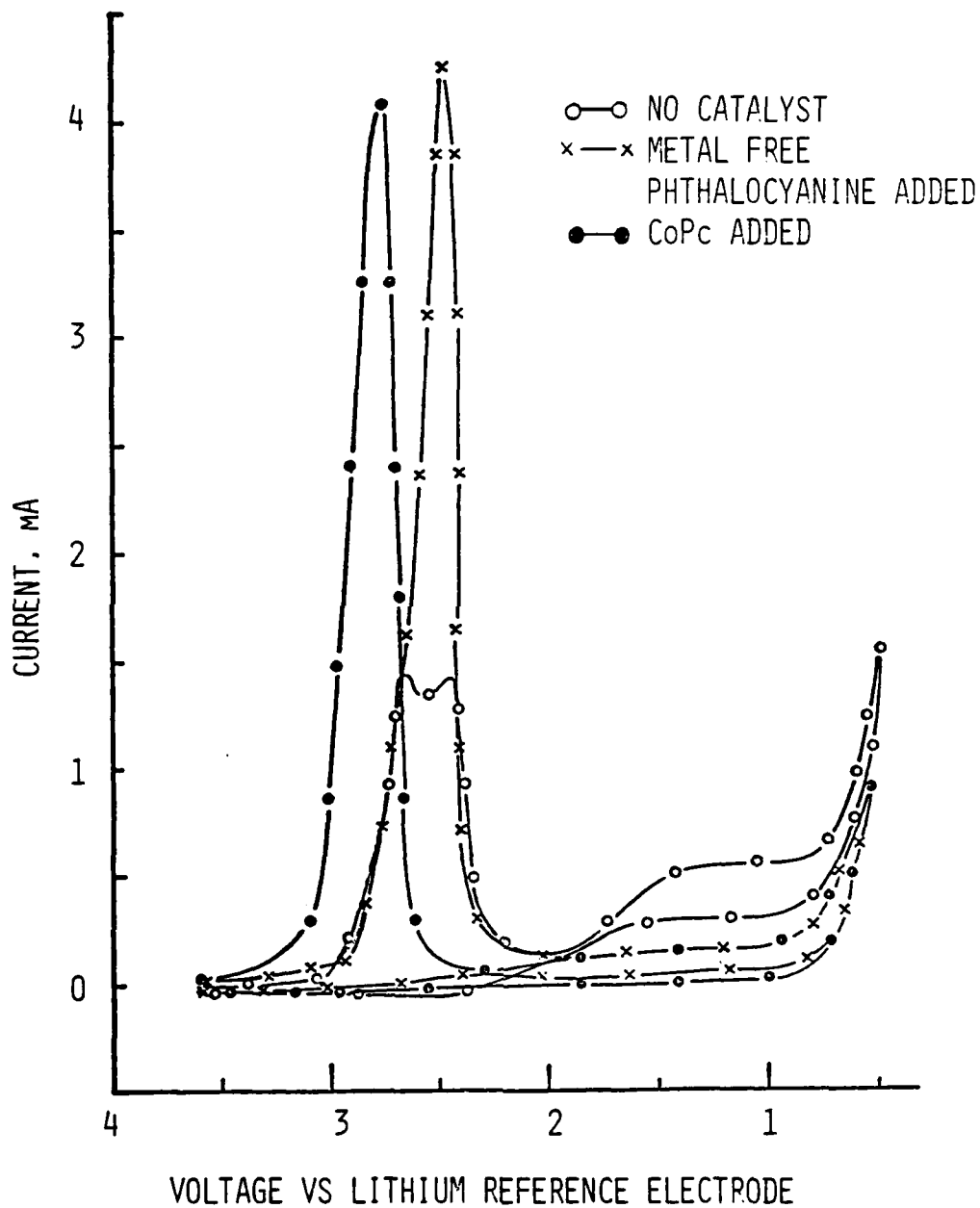


Figure 20. CYCLIC VOLTAMMOGRAMS AT PRESSURE ANNEALED PYROLYTIC GRAPHITE (0.178 cm^2) IN 1M $\text{LiAlCl}_4/\text{SOCl}_2$ ELECTROLYTE. SWEEP RATE 100 mv/sec.

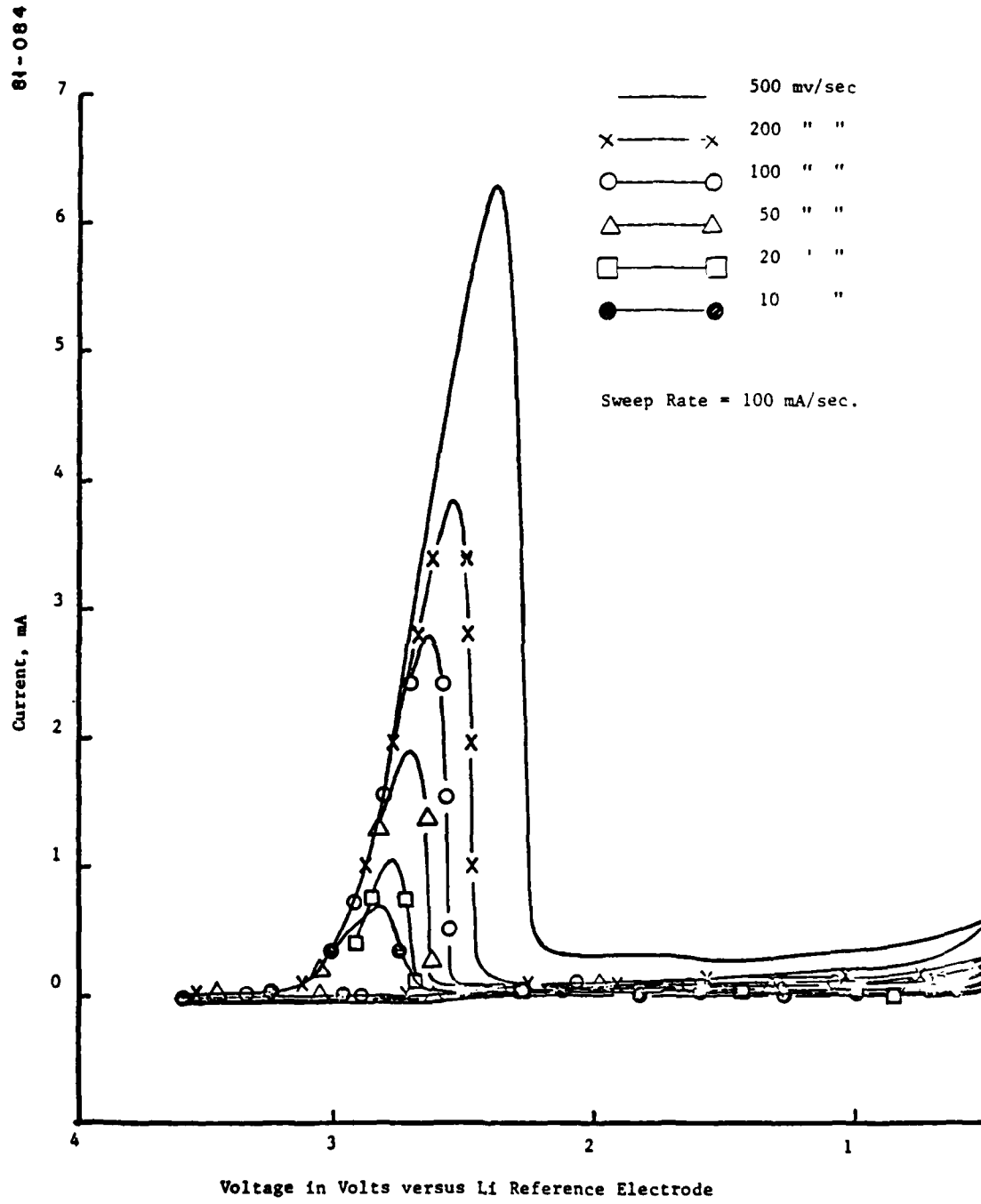
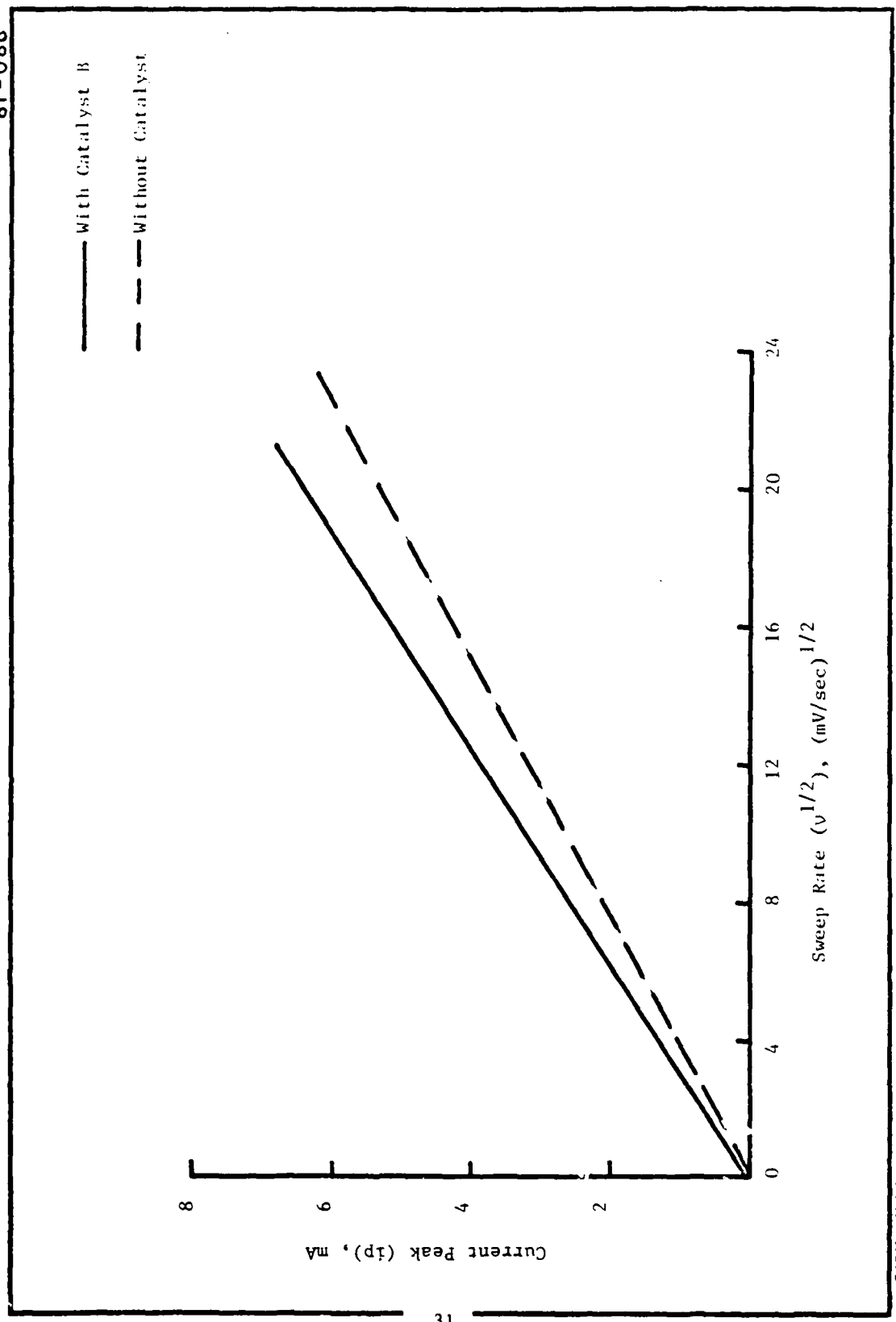


Figure 21. Effect of Sweep Rate on Cyclic Voltammograms at Pressure Annealed Pyrolytic Graphite Electrode ($A=0.178 \text{ cm}^2$) in 1.0M $\text{LiAlCl}_4/\text{SOCl}_2$ Electrolyte at 75°F .

81-086



FORM FM-10

Figure 22. Current Peak Bright (i_p) versus Square Root of Sweep Rate ($V^{1/2}$),
pressure Annealed Pyrolytic Graphite ($\Lambda=0.178 \text{ cm}^2$) in 1M LiAlCl₄/SOCl₂
at 750°C.

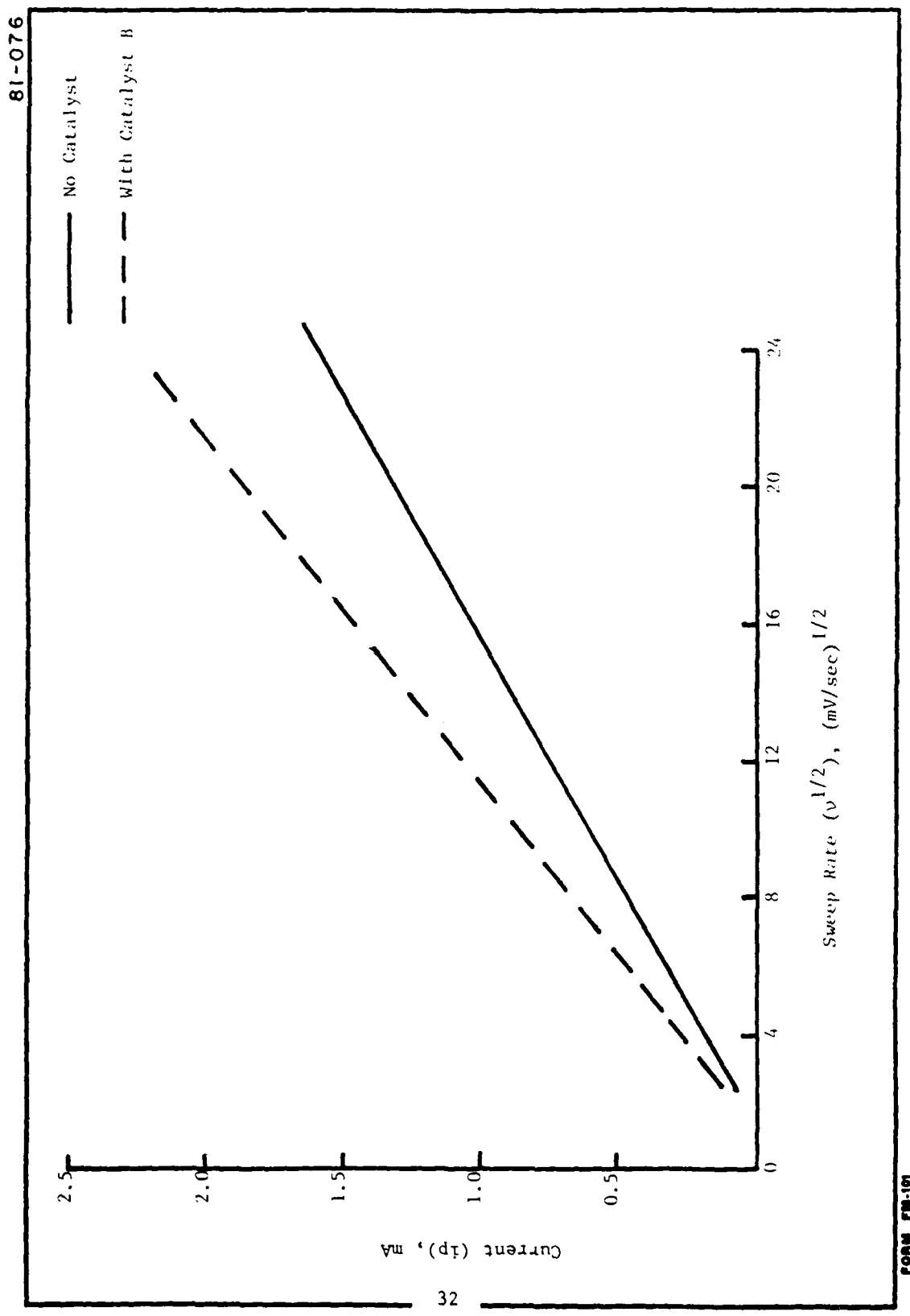


Figure 23. Current Peak Height (i_P) versus Square Root of Sweep Rate, Pt electrode ($\Lambda=0.175 \text{ cm}^2$) in 1M LiAlCl₄/CHCl₃, at Ambient Temperature.

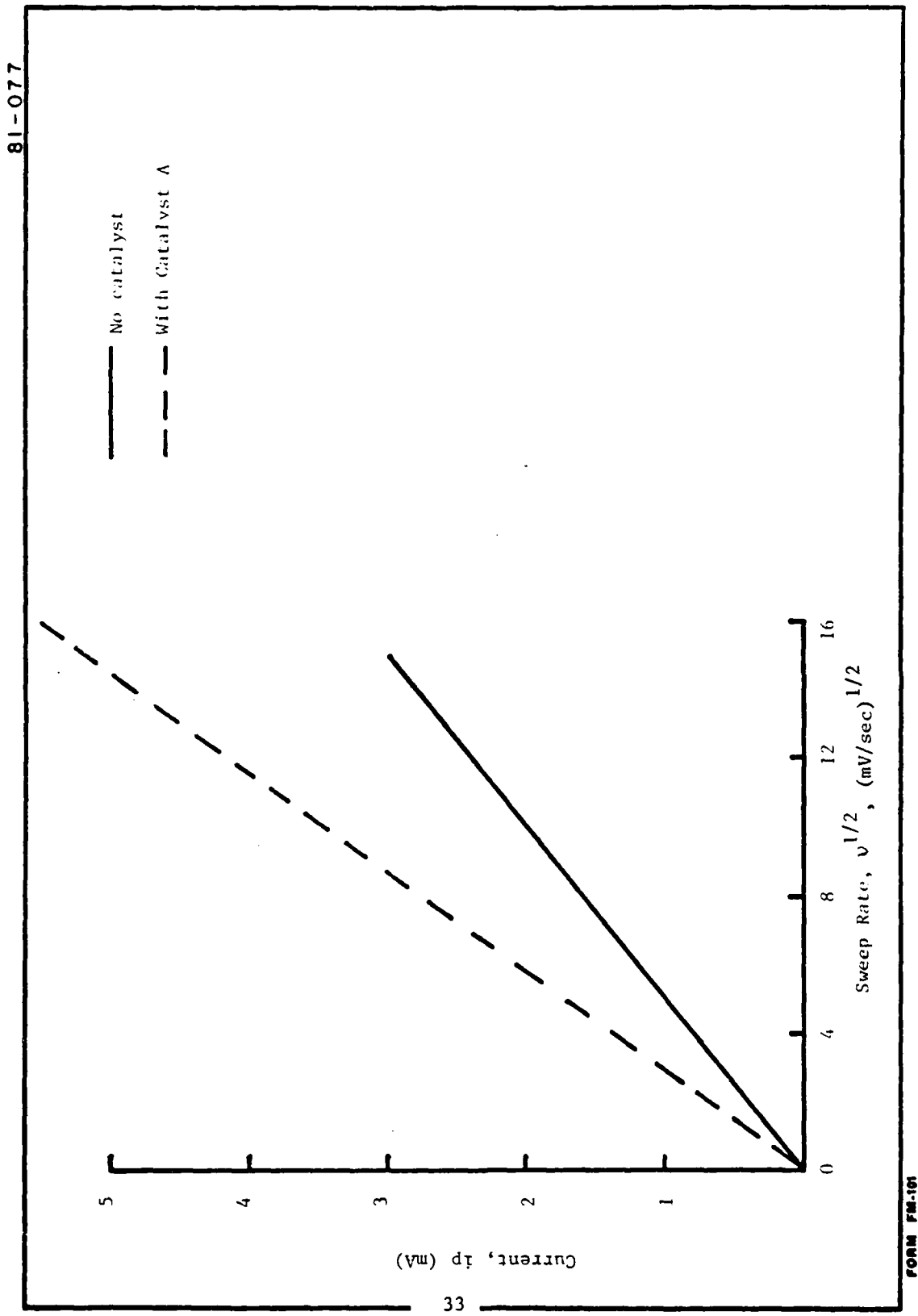


Figure 24. Current Peak Height (i_p) versus Square Root of Sweep Rate of Glassy Carbon Electrode (0.44 cm^2) in 1M LiAlCl₄/SOCl₂ at 30°F .

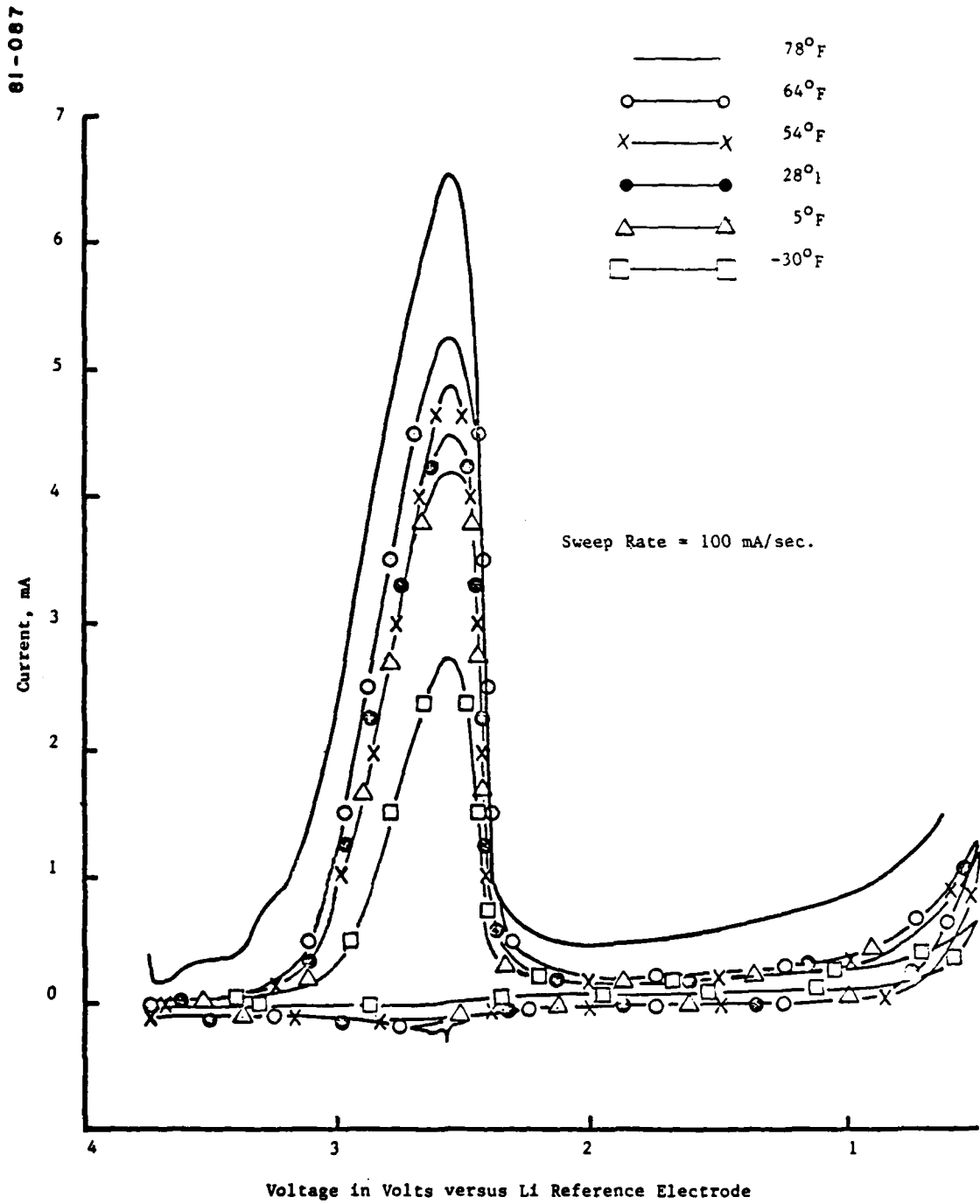


Figure 25. Effect of Temperature on Cyclic Voltammograms at Polycrystalline Carbon Electrode in 1.0M LiAlCl₄/SOCl₂ Electrolyte Containing FePc Catalyst.

81-083

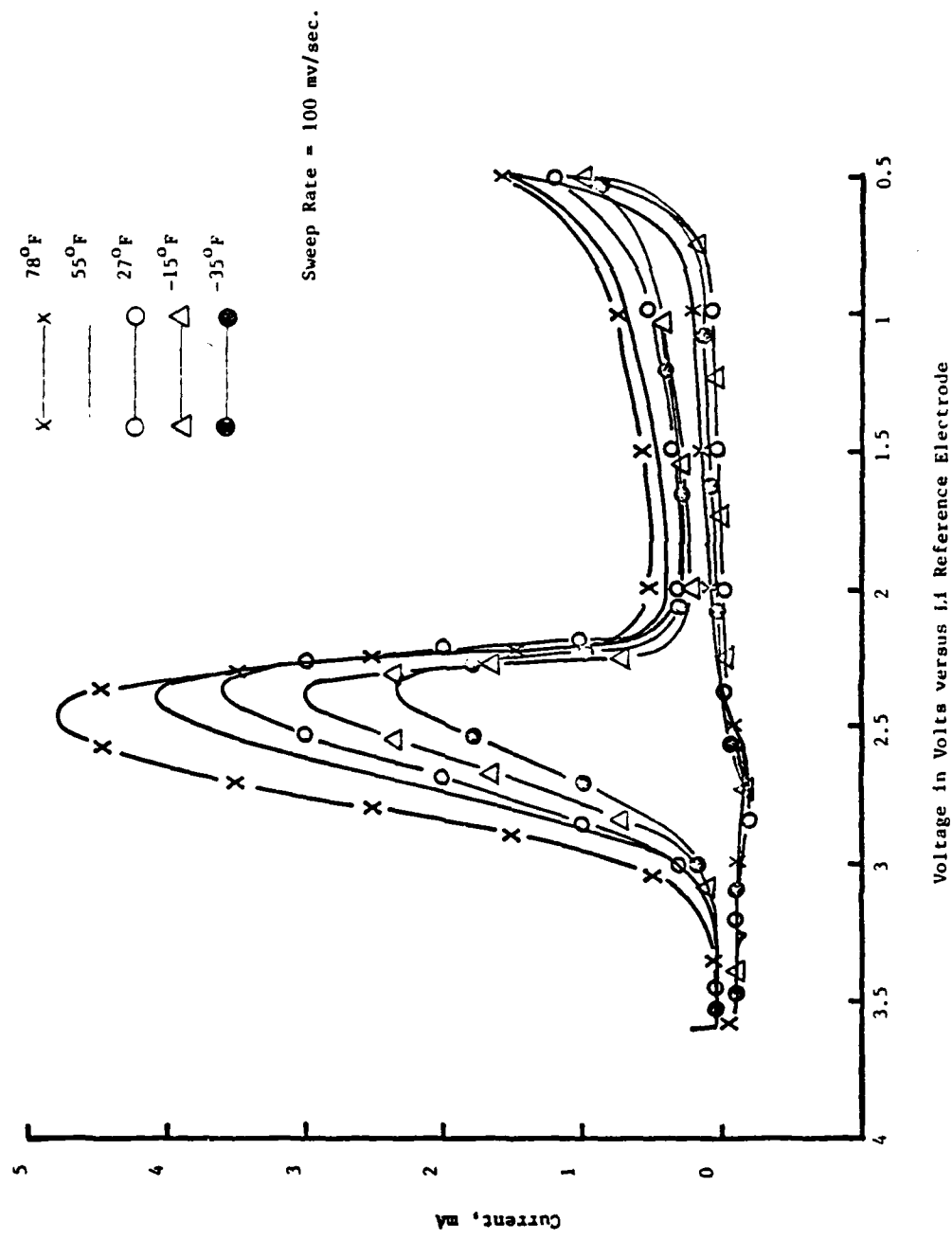


Figure 26. Effect of Temperature on Cyclic Voltammograms at Polycrystalline Carbon Electrode ($A=0.178 \text{ cm}^2$) in 1.0M $\text{LiAlCl}_4/\text{SOCl}_2$ Electrolyte.

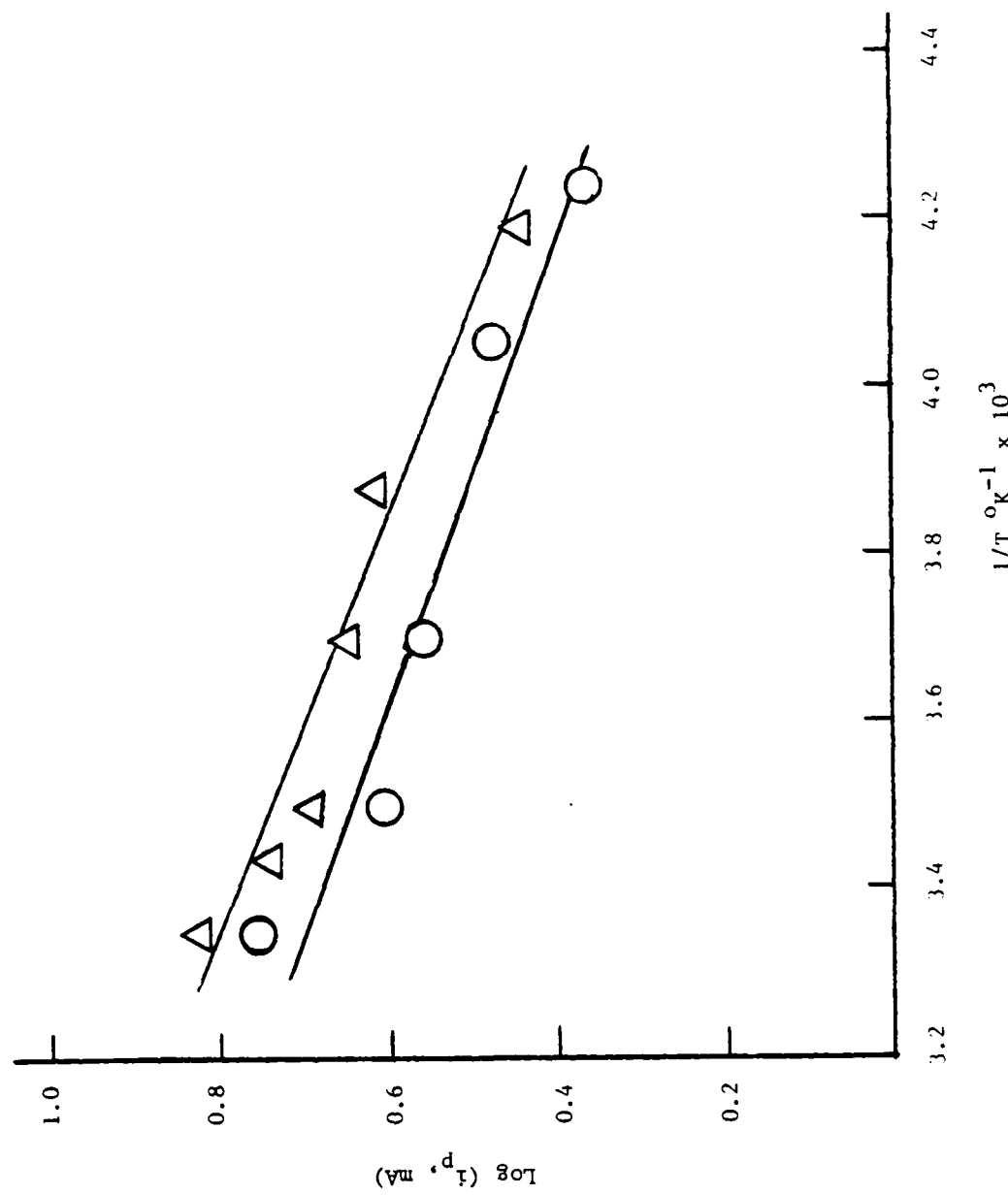


Figure 27. Arrhenius-type Temperature Dependence of Current Peak Heights

that the cathode performance is strongly influenced by electrolyte properties. The peak shift toward more negative potential with decrease in temperature is observed only with baseline cathodes. No such shift is found with catalyzed cathodes. This could be due to changes in activation polarization of uncatalyzed cathodes.

3. Rotating-Disc Electrode Studies

a. Experimental. Cyclic voltammetric studies in 1.5M LiAlCl₄/SOCl₂ solutions at various cathode surfaces indicated that the system is diffusion controlled. However, it should be noted that the reaction products which are strongly adsorbed on the cathodes, and the diffusion limitations, might have contributed to the current peak heights in cyclic voltammograms. Therefore, studies were carried out at a rotating-disc electrode.

Cyclic voltammograms were obtained at a glassy carbon electrode (0.458 cm²). An ASR rotator, manufactured by Pine Instrument Company, was used to rotate the disc electrode. Cyclic voltammograms were generated using PAR electrochemistry system Model 170.

As a first order reaction mechanism, the experimental currents in a rotating disc study are related to the rotation rate ω (in rpm) by the equation

$$\frac{1}{i} = \frac{1}{i_k} + \frac{1}{B\sqrt{\omega}} \quad (2)$$

where i_k is the kinetic current and B is a constant:

$$B = \frac{\sqrt{2\pi}}{60} n \cdot F v^{1/2} c_0 \left[0.621 s^{-2/3} (1 + 0.298 s^{-1/3} + 0.145 s^{-2/3}) \right] \quad (3)$$

where v = Kinematic viscosity

F = The Faraday constant

n = The number of electrons per mole of electroactive species
(SOCl₂ in our case)

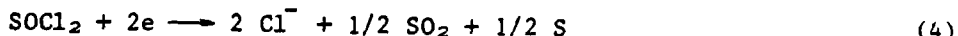
c_0 = The concentration of SOCl₂ in moles/cm³

s = v/D , where D = diffusion coefficient

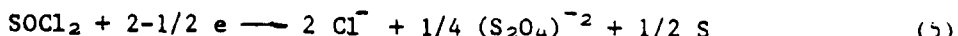
b. Effect of Electrode Rotation. Figure 28 shows the plots of i_p^{-1} vs $\omega^{-1/2}$ from the rotating disc data for SOCl_2 reduction at glassy carbon electrode (0.458 cm^2) in $1.5\text{M LiAlCl}_4/\text{SOCl}_2$ with and without FePc catalyst. At limiting currents; i.e., peak heights (i_p), the currents usually correspond to pure diffusion control for the SOCl_2 reduction. However, the plots indicate that the kinetic currents (intercepts) contribute to the limiting currents at 100 mv/second scan rate. Furthermore, in the presence of FePc catalyst, the kinetic current contribution to the limiting currents increases by 2.5 times (from 25.24 mA/cm^2 to 63.1 mA/cm^2). The i_k values decrease with decreasing scan rate in both cases. The i_p^{-1} vs $\omega^{-1/2}$ plots from the rotating disc data obtained at different scan rates in FePc added to $1.5\text{M LiAlCl}_4/\text{SOCl}_2$ electrolyte show (Figure 29) decreased kinetic currents with decreasing scan rate.

From the slopes of the straight lines in Figure 28, the B value can be calculated. For a similar reaction mechanism, the slopes should be equal as the changes in the values of parameter in equation 2 are minimal with the addition of FePc catalyst to the electrolyte. However, in the presence of FePc catalyst, the B value increases from 0.467 to 0.633. This increase could be attributed to the modification in the overall reaction mechanism as follows:

At baseline cathode:



At FePc catalyzed cathode:



The diffusion coefficient of SOCl_2 , calculated from the above B values, is $1.8 \times 10^{-5} \text{ cm}^2 \cdot \text{sec}^{-1}$. The effect of passive film in the cathode on diffusion rate is considered to be minimal under experimental conditions.

Plots of i^{-1} vs $\omega^{-1/2}$ yield parallel straight lines at potentials anodic to the peak-height (Figure 30), indicative of a first order process on SOCl_2 . Deviation from parallel straight lines at more anodic potential could be due to changes in the reaction mechanisms.

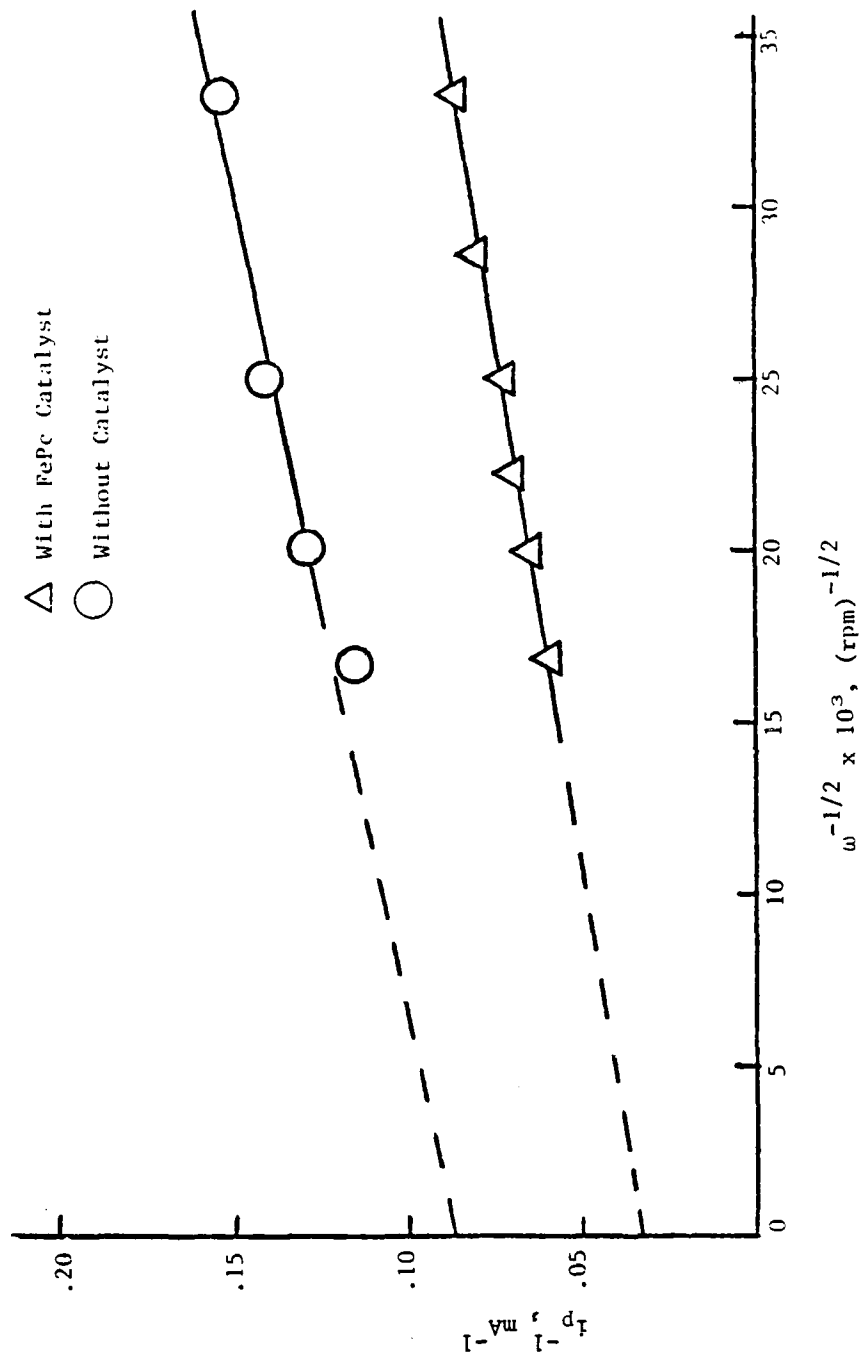


Figure 28. Plot of $1/i$ VS $1/\sqrt{\omega}$ From the Rotating Disk Data for Glassy Carbon
 Electrode (0.458 cm^2) in 1.5M LiAlCl₄/SOCl₂ at Room Temperature,
 (Scan Rate 100 mV/second)

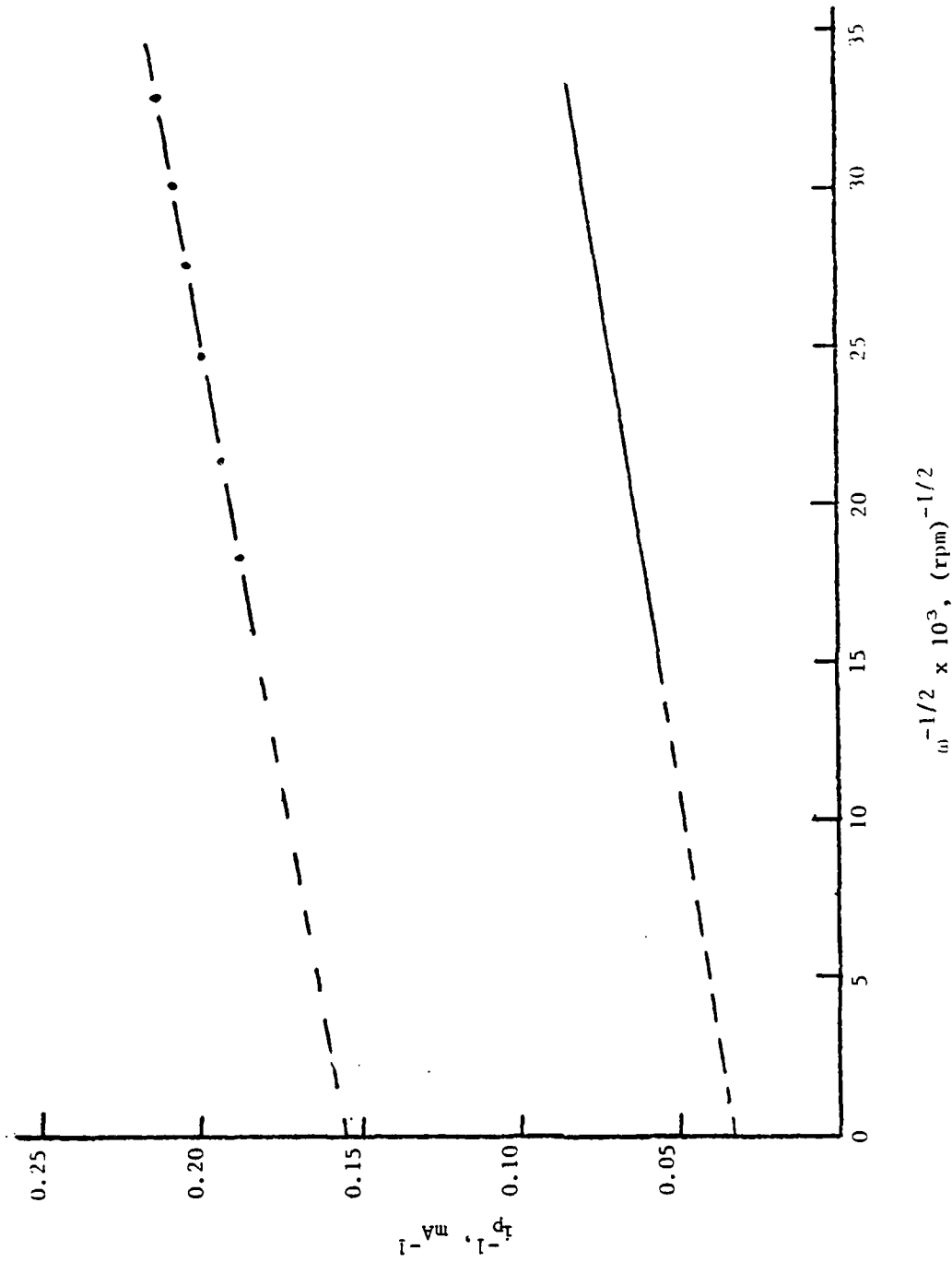


Figure 29. Plots of $i_{\bar{A}}^{-1}$ vs $\omega^{-1/2}$ from the Rotating Disc Data for Glassy Carbon Electrode (0.458 cm²) in 1.5M LiAlCl₄/FePc at different Scan Rates (--- 100 mV/seconds, -·- 1 mV/seconds)

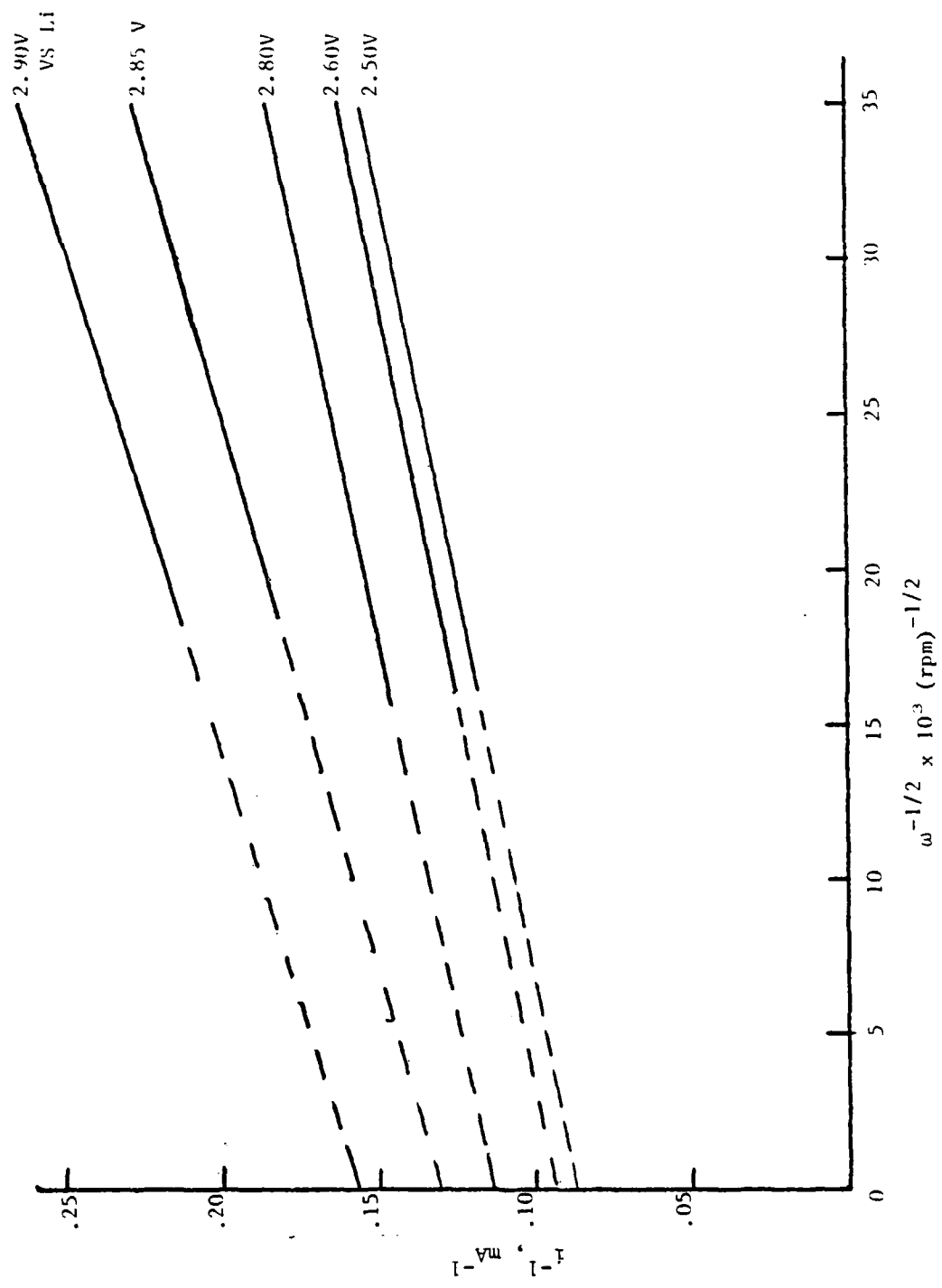


Figure 30. Plot of i^{-1} vs $\omega^{-1/2}$ at different Potentials From the Rotating Disc Data for Glassy Carbon Electrode (0.458 cm²) in $1.5\text{M LiAlCl}_4/\text{SOCl}_2$ at RT.

At 0°F, the peak heights decrease drastically at catalyzed and uncatalyzed electrodes. In Figure 31, the plots of i_p^{-1} vs $\omega^{-1/2}$ at low sweep rates yield straight lines. The kinetic current contribution becomes predominant at 0°F even though it decreases with lowering the sweep rate. Further studies are needed to fully understand the mechanisms.

D. IMPEDANCE MEASUREMENTS

1. Introduction

Determination of cell internal resistance and charge transfer resistance is essential in determining the sources of electrode overpotential. Since both the electrolyte physical properties and cathode structure and its reaction kinetics contribute to the polarization, we evaluated both these important factors. The effect of temperatures on the electrolyte conductivity and viscosity, and the AC impedance of measurements at carbon surface were evaluated.

Our starting electrolyte for this program was 1.5M LiAlCl₄/SOCl₂. Improvements to achieve higher conductivity and lower viscosity were needed for better mass transport properties at low operating temperatures. Therefore, conductivity and viscosity measurements between -40°F and 77°F were made for both 1.0M and 1.5M LiAlCl₄/SOCl₂ so as to compare these variables on the electrolyte composition.

2. Electrolyte Physical Properties

a. Conductivity. Conductivity measurements were made employing a General Radio Impedance Comparator Bridge and Jones-type conductivity cell having bright platinum electrodes. The electrodes were cleaned with chromic acid cleaning solution, washed thoroughly with distilled water and finally dried before each experiment. The cells were calibrated at 25°C with KCl solutions, and were used to duplicate experiments. The cell constants were 114.63 and 130.50 cm⁻¹.

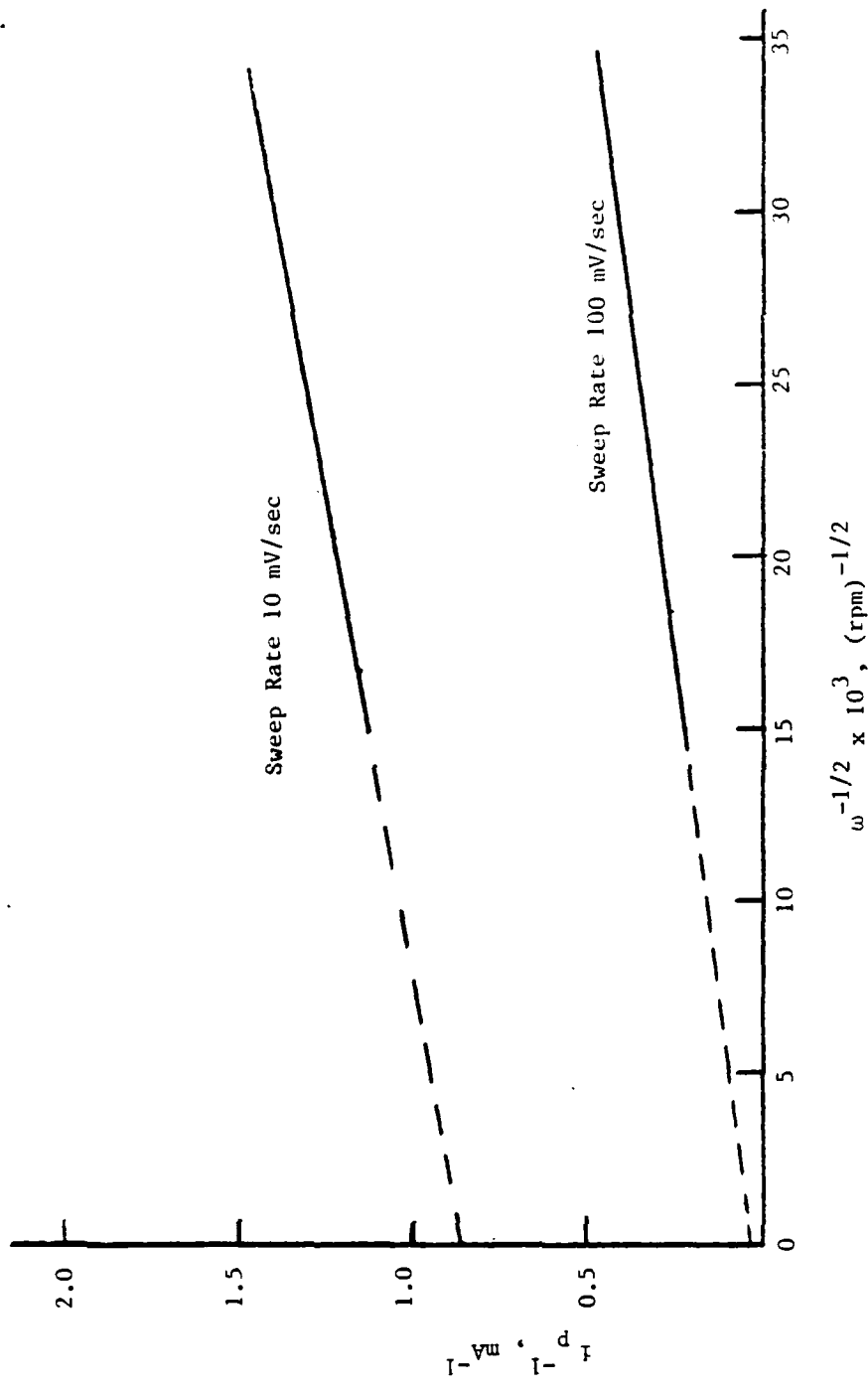


Figure 31. Plot of $1/h^0$ vs $\omega^{-1/2}$ from the relative disc data for glassy carbon Electrode (0.458 cm^2) in $1.5M \text{ LiAlCl}_4/\text{SOCl}_2$ at 0°F .

Resistance, R measurements of the electrolyte solutions were made at 10 KHz over the temperature range. From the resistance value, the specific conductance, L_s in $\text{ohm}^{-1} \text{ cm}^{-1}$, was calculated from the standard equation:

$$L_s = \frac{L}{AR}$$

where,

L = Electrode separation

A = Electrode area, cm^2

The temperature dependence of specific conductance of electrolyte is shown in Figure 32. The conductivity of 1.5M LiAlCl₄/SOCl₂ is higher than that of 1.0M LiAlCl₄/SOCl₂. Furthermore, addition of catalyst decreases the conductivity slightly throughout the temperature range studied.

b. Viscosity. Viscosity measurements were made employing Cannon-Zhukov capillary type viscometers calibrated with deionized water at 25°C. Measurements between -40°F and 77°F were carried out in a Conrad/Missimer environmental chamber. The temperatures were read with a Doric thermocouple temperature indicator. Viscometer flow times were measured with a Precision Scientific Timer giving readings to 0.1 second.

The viscosity versus temperature data are plotted in Figure 33. An Arrhenius temperature dependency of viscosity is observed except at low temperature. The increase in viscosity with decrease in temperature is much more severe with 1.5M LiAlCl₄/SOCl₂ than with 1.0M LiAlCl₄/SOCl₂. Such an effect influences the conductivity as observed in Figure 32.

81-078

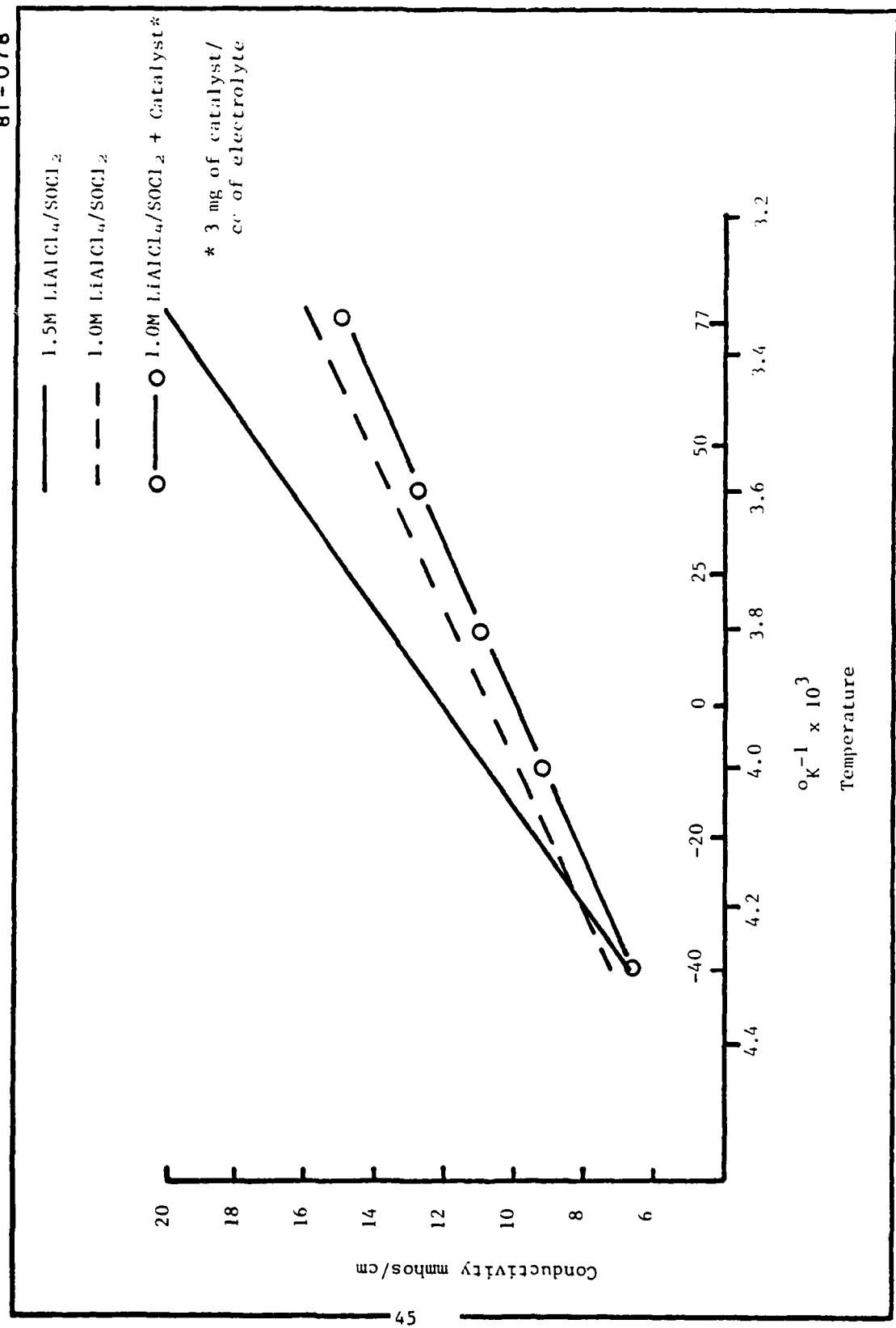
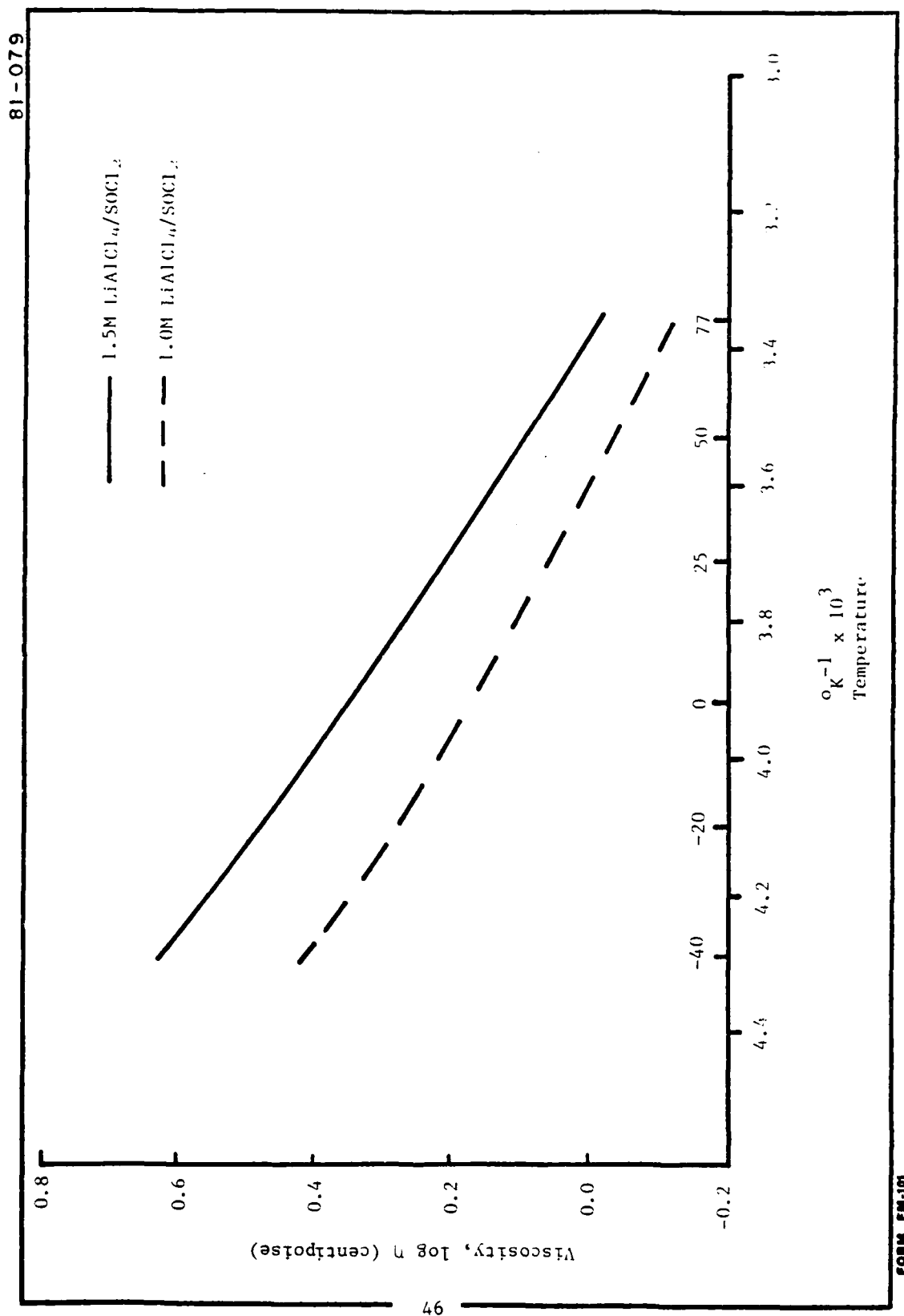


Figure 32. Effect of Temperature on the Conductivity of LiAlCl₄/SOCl₂ Electrolyte.

Figure 33. Effect of Temperature on LiAlCl₄/SOCl₂ Electrolyte Viscosity.



3. AC Impedance Measurements

a. Introduction. Physical and chemical processes taking place at the electrode interface influence the overpotential of an electrode system. Three types of processes described in Section II-A contribute to the total electrode overpotential in Li/SOCl₂ system.

Two non-steady state measurement techniques, galvanostatic single current pulse and AC impedance measurements are generally used to determine the type and magnitude of overpotentials. Recent successful AC impedance studies (6,7) of lithium anodes prompted us to utilize this technique for porous electrode.

Alternating current impedance measurements are attractive to kinetic reaction studies, but the interpretation of experimental data obtained on a porous electrode can cause substantial complications, especially when adsorption and desorption processes are involved. However, recent advances in electronics have enabled the acquisition of a complete impedance spectrum within minutes by the use of the fast Fourier transform (FFT) algorithm, which allows Fourier analyses to be carried out readily upon complex input signals.

The theory of electrochemical impedance measurements of porous electrodes is very complex and will not be given here(8). Basically, a spectrum analyzer determines impedance spectra by noise response impedance analysis; a white noise source generated by an analyzer is delivered to the cell and the current response is subjected to FFT analysis. The frequency dependent impedance and phase angle are displayed in the CRT and can be recorded easily.

b. Experimental. AC impedance data were obtained at Sandia National Laboratories* using a Hewlett Packard 3722A noise generator and a PAR Potentiostat 173. A Hewlett-Packard 9845T desk top computer was used to reduce the data. Impedance measurements at both steady state and dynamic conditions were made over the frequency range of 0.01 Hz to 1000 Hz.

*Experiments were carried out by Dr. Frank M. Delnick of Sandia National Laboratories.

The electrochemical cell consisted of a carbon electrode and a platinum counter electrode. Impedance measurements of the cathodes were made with and without iron phthalocyanine catalyst in 1.5M LiAlCl₄/SOCl₂ electrolyte (3 mg FePc per cc of electrolyte). Initial impedance experiments of baseline porous carbon electrodes with and without catalyst revealed that the electron transfer process was extremely slow at open circuit voltage and the impedance spectrum had a very large diameter. In order to minimize problems associated with high surface area porous electrodes, a stress annealed pyrolytic graphite electrode ($A=0.178 \text{ cm}^2$) was used.

c. Results. In Figures 34 and 35, the complex impedance of carbon electrodes with and without FePc catalyst respectively, in 1.5M LiAlCl₄/SOCl₂ electrolyte, are given. The diameter of the semicircle represents the Faradaic resistance if the capacitance value is small. For a diffusion controlled reaction, a straight line with a phase angle of 45° is usually obtained in the complex impedance. For a porous electrode the phase angle should be 22°.

The impedance of carbon electrodes in 1.5M LiAlCl₄/SOCl₂ with and without FePc catalyst shows a semicircle with a large diameter. The diameter decreases with FePc catalyst. Still, very high resistance due to charge transfer process exists, which is indicative of very slow reaction rates at open circuit voltage. The open circuit potentials vs platinum electrode were -0.322V and -0.511V for cathodes with and without FePc catalyst.

Impedance measurements were made on catalyzed cathodes under dynamic conditions. Figures 36 through 38 show the complex impedance at discharge rates of 34, 112 and 675 $\mu\text{A}/\text{cm}^2$. The current rates remained constant at 34 and 112 $\mu\text{A}/\text{cm}^2$ throughout the experimental time (30 minutes at each experiment); however the discharge current, 675 $\mu\text{A}/\text{cm}^2$ decreased slowly with time (675 $\mu\text{A}/\text{cm}^2$ to 450 $\mu\text{A}/\text{cm}^2$). At 34 and 112 $\mu\text{A}/\text{cm}^2$ discharge, the charge transfer resistance decreased but the reaction rates were still very slow. At 675 $\mu\text{A}/\text{cm}^2$, the reaction is completely diffusion controlled as shown in Figure 38 by a straight line with a phase angle of 42°. Furthermore, when the impedance measurements were made at open circuit voltage after passing 675 $\mu\text{A}/\text{cm}^2$ current for nearly 30 minutes, as shown in Figure 39, the reaction is still diffusion controlled.

Additional experiments are needed to understand and establish various resistances (ionic, faradaic, etc.) which contribute to the cathode overpotential.

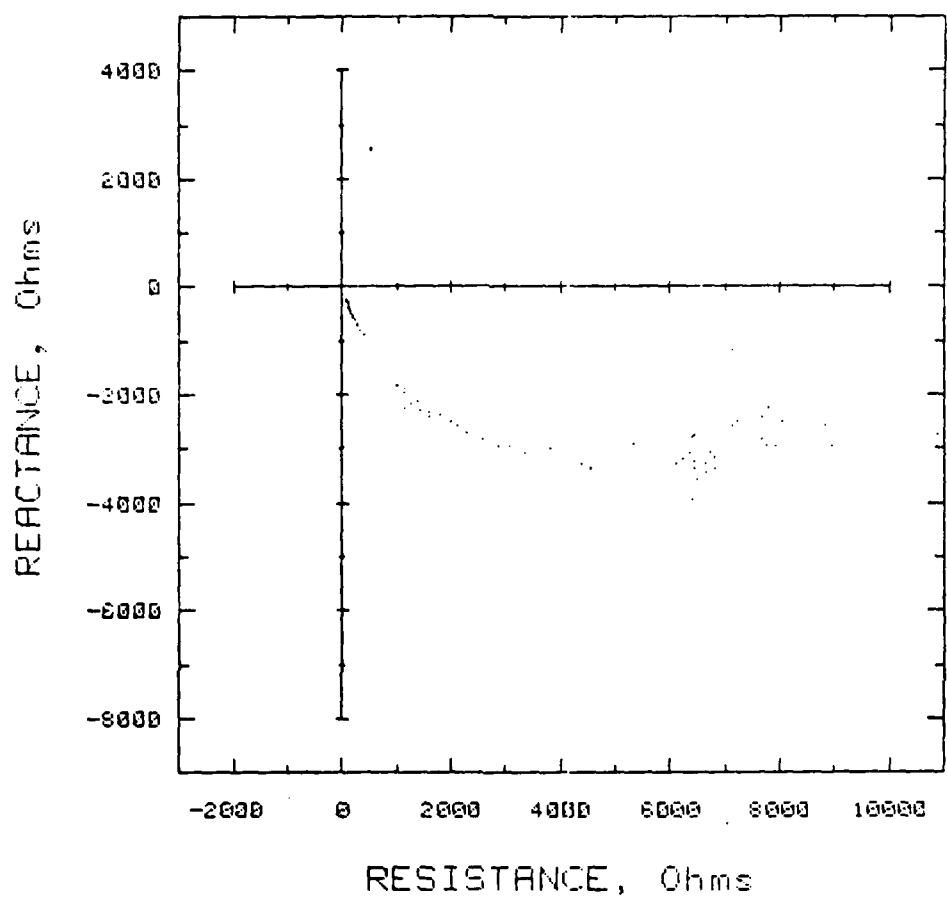


Figure 34. Impedance of Stress Annealed Pyrolytic Graphite Electrode (0.178 cm^2) in 1.5M $\text{LiAlCl}_4/\text{SOCl}_2$ Containing FePc Catalyst.

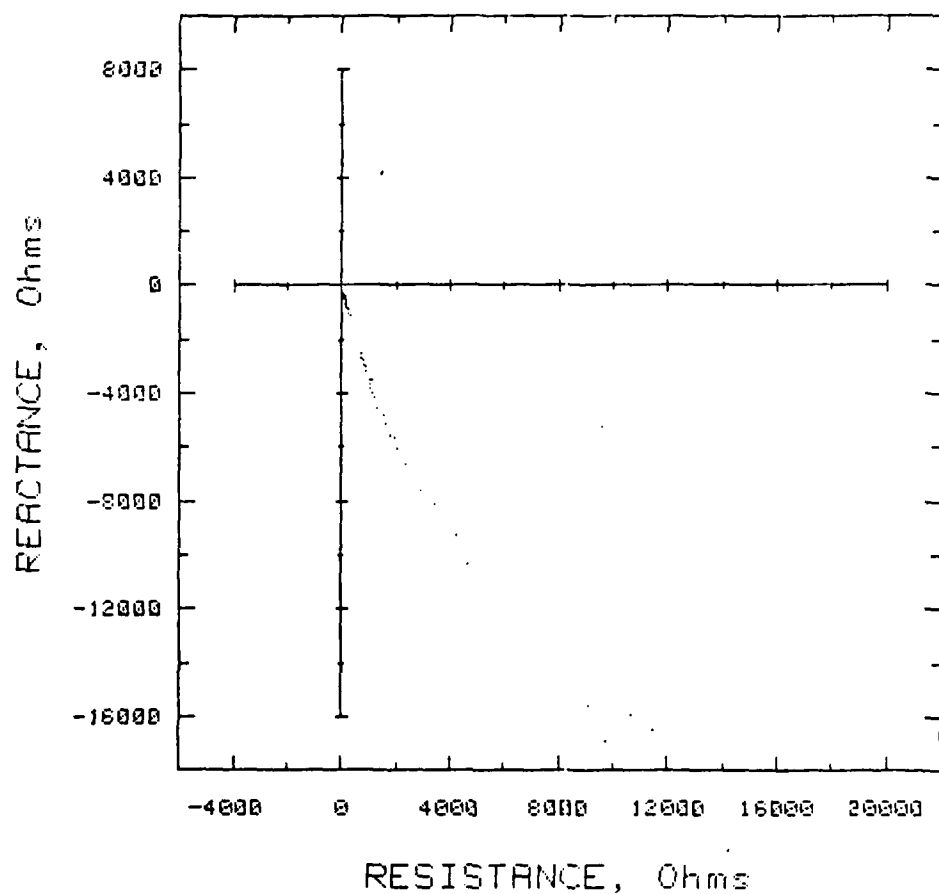


Figure 35. Impedance of Stress Annealed Pyrolytic Graphite Electrode (0.178 cm^2) in $1.5\text{M LiAlCl}_4/\text{SOCl}_2$ Electrolyte at 75°F .

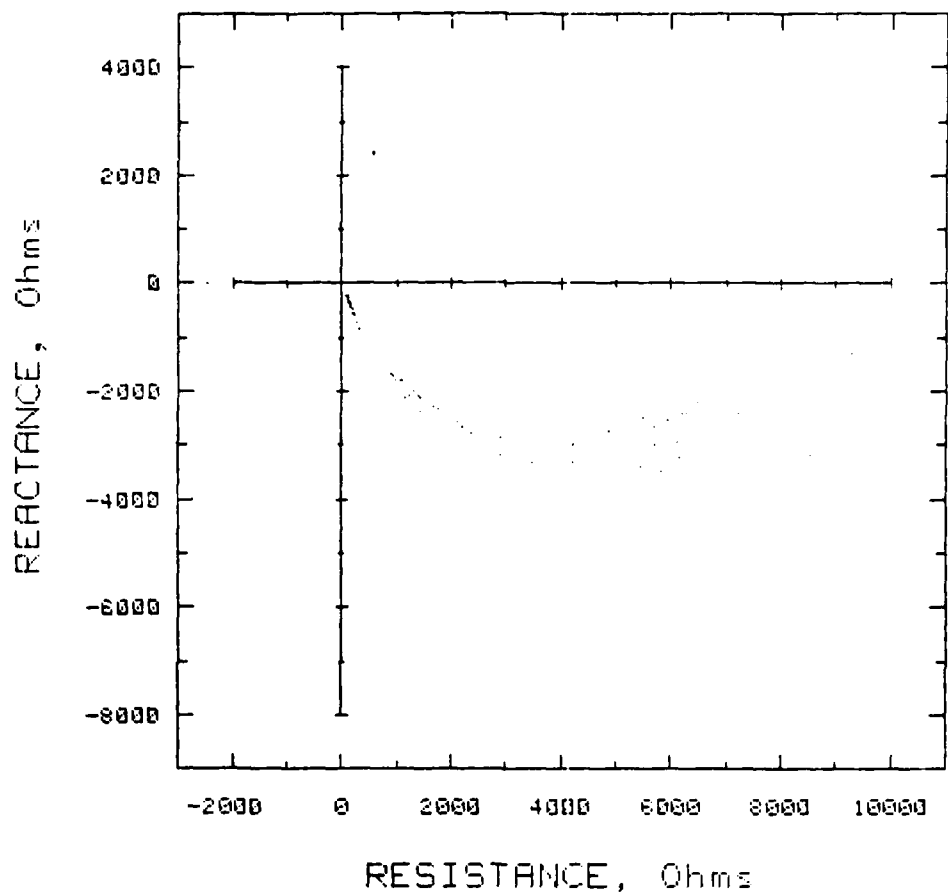


Figure 36. Impedance of Stress Annealed Pyrolytic Graphite Electrode (0.178 cm^2) at a Discharge Rate of $34 \mu\text{A}/\text{cm}^2$ in $1.5\text{M LiAlCl}_4/\text{SOCl}_2 + \text{FePc}$.

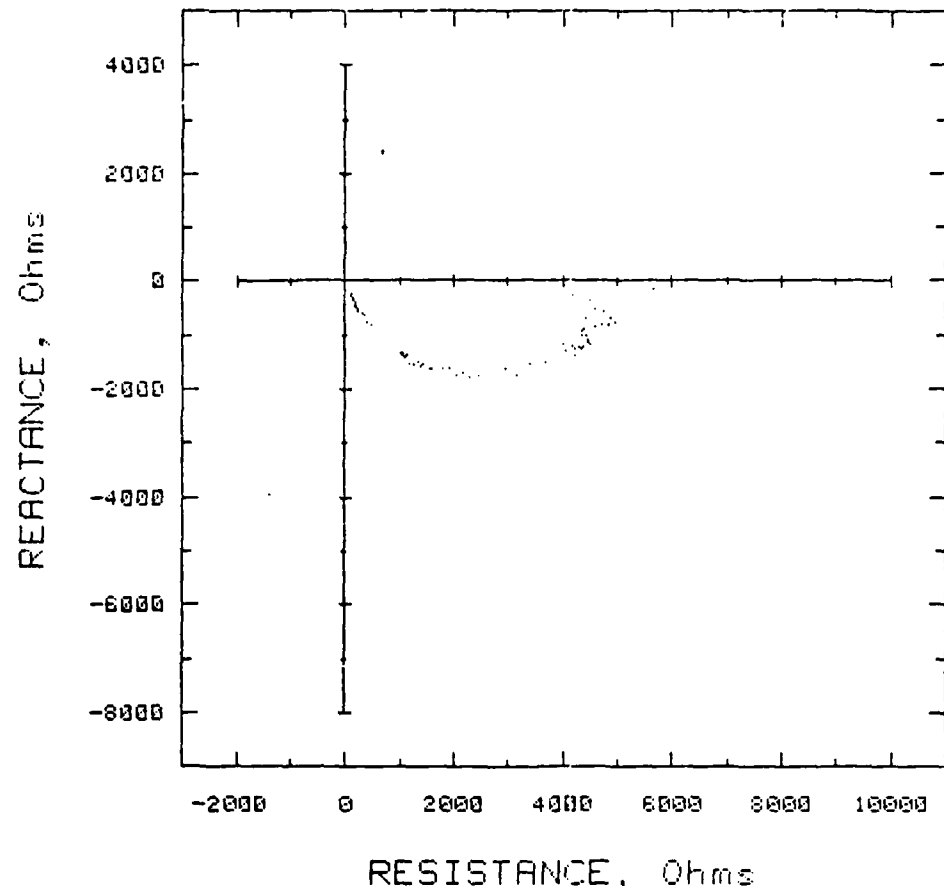


Figure 37. Impedance of Stress Annealed Pyrolytic Graphite Electrode (0.178 cm^2) at a Discharge Rate of $112 \mu\text{A}/\text{cm}^2$ in $1.5\text{M LiAlCl}_4/\text{SOCl}_2 + \text{FePc}$.

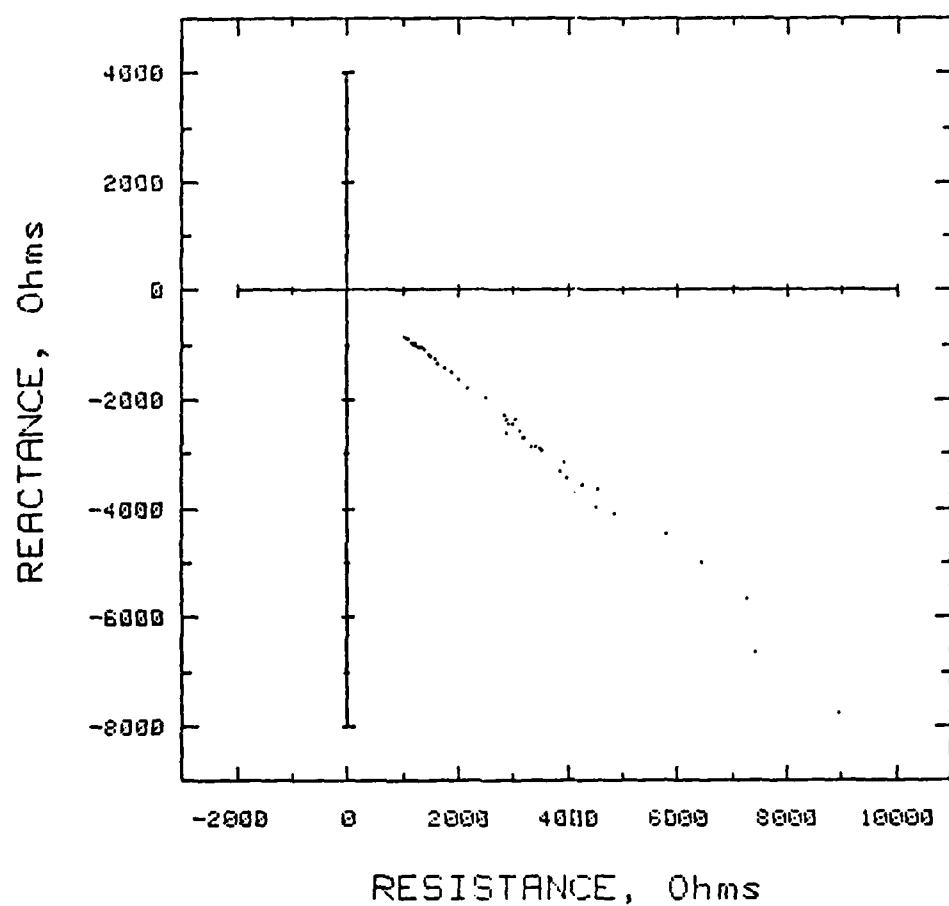


Figure 38. Impedance of Stress Annealed Pyrolytic Graphite Electrode (0.178 cm^2) at a Discharge Rate of $675 \mu\text{A}/\text{cm}^2$ in $1.5\text{M LiAlCl}_4/\text{SOCl}_2 + \text{FePc}$.

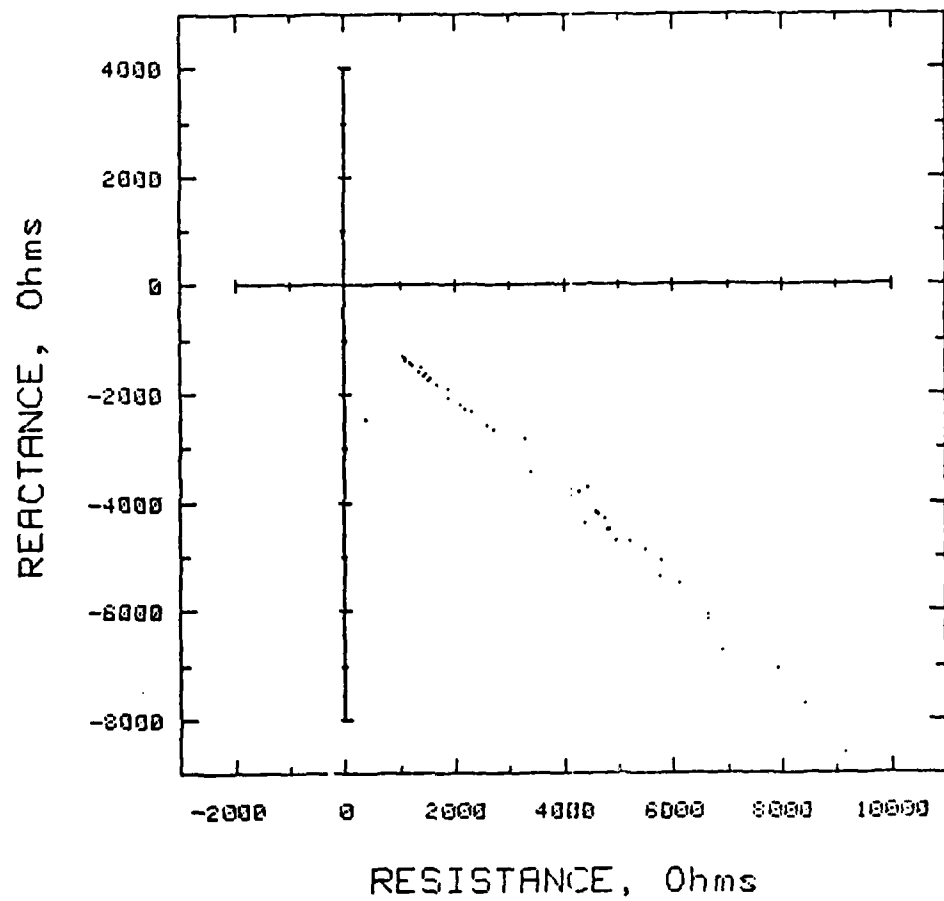


Figure 39. Impedance of Stress Annealed Pyrolytic Graphite Electrode (0.178 cm^2) at Open Circuit Voltage (After 30 minutes at $675 \mu\text{A}/\text{cm}^2$ discharge) in $1.5\text{M LiAlCl}_4/\text{SOCl}_2 + \text{FePc}$.

III. CATHODE PERFORMANCE IMPROVEMENTS

A. INTRODUCTION

The electrochemical reduction of thionyl chloride takes place at the cathode surface and the reduction rate is known to depend strongly on the cathode material. The widely accepted cathode reaction



proceeds smoothly at low rates upon various metals and non-metals, but it has been found that high rates can be achieved only by using carbon black substrates doped with or without electrocatalysts (5). Furthermore, the cathode polarization and reaction zone thickness strongly depend on cathode variables such as (a) cathode substrate, (b) cathode thickness, and (c) cathode density. These three cathode variables are optimized to achieve a high efficiency Li/SOCl₂ cell.

1. Carbon Substrates

Since it is known that acetylene black carbons catalyze the SOCl₂ reduction better than any other carbon reported in the literature, both 50% and 100% compressed grade Shawinigan acetylene blacks (SAB) were evaluated for their effect on cathode performance. In addition, the effect of (CoPc)_n and FePc catalysts were examined. These catalysts were doped only on 100% SAB because of its superior performance observed over 50% SAB.

2. Cathode Thickness

At high discharge rates, only a small part of the available cathode surface participates in the electrochemical SOCl₂ reduction process at porous teflonated carbon cathodes. This part of the electrode structure is often referred to as the reaction zone. The reaction zone thickness is influenced by both kinetics and

mechanism of electrochemical reduction. In addition, it is known that the cathode thickness influences the reaction zone thickness (depth of penetration). Therefore, the effect of cathode thickness on both voltage and performance of cathode were studied. Cathodes of thickness, 0.010, 0.015, 0.020, 0.030 and 0.040 inches were fabricated for each substrate described above by the standard cathode fabrication process described earlier.

3. Cathode Density

Teflonated porous carbon electrodes are commonly used in Li/SOCl₂ systems. The amount of Teflon binder influences the cathode density, conductivity, surface area, etc. Therefore, in order to optimize the Teflon amount on these physical properties which influence the cathode performance, cathodes were fabricated containing 5, 10, and 15% by weight Teflon binder. In Figure 40, cathode density dependence on the Teflon content is plotted for three different carbon substrates. Approximately 20% increase in cathode density is observed with 100% SAB compared to that of cathode with 50% SAB substrate. The drop in density with 5% (CoPc)_n doped 100% SAB may be due to porosity created during heat treatment at 550–600°C.

B. EVALUATION OF CATHODE PERFORMANCE

1. Introduction

Cathode performance was evaluated by discharging laboratory Li/SOCl₂ cells at a fixed 10 mA/cm² current rate. The effect of cathode substrate, thickness and density, on the discharge performance were examined at 75, 0, 20, and -40°F. All cells were activated at ambient temperature and cooled to appropriate temperature with a constant current load equivalent to 0.2 mA/cm² to avoid passivation problems associated with Li/SOCl₂ system. All experiments were duplicated and if a variation was found, it was repeated until reproducible results were obtained. A total of 40 cathodes were fabricated and evaluated.

2. Discharge Performance

Discharge characteristics at a constant current rate of 10 mA/cm² were studied in our standard laboratory cell fixture. In order to maintain identical experimental

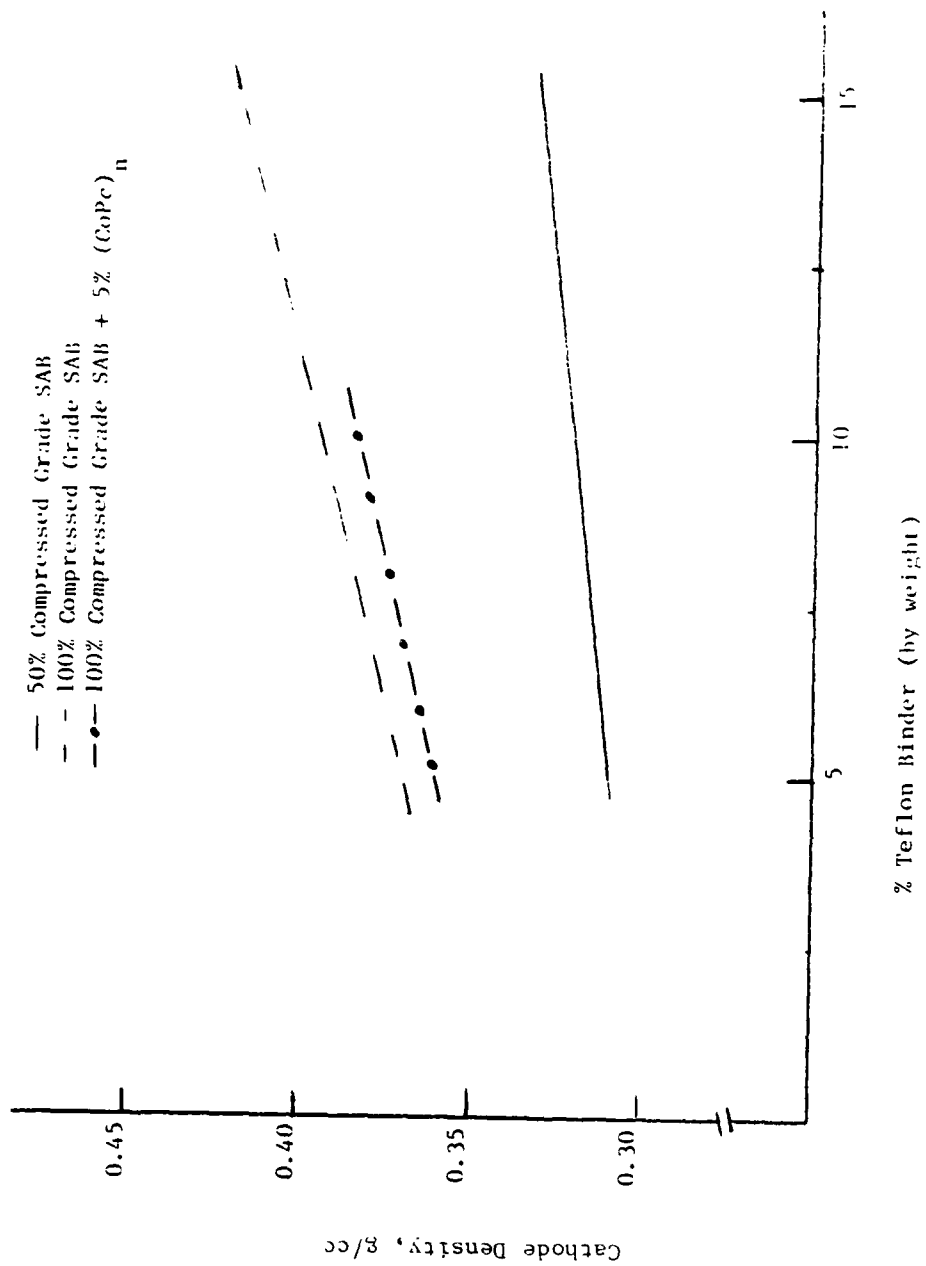


Figure 40. Effect of Teflon Content on the Cathode Density

conditions, cells containing cathodes of constant density were built and discharged together for every operating temperature. For example, cathodes having thicknesses of 0.010, 0.015, 0.020, 0.030 and 0.040 inches, fabricated from a carbon mix containing 5% Teflon binder and 50% SAB, were evaluated in duplicate together at 0°F. This procedure maintained a constant cooling time and exposed the cells to the same fluctuations in temperature and discharge rate.

In Figures 41-43, the effect of cathode density on the discharge performance of cathodes fabricated from 50% SAB, 100% SAB and 5% (CoPc)_n doped 100% SAB are given, respectively. No significant change in performance is observed (Figure 41) with 50% compressed grade Shawinigan acetylene black cathode substrate containing 5-15% Teflon binder. However, cathodes fabricated with 100% SAB with and without (CoPc)_n catalyst exhibit best performance with 5% Teflon binder (Figures 42 and 43). Similar behavior was observed for FePc catalyzed cathodes.

The discharge performance of cathodes fabricated from various cathode substrates is compared in Figure 44. All the cathodes contained 5% Teflon binder and the cells were discharged at ambient temperature with a constant current load equivalent to 10 mA/cm². Significant performance improvements are achieved with catalyzed cathodes. As the cathode thickness increases, the improvement in cathode performance increases with catalyzed cathodes. However, the slope of the line decreases with cathode thickness regardless of cathode thickness and also regardless of cathode substrate.

In Figure 45, the cell voltage at 50% depth-of-discharge with respect to cathode thickness is compared for the cells described in Figure 44. The cell voltage remains constant for cathodes containing 50% SAB, whereas all others increased with cathode thickness. Dramatic voltage improvements are achieved with FePc catalyzed cathodes.

Low temperature (0°F) performance of cells described in Figure 44 is given in Figures 46 through 55. In general, lowering the temperature results in a decrease in electrochemical cell performance irrespective of cathode thickness and cathode

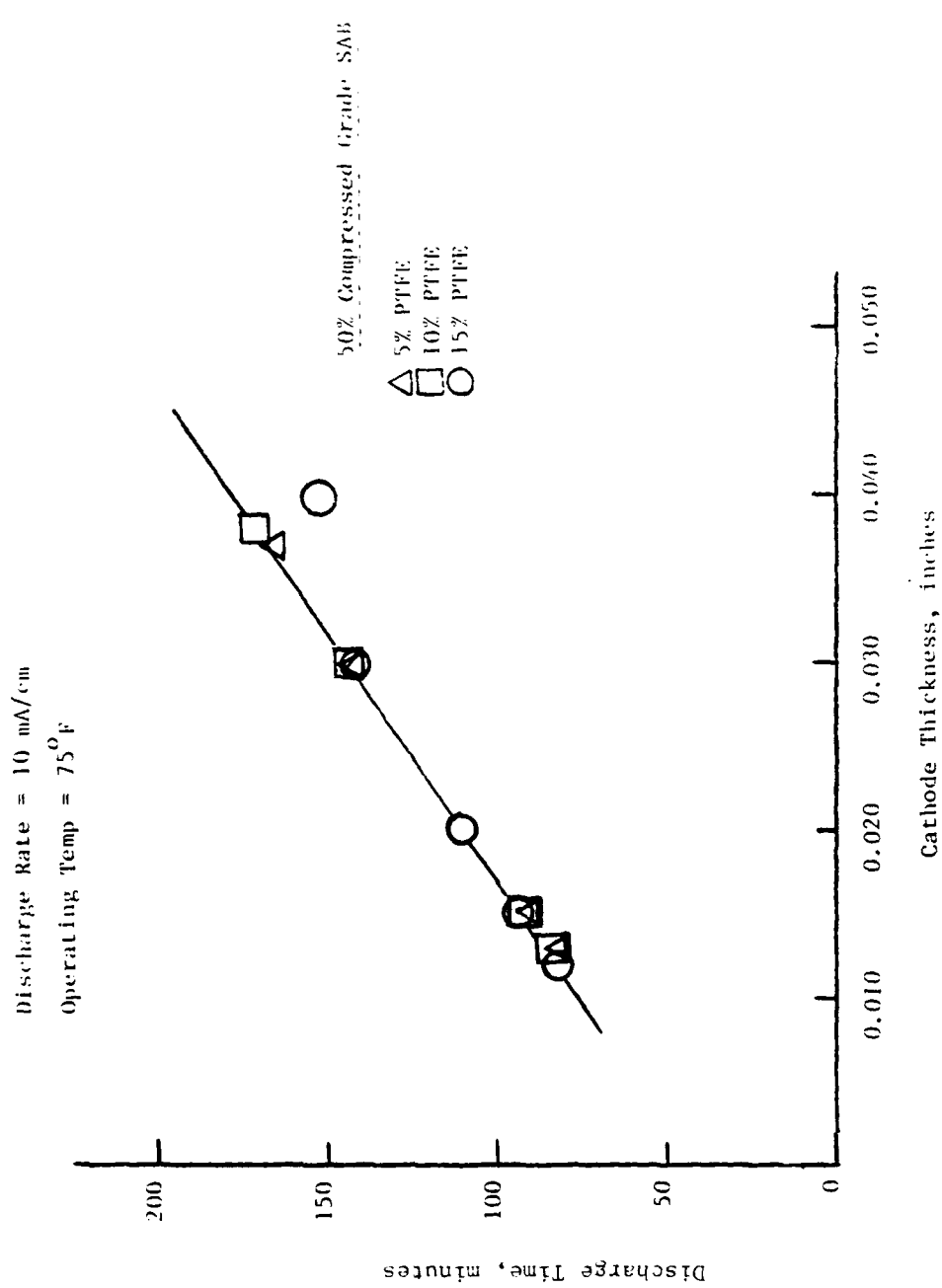


Figure 41. Effect of Cathode Variables (Teflon binder content with 50% Compressed Anode SAB) on the Discharge Performance of Li/SOCl₂ Cells with 1.5M LiAlCl₄/SOCl₂ Electrolyte

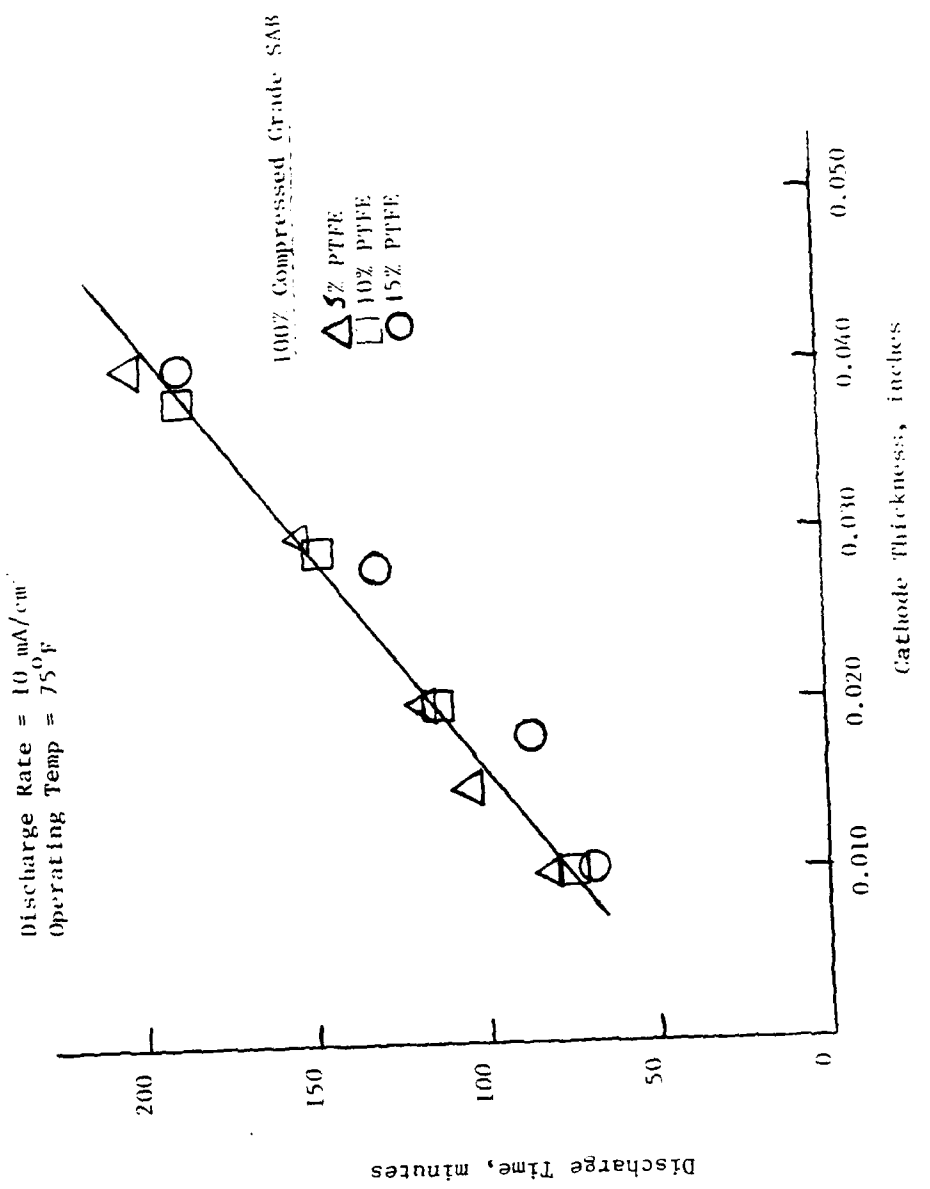


Figure 42. Effect of Cathode Variable (Teflon Binder Content with 100% Compressed Grade SAB) on the Discharge Performance of Li/SOCl₂ Cells with 1.5M LiAlCl₄/SOCl₂ Electrolyte

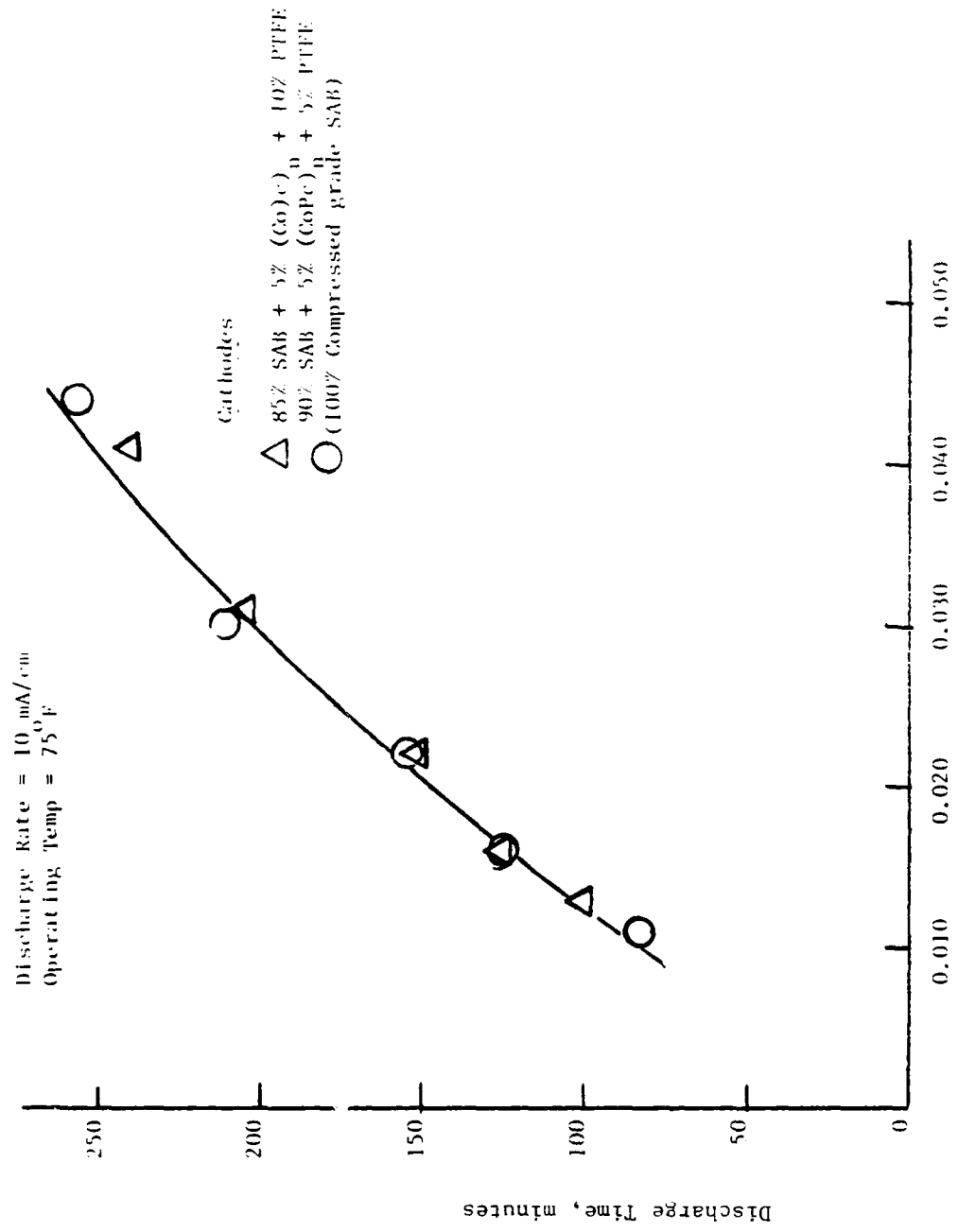


Figure 43. Effect of Cathode Variables (Teflon Binder Content with (CoPC)_n, Catalyzed Carbon Substrate) on the Discharge Performance of Li/SOCl₂ Cells with 1.5M LiAlCl₄/SOCl₂ Electrolyte

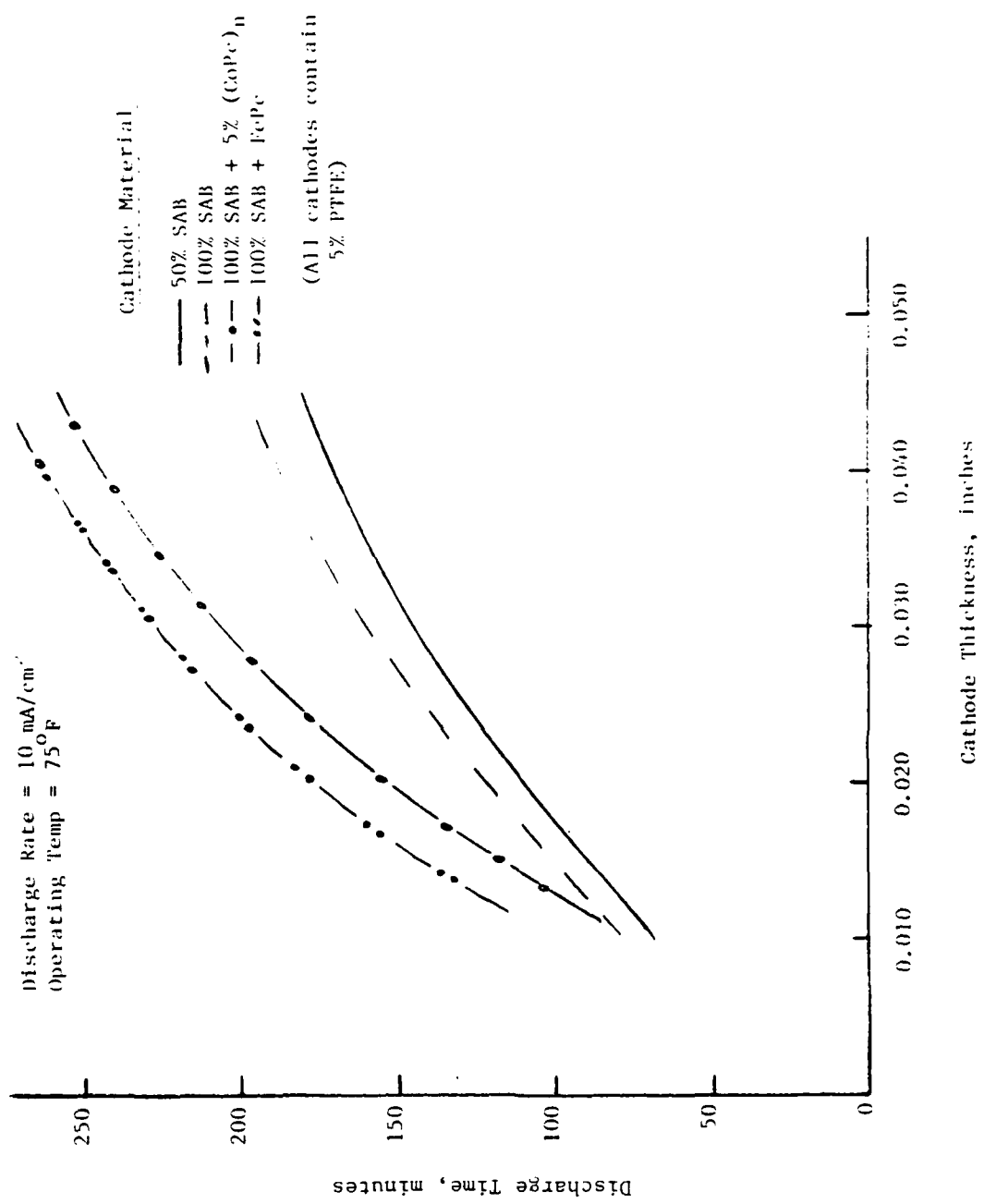


Figure 44. Effect of Cathode Variables (Cathode Substrates) on the Discharge Performance of Li/SOCl₂ with 1.5M LiAlCl₄/SOCl₂ Electrolyte

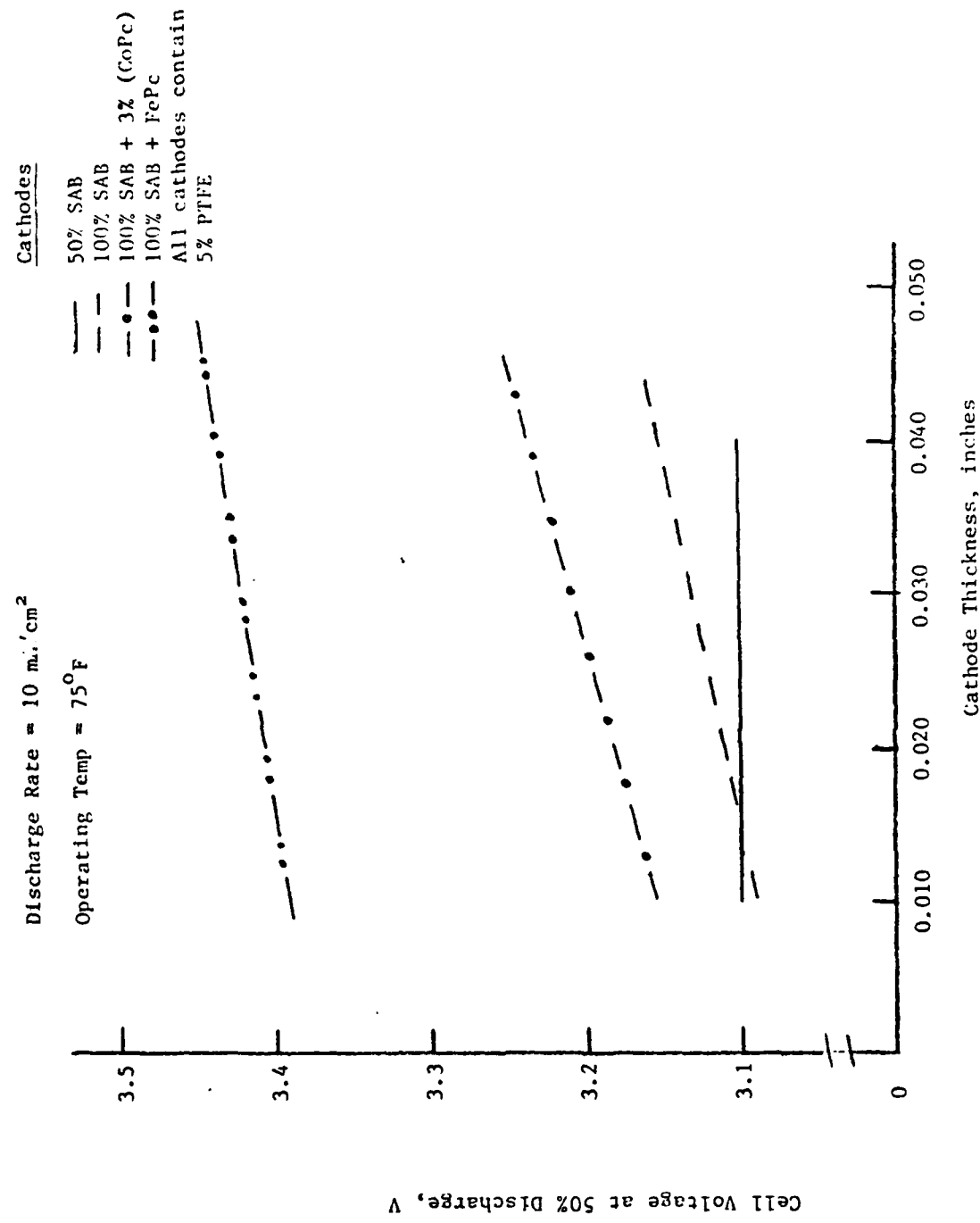


Figure 45. Effect of Cathode Variables on Voltage of Li/SOCl₂ Cells with 1.5M LiAlCl₄/SOCl₂ Electrolyte at 10 mA/cm² and 75° F.

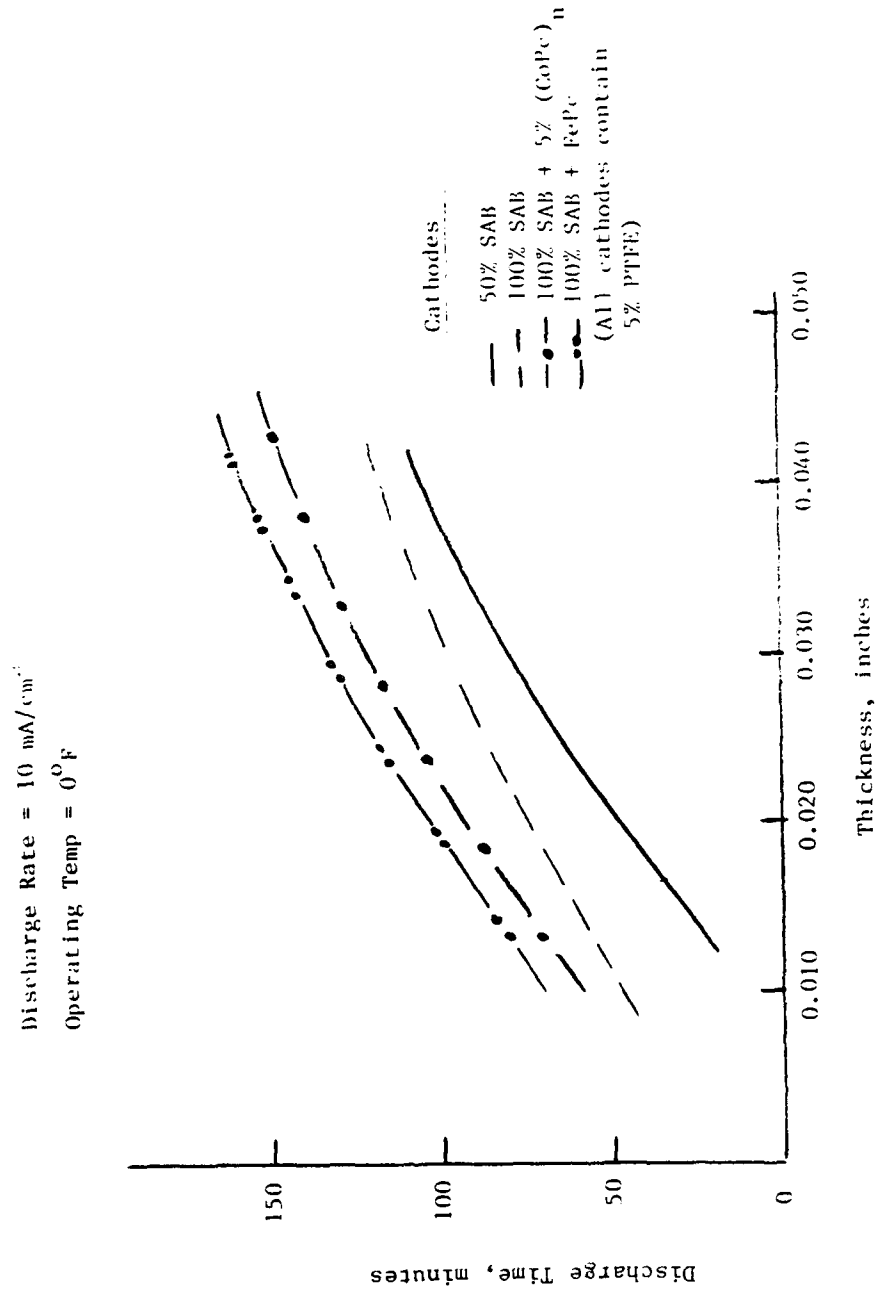


Figure 46. Effect of Cathode Variables (Cathode Substrates) on the Discharge Performance of Li/SOCl₂ Cells with 1.5M LiAlCl₄/SOCl₂ Electrolyte at 10 mA/cm² and 0° F

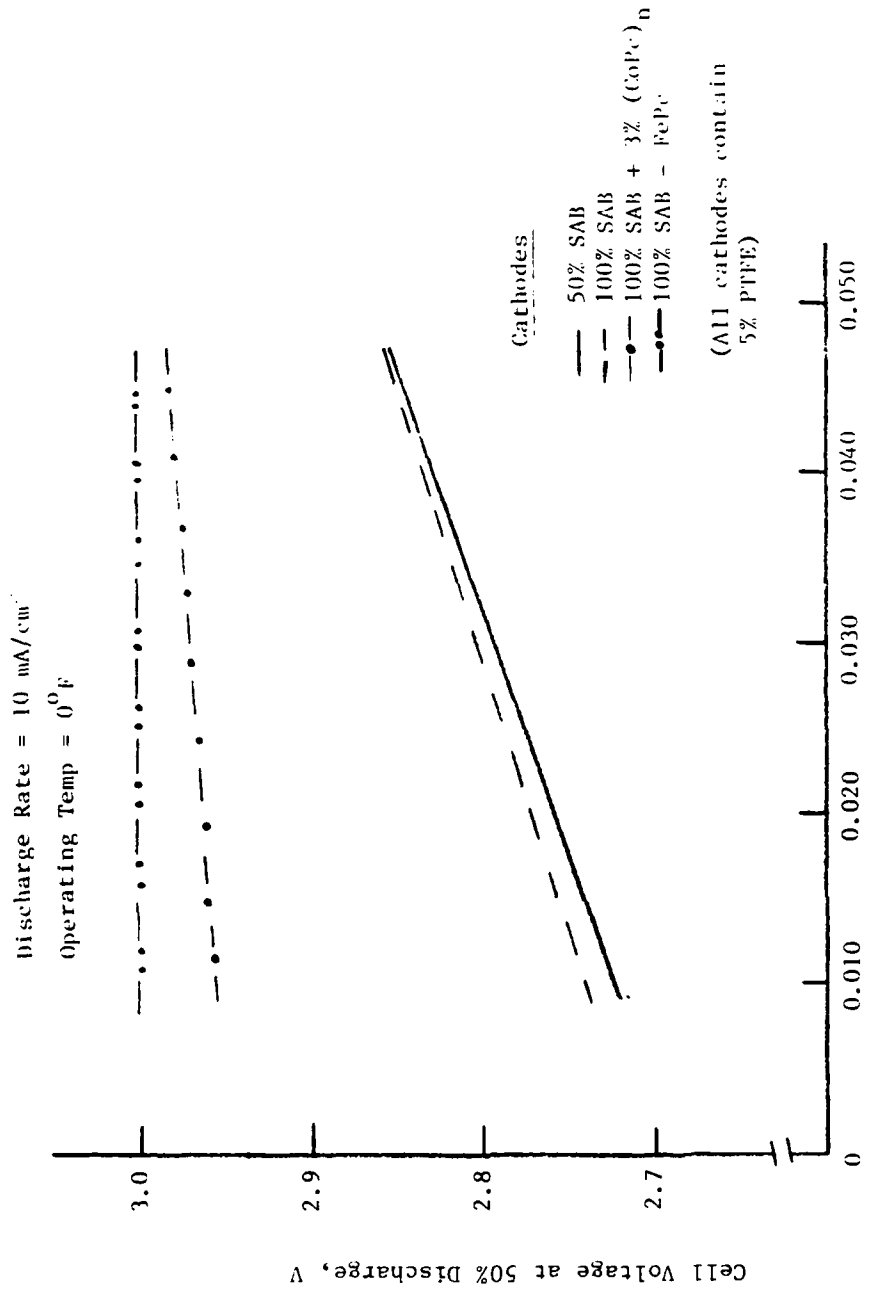


Figure 47. Effect of Cathode Variables on Voltage of Li/SOCl₂ Cells with 1.5M LiAlCl₄/SOCl₂ Electrolyte at 10 mA/cm² and 0° F.

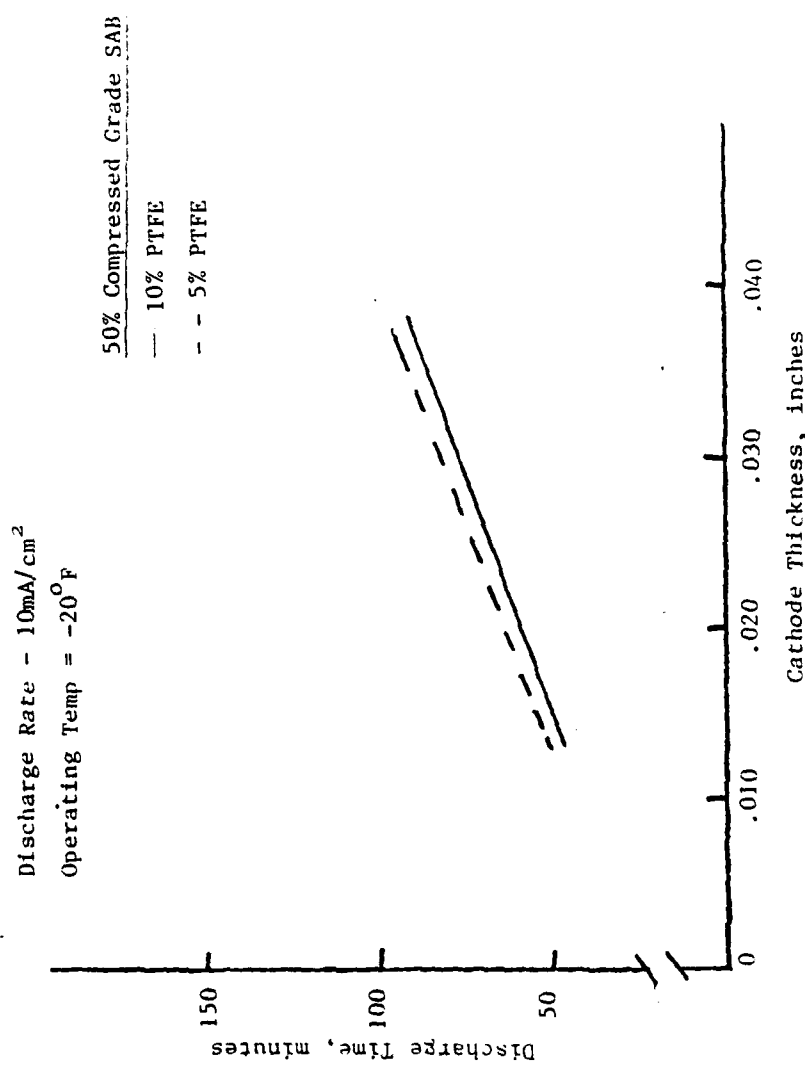


Figure 48. Effect of Cathode Variables (Teflon Binder with 50% Compressed Grade SAB) on Li/SOCl₂ Cell Life with 50% SAB in 1.5M LiAlCl₄/SOCl₂ at -20°F

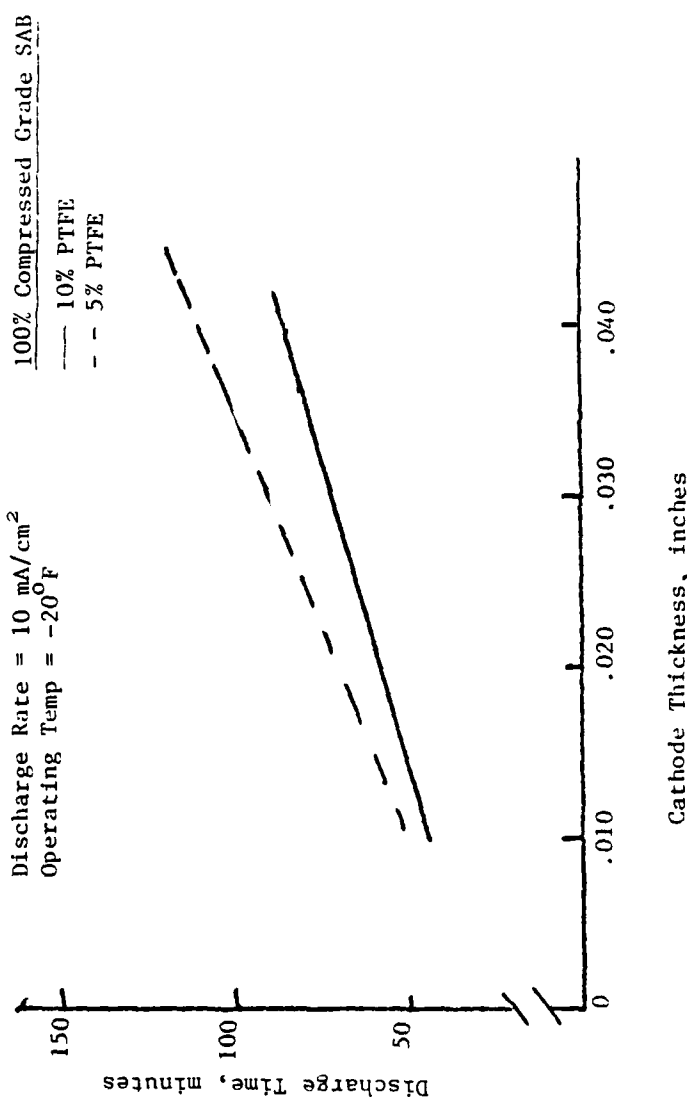


Figure 49. Effect of Cathode Variables (Teflon Binder with 100% Compressed Grade SAB) on Li/SOCl₂ Cell Life with 100% SAB in 1.5M LiAlCl₄/SOCl₂ at -20°F

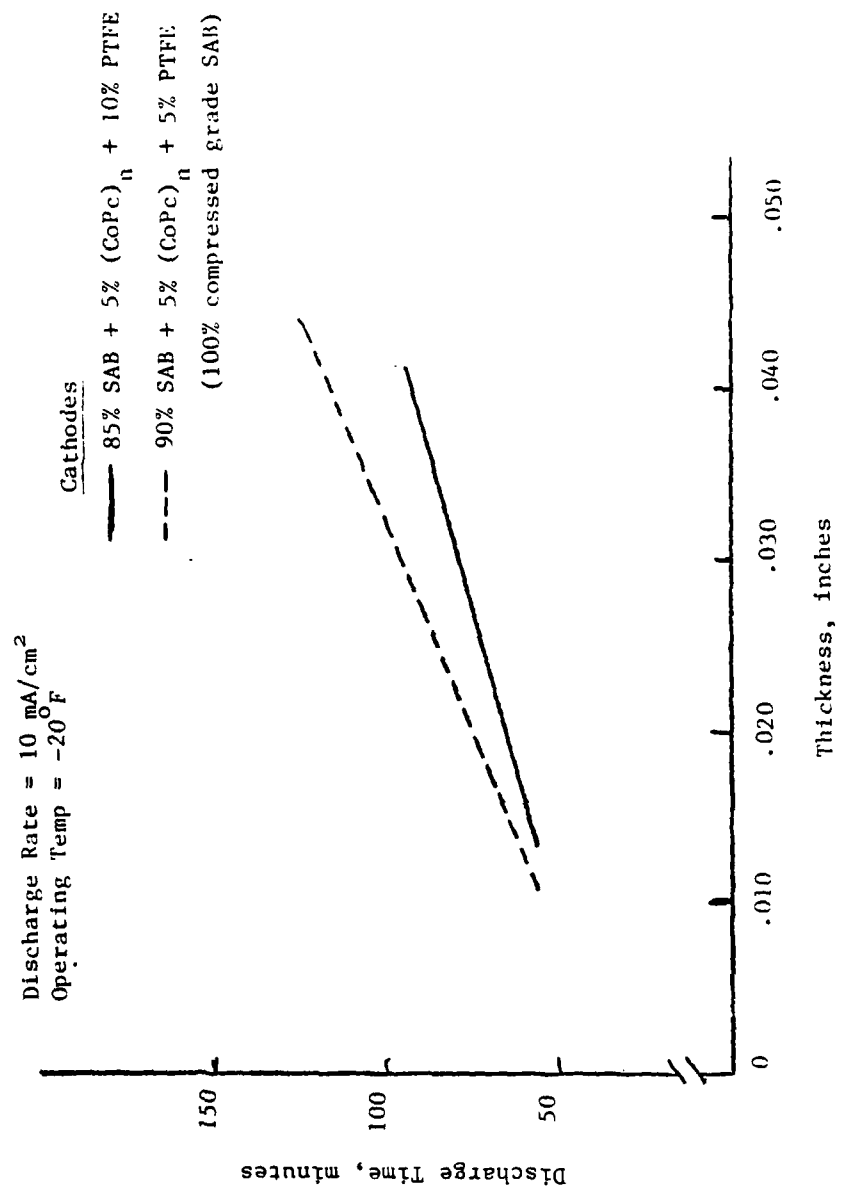


Figure 50. Effect of Cathode Variables (Teflon Binder with (CoPc)_n Catalyzed Carbon Substrate) on Li/SOCl₂ Cell Life with 5% (CoPc)_n Catalyzed Cathodes in 1.5M LiAlCl₄/SOCl₂ at -20° F

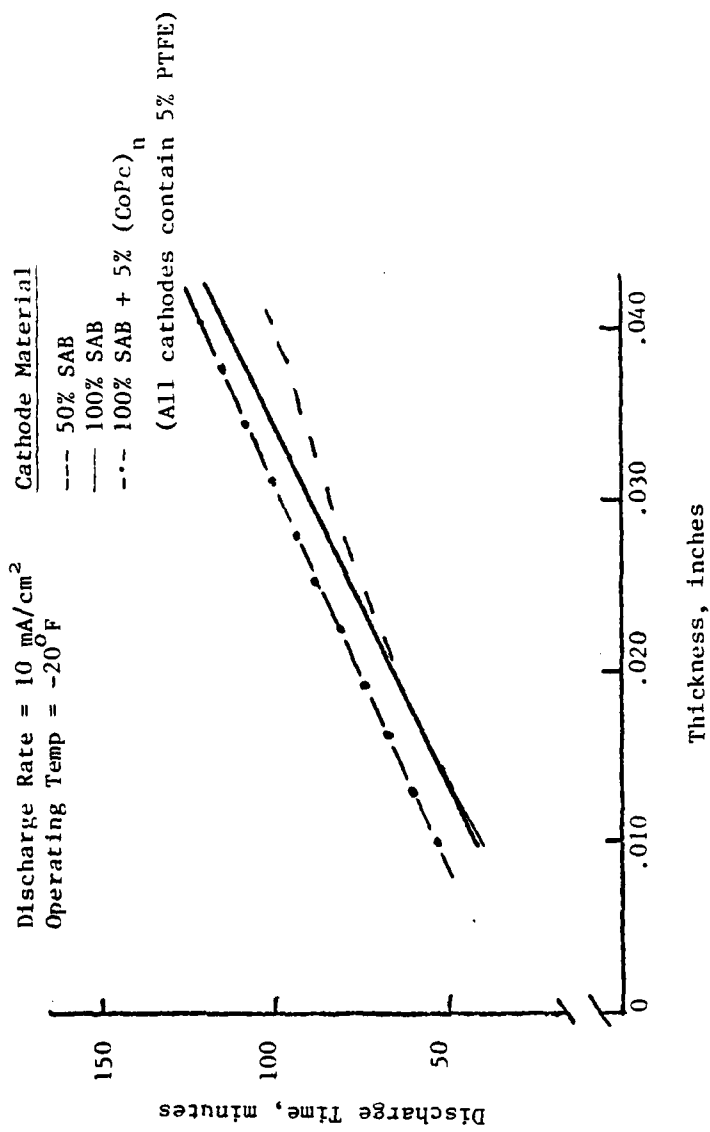


Figure 51. Effect of Carbon Substrates on the Li/SOCl₂ Cell Discharge Time in 1.5M LiAlCl₄/SOCl₂ at -20° F.

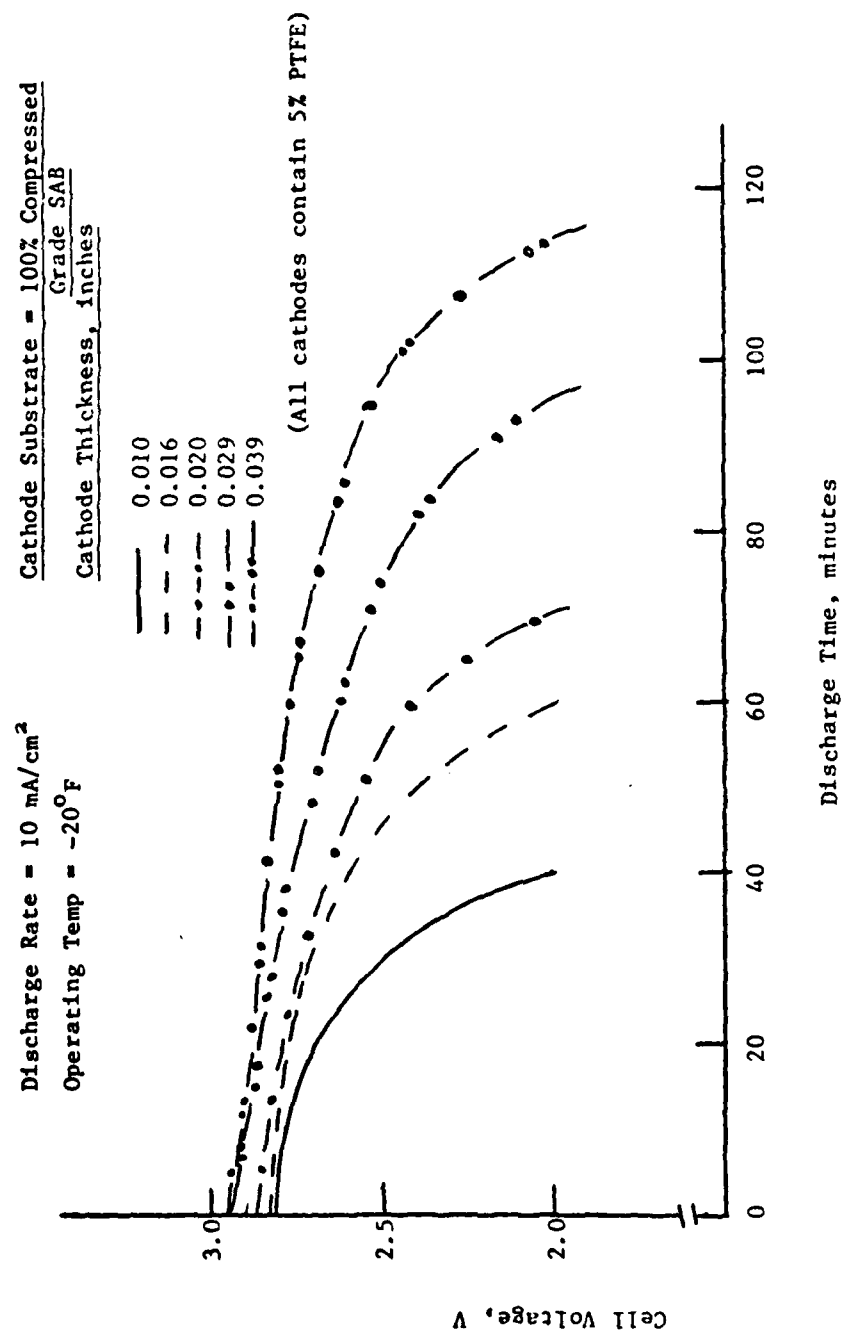


Figure 52. Effect of Cathode Thickness on Discharge Characteristics of Li/SOCl₂ Cells with 1.5M LiAlCl₄/SOCl₂ Electrolyte

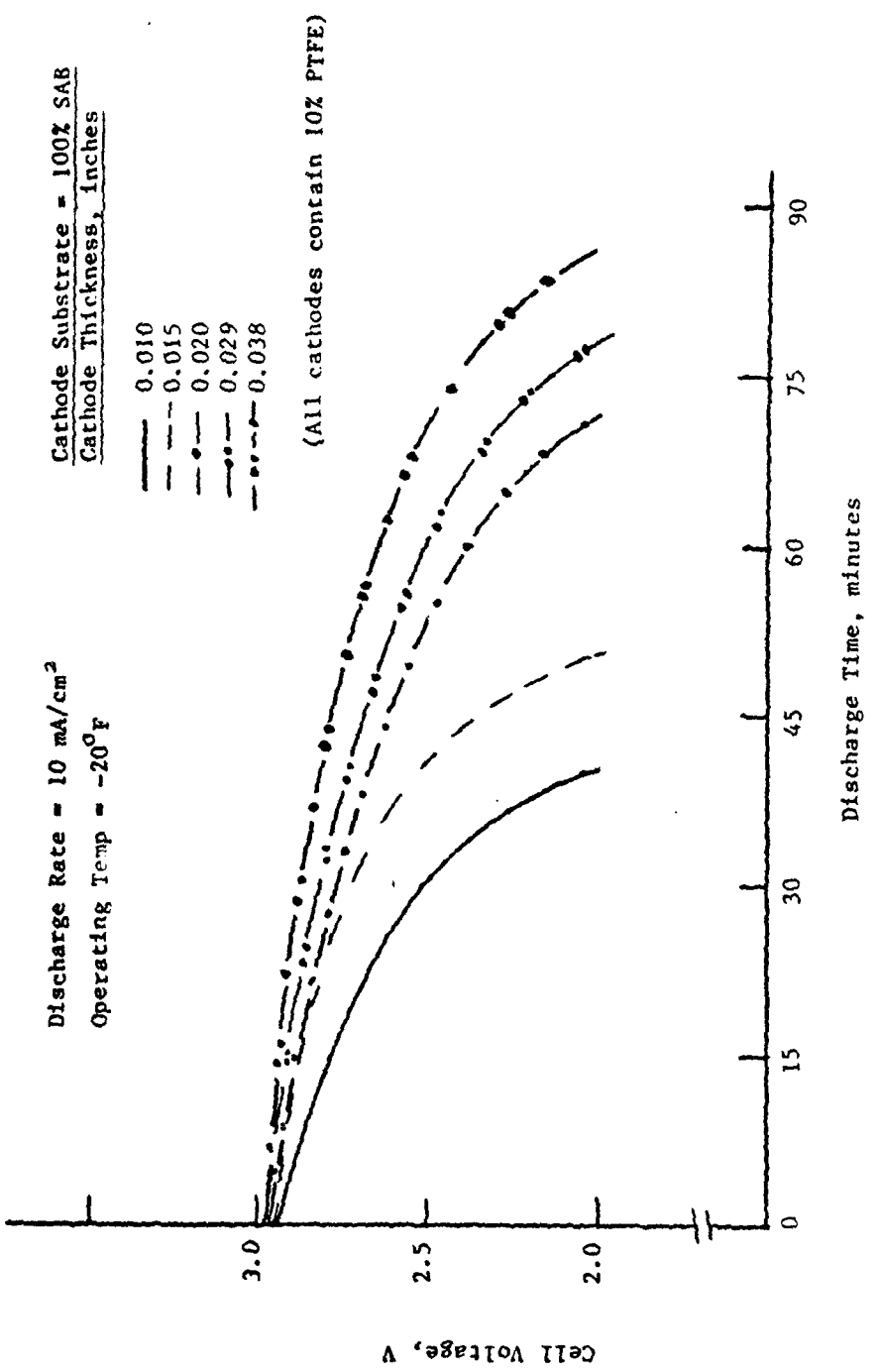


Figure 53. Effect of Cathode Thickness on Discharge Performance Characteristics of Li/SOCl₂ Cells with 1.5M LiAlCl₄/SOCl₂ Electrolyte (10% PTFE).

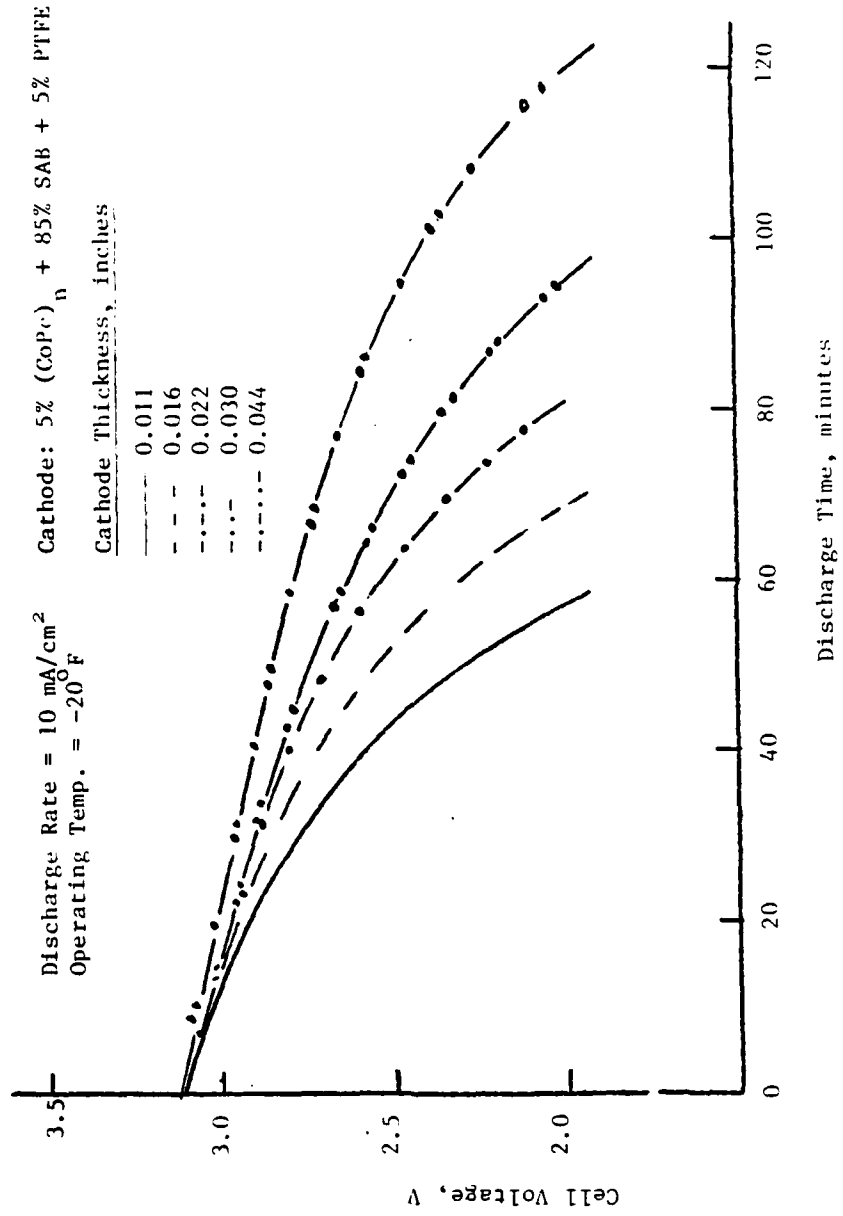


Figure 54. Effect of Cathode Thickness on Discharge Performance of Li/SOCl₂ with Catalyzed Cathode Containing 5% Teflon Binder in 1.5M LiAlCl₄/SOCl₂.

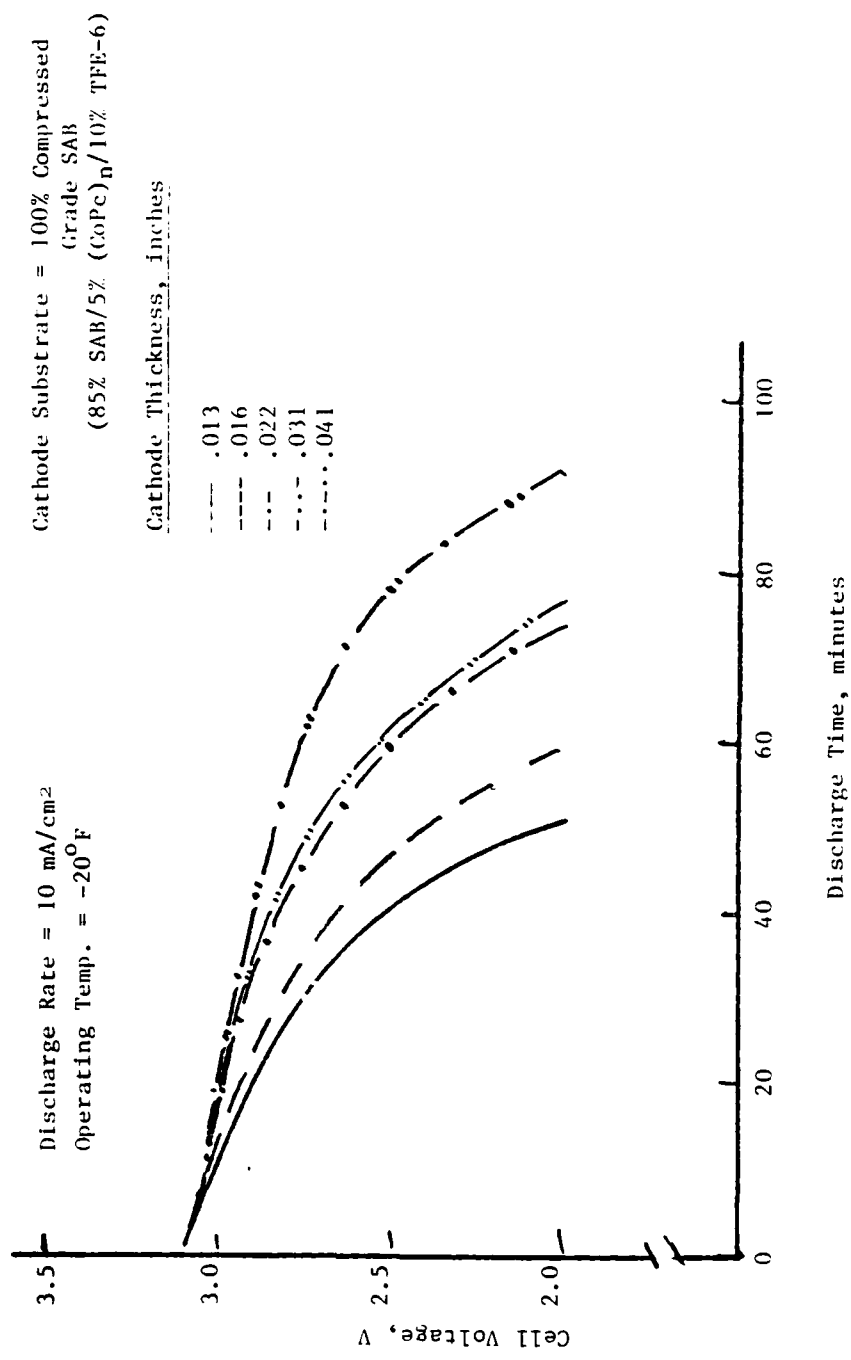


Figure 55. Effect of Cathode Thickness on Discharge Characteristics of Li/SOCl₂ Cells with Catalyzed Cathode Containing 10% Teflon Binder in 1.5M LiAlCl₄/SOCl₂ Electrolyte.

substrate (Figure 46). Furthermore, the extent of deterioration of cell performance with lowering temperature is influenced by the amount of Teflon binder in the cathode. The optimum amount of Teflon binder seems to be 5% or less by weight in the final cathode components.

C. PERFORMANCE OF OPTIMIZED CATHODES

1. Introduction

The systematic evaluation of baseline cathode performance during the program period has resulted in the optimization of cathode(s) for Li/SOCl₂ cells. The optimized cathodes contained (by weight):

a) Baseline Cathode

- o 95% - 100% compressed-grade Shawinigan acetylene black carbon substrate, (100% SAB)
- o 5% Teflon-6 binder

b) Catalyzed Cathode (CoPc)_n

- o 5% polymeric cobalt phthalocyanine
- o 90% - 100% SAB
- o 5% Teflon-6

c) Catalyzed Cathode, FePc

- o 95% - 100% SAB
- o 5% Teflon-6
- o 1-3 mg of FePc/cc of electrolyte (both neutral and acidic electrolytes)

2. Laboratory Cell Performance

Both half-cell measurements and cell discharge performance were made on the optimized cathodes at 75, 32, 0, -20 and -40°F. Cathodes of 0.020 inch thickness were employed during evaluation studies.

In Figures 56, the polarization characteristics of Li/ SOCl_2 with three different cathodes are compared. As previously observed, the cathode polarization decreases with catalyzed cathodes; the greatest decrease is achieved with FePc. Lowering the operating temperature from 75 to 32 $^{\circ}\text{F}$ results in a 125 mV increase in cathode polarization, irrespective of cathode type. The increase seems to be due to the increase in resistance as can be seen in Figure 57. Further lowering of temperature causes severe cell polarization and causes drop in the rate capability as observed with the cathodes described in Section II.

The discharge performance of Li/SOCl₂ cells with and without catalyzed cathodes shows that both high voltage and longer discharge times are achieved with catalyzed cathodes as shown in Figure 58. At low operating temperatures, the cell voltage, as well as cell life, decrease drastically as shown in Tables 2 and 3. Furthermore, the operating temperature also alters the voltage profile with the depth of discharge. This could be partly due to changes in electrolyte conductivity and viscosity.

Comparison of the results obtained on optimized cathodes and on our best starting cathodes show no severe changes in both polarization and discharge characteristics. This is anticipated because the optimized cathodes contained the same composition and underwent similar fabrication procedures as those of our initial cathodes.

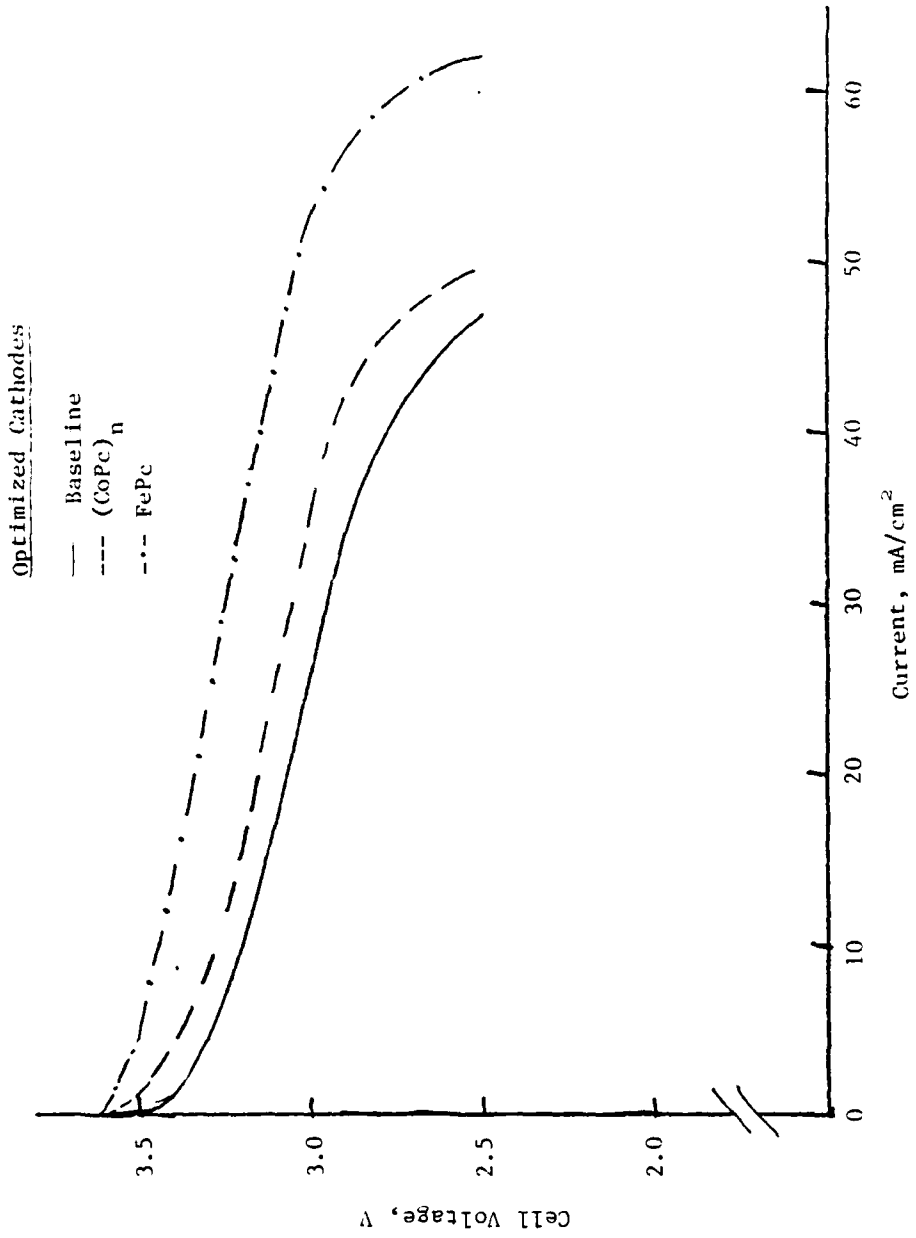


Figure 56. Polarization Characteristics of Li/SOCl_2 Cells at 75°F .

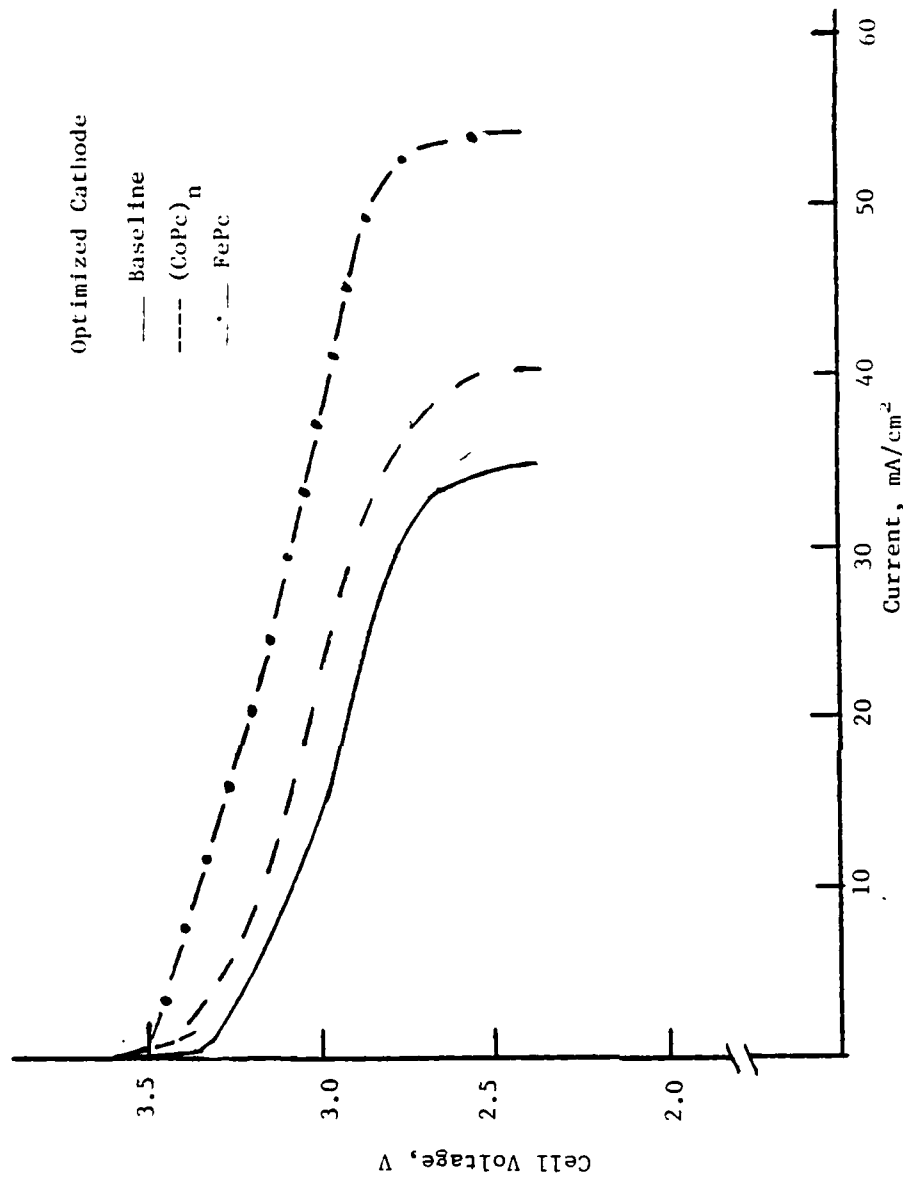


Figure 57. Polarization Characteristics of Li/SOCl_2 Cells with Optimized Cathodes at 32°F

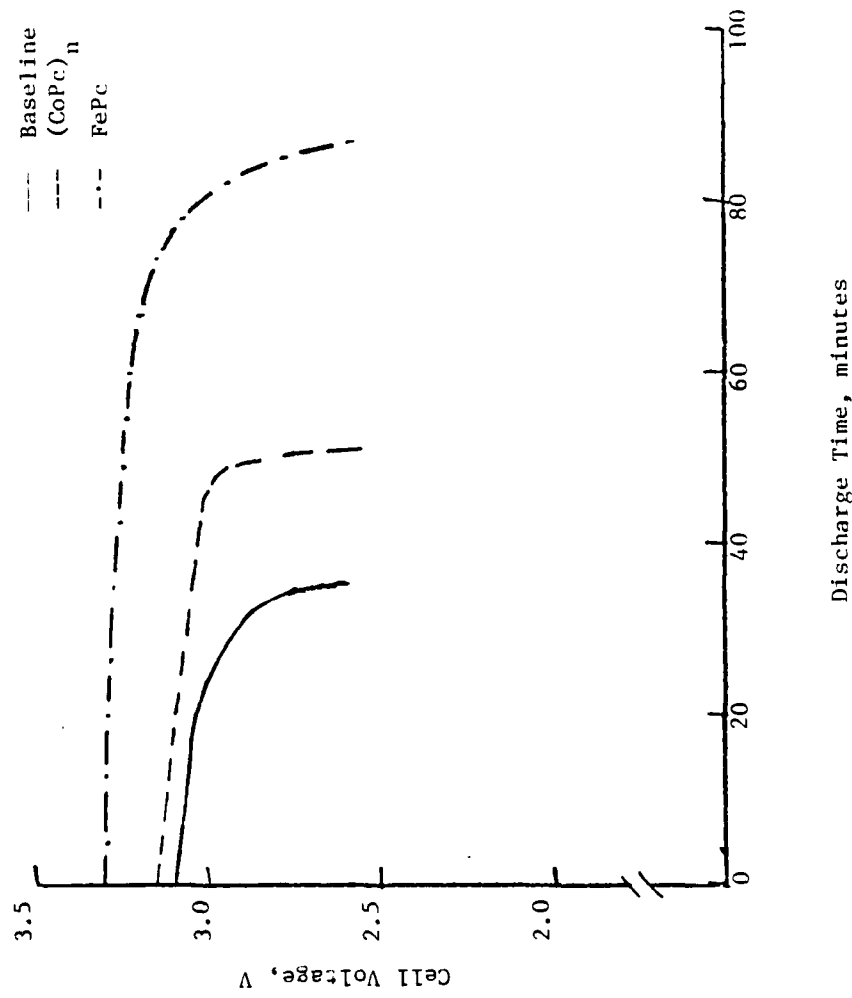


Figure 58. Discharge Characteristics of Li/SOCl₂ Cells at 20 mA/cm² and 75° F.

Table 2. Effect of Temperature on Discharge Characteristics of Li/SOCl₂ Cells with Optimized Cathodes and 1.5M LiAlCl₄/SOCl₂ at 10 mA/cm²

Temp, °F	Baseline Cathode			with Catalyst B			with Catalyst C		
	Avg. Cell Voltage, V	Discharge Time, min	Voltage, V	Avg. Cell Voltage, V	Discharge Time, min	Voltage, V	Avg. Cell Voltage, V	Discharge Time, min	Voltage, V
75	3.12	125	3.21	170	3.35	215			
32	3.02	77	3.10	96	3.16	155			
0	2.98	68	3.07	78	3.10	110			
-20	2.80	52	2.86	64	2.95	66			

*Average cell voltage is the voltage at 50% depth of discharge.

Table 3. Effect of Temperature on Discharge Characteristics of Li/SOCl₂ Cells with Optimized Cathodes and 1.5M LiAlCl₄/SOCl₂ at 20 mA/cm²

Temp., °F	Baseline Cathode Avg. Cell Voltage, V	with Catalyst B		with Catalyst C	
		Avg. Cell Discharge Time, min	Discharge Voltage, V	Avg. Cell Voltage, V	Discharge Time, min
75	3.03	38	3.07	46	3.26
32	3.00	32	3.04	38	3.15
0	2.77	22	2.87	25	2.95
-20	2.55	4	2.63	6	2.70

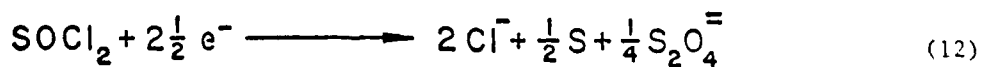
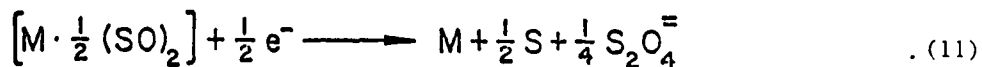
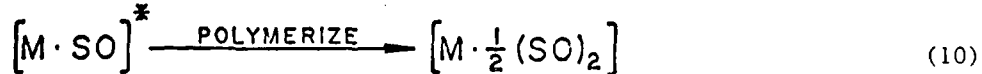
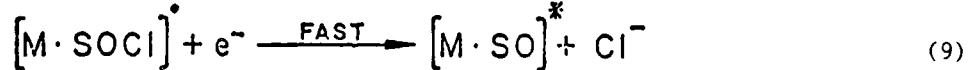
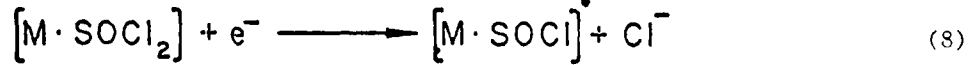
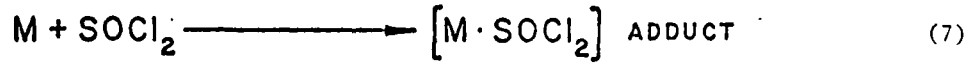
*Average Cell Voltage is the voltage at 50% depth of discharge.

IV. SUMMARY AND CONCLUSIONS

The rate of SOCl_2 reduction is strongly influenced by the carbon substrate of Teflonated porous cathode. Electrocatalysts, such as cobalt and iron phthalocyanine complexes increase the rate of SOCl_2 reduction and hence the rate capability of the system. These complexes, unlike other cathode dopants such as copper, nickel, and platinum, are true catalysts for the electrochemical reduction of SOCl_2 . Furthermore, they catalyze both electrochemical and chemical reactions of intermediate species.

Small amounts of catalysts in the carbon pore structure results in significant improvements in both cell voltage and specific cathode capacity; FePc catalyst shows the greatest catalytic effect. The improvement in cell voltage is attributed to the lowering of activation polarization due to elementary processes taking place at the cathode. The increase in specific cathode capacity could be due to increases in the reaction zone thickness and/or modification in reaction mechanisms.

Catalyzed cathodes also increase the cell limiting current. The increases are 10 and 25% with $(\text{CoPc})_n$ and FePc catalysts respectively. The increase is not caused by changes in physical properties of cathodes. The cyclic voltammograms of SOCl_2 reduction at stress annealed pyrolytic graphite electrode also show significant increase in the current peak heights. Therefore, it is strongly believed that the electrocatalysts not only catalyze the SOCl_2 reduction rate, but also modify the reduction mechanisms. Based on the results, the projected mechanisms at catalyzed cathode are:



At FePc catalyzed cathode, the above reaction mechanism proceeds. However, at $(CoPc)_n$ catalyzed cathodes, the reactive adduct $(M\cdot SO)^*$ might also dissociate to give free unstable SO molecule which is known to undergo disproportionation to S and SO_2 . Therefore, the overall reduction mechanism at $(CoPc)_n$ catalyzed cathode might involve less than 2-1/2 e^- per mole of $SOCl_2$, but more than $2e^-$. However, it should be noted that, due to fast second electron reduction (equation 9), the reaction mechanism is simplified at the catalyzed cathodes, whereas at the baseline cathode, the $SOCl^{\cdot}$ radical might promote a disproportionate reaction to unwanted chemical species. This could potentially lead to a safer Li/ $SOCl_2$ cell/battery.

The catalytic activity from adduct formation arises by overlapping a dz^2 orbital of Co or Fe with the sp^3 orbital of sulfur. In thionyl chloride, one of the sp^3 orbitals is non-bonded and contains two electrons; the dz^2 orbitals of Co and Fe are empty. Therefore, the charge transfer can occur easily from the electron-filled sulfur sp^3 orbital to the dz^2 orbital. The greater catalytic activity of FePc for the electrochemical reduction of $SOCl_2$ and also for the Stroger adduct formation with SO (equation 10) may be due to higher orbital overlapping.

The operating temperature affects the Li/ $SOCl_2$ cell performance severely. Both cell voltage and rate capability decrease with decreasing operating temperature. In addition, at operating temperatures of $-20^{\circ}F$ and below, the rate capability of Li/ $SOCl_2$ cells decreases drastically and no useful discharge times can be achieved at discharge rates of greater than 10 mA/cm^2 even with FePc catalyzed cathodes.

The conductivity of electrolyte decreases by more than threefold when temperature is lowered from 75 to $-40^{\circ}F$. This causes an increase in the polarization due to ohmic resistance. Furthermore, the changes in electrolyte viscosity also effect the overall cell performance, particularly at high rate and/or low operating temperature.

V. RECOMMENDATIONS

The feasibility of attaining improved rate performance and efficiency in the Li/SOCl₂ system using electrocatalyst(s) was clearly demonstrated in this program in laboratory cells. Future work needs to focus on confirming the established performance attributes of electrocatalyst(s) at the hardware cell level. Specifically, we recommend the following:

- o Conduct parametric studies on the hardware cell performance using "D-sized" cells that contain catalyzed cathodes. In addition to the general performance characterizations as a function of discharge rates and temperature, the parametric studies should include storage time so as to evaluate the effect of electrocatalyst(s) on Li passivation.
- o Confirmation of the proposed model reaction mechanism via monitoring of the pressure behavior at the hardware level and via quantitative analysis of LiCl, Li₂S₂O₄, and S. If the overall model reaction proposed is correct, either little or no SO₂ should be generated. Li₂S₂O₄ should be present in lieu of SO₂.
- o Conduct AC impedance measurements on both laboratory and hardware cells with respect to depth of discharge so as to understand the rate of lithium chloride film resistance on cell performance.

VI. REFERENCES

1. W. K. Behl, J. A. Christopoulos, S. Ramirez and S. Gilman, *J. Electrochem. Soc.* 120, 1619 (1973).
2. J. J. Auborn, K. W. French, S. I. Lieberman, V. K. Shah and A. Heller, *J. Electrochem. Soc.* 120, 1613 (1973).
3. G. E. Blomgren, V. Z. Leger, T. Kalnoki-Kis, M. L. Kronenberg and R. J. Brodd, in "Power Sources," J. Thomson, Editor, p.583, Academic Press, (1979).
4. A. N. Dey, *Thin Solid Films*, 43, 131 (1977).
5. N. Doddapaneni, *Extended Abstracts of the Electrochemical Society*, Vol. 81-1, 218-219 (1981).
6. J. Phillips, J. C. Hall and H. F. Gibbard, *Extended Abstracts of Electrochem. Soc.*, Vol. 80-2, 165-167, (1980).
7. F. M. Delnick and C. D. Jaeger, *Extended Abstracts of Electrochem. Soc.* Vol. 81-2, 223-225 (1981).
8. V. G. Levich, "Physicochemical Hydrodynamics," Prentice Hall, Englewood Cliffs, NJ (1962).

VII. ACKNOWLEDGEMENTS

The author acknowledges the support of this research by the U.S. Army Electronics Research and Development Command under Contract No. DAAK20-81-C-0381 and the experimental assistance of Mr. Steven J. Geib. The author further acknowledges the helpful discussions with Drs. David L. Chua, Hanumanthiah Venkatasetty, Sol Gilman and Wishvender K. Behl during the conduct of this program.

DISTRIBUTION LIST

Defense Technical Info Ctr ATTN: DTIC-TCA Cameron Station (Bldg 5) Alexandria, VA 22314	(12)	Commander US Army Electronics R&D Command Fort Monmouth, NJ 07703
Cdr, Naval Surface Weapons Ctr White Oak Laboratory ATTN: Library, Code WX-21 Silver Spring, MD 20910	(1)	DELET-DD (1) DELET-DT (1) DELSD-L (Library) (1) DELSD-L-S (Stinfo) (2) DELET-PR (S. Gilman) (17)
Commandant, Marine Corps HQ, US Marine Corps ATTN: Code LMC, INTS (In Turn) Washington, DC 20380	(1)	NASA Scientific & Tech Info Facility Baltimore/Washington Intl Airpt PO Box 8757, MD 21240 (1)
Rome Air Development Center ATTN: Documents Library (TSLD) Griffiss AFB, NY 13441	(1)	CMDR, MICOM ATTN: DRCPM-HDE Redstone Arsenal, AL 35809 (1)
AFGL/SULL S-29 • HAFB, MA 01731	(1)	Foote Mineral Company Route 100 Exton, PA 19341 ATTN: Dr. H. Grady (1)
HQDA (DAMA-ARZ-D/Dr. F.D.Verderame) Washington, DC 20310	(1)	Eagle-Picher Industries, Inc. Electronics Division P.O. Box 47 Joplin, Missouri 64801 ATTN: Mr. Robert L. Higgins (1)
Cdr, Harry Diamond Laboratories ATTN: Library 2800 Powder Mill Road Adelphia, MD 20783	(1)	Yardney Electric Company 82 Mechanic Street Pawcatuck, CT 06379 ATTN: Technical Library (1)
Director US Materiel Sys Anal Actv ATTN: DRXSY-T Aberdeen Prov Grnd, MD 21005	(1)	Duracell International, Inc. Northwest Industrial Park Burlington, MA 01803 ATTN: Dr. A.N. Dey (1)
Cdr, USA Signals Warfare Lab ATTN: DELSW-OS Vint Hill Farms Station Warrenton, VA 22186	(1)	Exxon Research & Engineering Co. Corporate Research Laboratory Linden, NJ 07036 ATTN: Dr. R. Hamlen (1)
Commander USA Mobility Eqp Res & Dev Cmd ATTN: DRDME-R Fort Belvoir, VA 22060	(1)	Argonne National Laboratories 9700 South Cass Argonne, IL 60439 ATTN: Dr. E.C. Gay (1)
Cdr. Harry Diamond Labs ATTN: DELHD-CO,TD (In Turn) 2800 Powder Mill Road Adelphia, MD 20783	(1)	

Union Carbide Corporation Battery Products Division P.O. Box 45035 Westlake, Ohio 44145 ATTN: C. M. Langkau	(1)	GTE Laboratories, Inc. 520 Winter Street Waltham, MA 02154 ATTN: Dr. Ronald McDonald	(1)
General Motors Corp. Research Laboratories General Motors Technical Center 12 Mile and Mounds Roads Warren, MI 48090 ATTN: Dr. J.L. Hartman	(1)	Electrochimica 2485 Charleston Road Mountain View, CA 94040 ATTN: Dr. Eisenberg	(1)
Duracell International, Inc. S. Broadway Tarrytown, NY 10591 ATTN: J. Dalfonso	(1)	Energy Storage & Conversion Dept. TRW Systems One Space Park Redondo Beach, CA 90278 ATTN: Dr. H.P. Silverman	(1)
North American Rockwell Corp. Atomics Internation Division Box 309 Canoga Park, CA 91304 ATTN: Dr. L. Heredy	(1)	Sanders Associates, Inc. 24 Simon Street Mail Stop NSI-2208 Nashua, NH 03060 ATTN: J. Marshall	(1)
General Electric Research & Development Center P.O. Box 8 Schenectady, NY 12301 ATTN: Dr. Stefan Mitoff	(1)	Power Conversion, Inc. 70 MacQuesten Pkwy Mount Vernon, NY 10550 ATTN: Stuart Chodosh	(1)
University of California Department of Science & Research Santa Barbara, CA 93100 ATTN: Dr. J. Kennedy	(1)	Portfolio Manager Hooker Chemicals & Plastics Corp. M.P.O. Box 8 Niagara Falls, NY 14302	(1)
Gulton Industries, Inc. Metuchen, NJ 08840 ATTN: Mr. S. Charlip	(1)	G207 S.R.I. Menlo Park, CA 94025 ATTN: Dr. Leonard Nanis	(1)
INCO Research and Development Center Sterling Forest Suffern, NY 10901 ATTN: Nehemiah Margalit	(1)	Bell Laboratories 600 Mountain Avenue Murray Hill, NJ 07974 ATTN: Dr. J.J. Auborn, Rm 1A-317	(1)
Director Propulsion and Power Division Mail Code EP5 NASA-Johnson Space Center Houston, Texas 77058 ATTN: Mr. B. J. Bragg	(1)	Jet Propulsion Laboratory 4800 Oak Grove Drive Pasadena, CA 91103 ATTN: Mr. Harvey Frank Mail Stop 198-220	(1)
		Naval Surface Weapons Center White Oak Laboratory, Code R-33 (M/S A026) Silver Spring, MD 20910 ATTN: Dr. D. Ernst	(1)
		Energy Conversion Branch Code 3642 Naval Underwater Systems Center Newport Laboratory Newport, RI 02840 ATTN: Mr. J. R. Moden	(1)

NASA Lewis Research Center
Mail Stop 6-1
21000 Brookpark Road
Cleveland, OH 44135
ATTN: Dr. Stuart Fordyce (1)

EIC, Inc.
Newton, MA 02158
ATTN: S.B. Brummer (1)

Altus Corp.
440 Page Mill Road
Palo Alto, CA 94306
ATTN: Douglas Glader (1)

MS 488
NASA Langley Research Center
Hampton, VA 23665
ATTN: J. Bene (1)

Research and Development Division
The Gates Rubber Co.
999 S. Broadway
Denver, CO 80217
ATTN: Mr. Eddie T. Seo (1)

Mail Stop 8C-62
Boeing Aerospace Company
P.O. Box 3999
Seattle, WA 98124
ATTN: Mr. Sidney Gross (1)

Honeywell Technology Center
10701 Lyndale Avenue, South
Bloomington, MN 55420
ATTN: Dr. H.V. Venkatasetty (1)

Jet Propulsion Laboratory
M.S. 198-220
4800 Oak Grove Drive
Pasadena, CA 91103
ATTN: Mr. Aiji Uchiyama (1)

Naval Surface Weapons Center
White Oak Laboratory, Code R-33
Silver Spring, MD 20910
ATTN: Dr. Frank Bis (1)

Dr. Jerry J. Smith
ONR Chemical Program
Arlington, VA 22217 (1)

Saft Corporation of America
711-A Industrial Blvd.
P.O. Box 1284
Valdosta, GA 31601
ATTN: Mr. Lou Adams (1)

Gould Laboratories-Energy Research
40 Gould Center
Rolling Meadows, IL 60008
ATTN: Dr. J. Hall (1)

Electrochem Industries (E-I) Inc.
9990 Wehrle Drive
Clarence, NY 14031
ATTN: Dr. C. Liang (1)

GTE Laboratories Incorporated
40 Sylvan Road
Waltham, MA 02254
ATTN: Dr. K. Klinedinst (1)

Harvey N. Seiger Associates
8 Beacon Hill Drive
Waterford, CT 06385
ATTN: Harvey N. Seiger, Ph.D. (1)

ECO Incorporated
P.O. Box 578
Buzzards Bay, MA 02532 (1)
ATTN: Myles Walsh

TRW/DSSG
Ballistic Missile Division
P.O. Box 1310 524/420
ATTN: Gordon L. Juvinall
San Bernardino, CA 92402 (1)

END
09-82